UNIVERSITÉ DE MONTRÉAL

MULTIPLE-INPUT MULTIPLE-OUTPUT COMMUNICATIONS SYSTEMS USING RECONFIGURABLE ANTENNAS

XINGLIANG LI
DÉPARTEMENT DE GÉNIE ÉLECTRIQUE
ÉCOLE POLYTECHNIQUE DE MONTRÉAL

THÈSE PRÉSENTÉE EN VUE DE L'OBTENTION
DU DIPLÔME DE PHILOSOPHIÆ DOCTOR
(GÉNIE ÉLECTRIQUE)
AVRIL 2015

UNIVERSITÉ DE MONTRÉAL

ÉCOLE POLYTECHNIQUE DE MONTRÉAL

Cette thèse intitulée :

MULTIPLE-INPUT MULTIPLE-OUTPUT COMMUNICATIONS SYSTEMS USING RECONFIGURABLE ANTENNAS

présentée par : LI Xingliang
en vue de l'obtention du diplôme de : Philosophiæ Doctor
a été dûment acceptée par le jury d'examen constitué de :

M. CARDINAL Christian, Ph. D., président
M. FRIGON Jean-François, Ph. D., membre et directeur de recherche
M. HACCOUN David, Ph. D., membre
M. FORTIER Paul, Ph. D., membre externe

DEDICATION

Dedicated to my family.

ACKNOWLEDGMENTS

It would not have been possible to complete this thesis without the help of all the kind people around me. I would like to thank the most important person in my life, my beloved wife Ran Cao, for her unconditional support, great patience and immense self-sacrifice. I will forever owe her a debt of gratitude for always having confidence in me, even in the times when I didn't. I would like to thank my parents, who have given me everything and have supported me all these years. And, I also owe a lot to Hanhan, my daughter, my life joy.

I would like to express my sincere gratitude to my supervisor, Prof. Jean-François Frigon, for his generous support and insightful guidance. His encouragement was invaluable to me during my doctoral study. This thesis would not have seen the light without his help. I would also like to thank the members of my thesis committee, Prof. Christian Cardinal, Prof. David Haccoun and Prof. Paul Fortier, for their valuable comments.

I would like to acknowledge all of my colleagues and friends in Poly-Grames, Diego Perea-Vega, Mohamed Jihed Gafsi, Vida Vakilian, Eddy Dailleux, Liang Han, Xuhua Shen, Ya Deng and Pengyan Zhang, for their suggestions, help and friendship.

Xingliang Li

RÉSUMÉ

Depuis les années 1990, l'utilisation des systèmes de communications sans-fil à entrées multiples-sorties multiples (MIMO) a été introduit pour fournir des transmissions fiables à grande vitesse. Cette thèse porte sur l'application et l'étude des systèmes MIMO avec des antennes reconfigurables, qui sont ajustable électroniquement pour produire différents diagrammes de rayonnement d'un seul élément d'antenne et ainsi offrir une diversité de diagrammes de rayonnement. En particulier, nous étudions le comportement de la capacité de canal des systèmes MIMO à sélection de diagrammes de rayonnement (PS-MIMO), et nous proposons aussi des algorithmes de sélection du diagramme de rayonnement atteignant la capacité maximale.

Tout d'abord, nous étudions l'application des antennes reconfigurables dans l'estimation des statistiques spatiales à long terme de canaux spatiaux avec grappes de multi-trajets (cluster). Nous proposons un estimateur de spectre de type Capon et une technique d'adaptation de la covariance (COMET) pour estimer conjointement l'angle moyen et l'étalement angulaire de la grappe spatiale avec des antennes reconfigurables. En second lieu, sur la base des statistiques à long terme du canal MIMO, nous proposons des algorithmes de sélection de diagramme de rayonnement MIMO (SPS-MIMO) pour atteindre la capacité maximale de canal ergodique. L'analyse de la maximisation de la capacité ergodique du système SPS-MIMO indique que le modèle statistique de sélection fournit des gains supplémentaires en améliorant la puissance du signal reçu et en décorrélant les signaux reçus avec différents diagrammes de rayonnement directionnels. Troisièmement, nous nous concentrons sur le modèle de sélection instantanée des diagrammes de rayonnement MIMO (IPS-MIMO) basé sur des informations instantanées d'état de canal (CSI) afin de maximiser la capacité instantanée pour chaque réalisation de canal. Nous démontrons que l'ordre de diversité des systèmes MIMO peut être multipliée par le nombre de diagrammes de rayonnement avec sélection de diagramme instantanée. Afin d'évaluer la capacité moyenne de l'IPS-MIMO, nous proposons un nouvel algorithme qui permet d'approximer étroitement la moyenne de la valeur maximale de la capacité du canal MIMO avec des trajets arbitrairement corrélés. Nous proposons également un algorithme pour sélectionner instantanément les diagrammes de rayonnement pour atteindre la capacité moyenne. En outre, sur la base d'une simple expression en forme fermée de la capacité coefficient de corrélation, nous sommes en mesure de proposer un algorithme de sélection de sous-ensemble de diagrammes qui offre un compromis entre performances et la complexité de l'algorithme de sélection.

En conclusion, des gains de performance importants peuvent être obtenus grâce à la

combinaison de l'utilisation d'antennes reconfigurables et de systèmes MIMO avec soit des algorithmes de sélection de diagramme de rayonnement statistique ou instantanée. La capacité des systèmes PS-MIMO à améliorer les performances du système, y compris la capacité et de l'ordre de la diversité, est démontrée par l'analyse théorique et des simulations numériques.

ABSTRACT

Since the 1990s, the use of multiple-input multiple-output (MIMO) systems has been introduced to modern wireless communications to provide reliable transmission at high data rates. This thesis focuses on the application of MIMO systems with reconfigurable antennas, which are electronically tunable to produce a number of radiation patterns at a single antenna element and provide pattern diversity. In particular, we investigate the capacity performance of the pattern selection MIMO (PS-MIMO) systems, and we also present maximum capacity achieving algorithms for radiation pattern selection.

First, we investigate the application of reconfigurable antennas in estimating long term spatial statistics of spatial clustered channels. We propose a Capon-like spectrum estimator and a covariance matching technique (COMET) to jointly estimate the mean angle and the angular spread of the spatial cluster with reconfigurable antennas. Second, based on the long term statistics of the MIMO channel, we propose statistical pattern selection MIMO (SPS-MIMO) algorithms to achieve maximum ergodic channel capacity. Analysis of the ergodic capacity maximization of the SPS-MIMO indicates that the statistical pattern selection provides additional gains by enhancing received signal power and decorrelating received signals with different directional radiation patterns. Third, we focus on the instantaneous pattern selection MIMO (IPS-MIMO) based on instantaneous channel state information (CSI) in order to maximize the instantaneous capacity for every channel realization. We prove that the diversity order of MIMO systems can be multiplied by the number of radiation patterns with instantaneous pattern selection. In order to evaluate the mean capacity of the IPS-MIMO, we propose a novel algorithm which closely approximates the mean of the maximum of the channel capacity of arbitrarily correlated MIMO channels. We also propose an algorithm for instantaneously selecting radiation patterns to achieve the mean capacity. In addition, based on a simple closed-form approximation to the capacity correlation coefficient, we are able to propose a subset pattern selection algorithm which enables the trade-off between performances and complexity.

In conclusion, important extra gains can be obtained as a result of combining the use of reconfigurable antennas and MIMO systems with either statistical or instantaneous radiation pattern selection. The capability of the PS-MIMO to improve system performances, including capacity and diversity order, is demonstrated through theoretical analysis and numerical simulations.

TABLE OF CONTENTS

LIST OF FIGURES

LIST OF ALGORITHMS

LIST OF APPENDICES

LIST OF ACRONYMS AND ABBREVIATIONS

3GPP	third generation partnership project
AS	angle spread = azimuth spread
AWGN	additive white Gaussian noise
BER	bit error rate
BPSK	binary phase-shift key
BS	base station
CDF	cumulative distribution function
CDMA	code division multiple access
CIR	channel impulse response
CRLH-LWA	composite right/left-handed leaky-wave antenna
CSI	channel state information
D-BLAST	diagonal Bell Labs layered space-time
DFT	discrete Fourier transform
DoA	direction-of-arrival
DoD	direction-of-departure
DoF	degree of freedom
EGC	equal gain combining
ESPAR	electronically steerable parasitic radiator
EVD	eigenvalue decomposition
FER	frame error rate
FET	field-effect transistor
iff	if and only if
i.i.d.	independent and identically distributed
ISI	inter symbol interference
LOS	line of sight
LWA	leaky-wave antenna
MEMS	micro-electromechanical systems
MGF	moment generating function
MIMO	multiple-input multiple-output
ML	maximum likelihood
MLSE	maximum-likelihood sequence estimation
MMSE	minimum mean square error
MRC	maximum ratio combining

MSE	mean square error
OFDM	orthogonal frequency division multiplexing
OSIC	ordered successive interference cancellation
OSTBC	orthogonal space-time block code
PAS	power azimuth spectrum
PDF	probability density function
PDP	power delay profile
PEP	pairwise error probability
RF	radio frequency
RMS	root mean square
Rx	receiver
SCM	spacial channel model
SER	symbol error rate
SINR	signal-to-interference-and-noise ratio
SISO	single-input single-output
SM	spatial multiplexing
SNR	signal-to-noise ratio
STBC	space-time block code
SVD	singular value decomposition
Tx	transmitter
ULA	uniform linear arrays
V-BLAST	vertical Bell Labs layered space-time
WLAN	wireless local area networks
ZF	zero-forcing

LIST OF SYMBOLS

$\triangleq$	variable definition
$\mathbb{E}[\cdot]$	expectation operator
$\otimes$	Kronecker product
$\odot$	Hadamard (element-wise) product
$\mathbb{R}$	real field
$\mathbb{C}$	complex field
a, α	scalar
$\mathbf{a}$	column vector
$\mathbf{A}$	matrix
$\mathbf{A}^T$	matrix transpose
$\mathbf{A}^H$	matrix conjugate transpose (Hermitian)
$\mathbf{A}^-$	generalized matrix inverse
$\det \mathbf{A}$	determinant of $\mathbf{A}$
$\mathrm{tr}\mathbf{A}$	trace of $\mathbf{A}$
$\|\mathbf{A}\|_F$	Frobenius norm of $\mathbf{A}$
$\mathrm{vec}\,(\mathbf{A})$	stacks $\mathbf{A}$ columnwisely into a column vector
$\mathrm{unvec}\,(\mathbf{a})$	restore the vector $\mathbf{a}$ to the original matrix
$r(\mathbf{A})$	rank of $\mathbf{A}$
$\mathbf{0}_{m\times n}$	zero matrix
$\lceil\cdot\rceil$	ceiling operator
$\lfloor\cdot\rfloor$	floor operator

CHAPTER 1

INTRODUCTION

1.1 Background and Motivation

Since the 1990s, the use of multiple transmit and receive antennas has been introduced to modern wireless communications. Computer simulations and theoretical analysis presented in the pioneering works by Winters [1] and Telatar [2] have shown that, by deploying these multiple-input multiple-output (MIMO) systems, the spectral efficiency in a point-to-point communication scenario can be increased linearly with the number of antennas. Therefore, MIMO is regarded as an essential technical breakthrough which serves as a promising solution to the ever increasing demand for high data rates in future wireless communications.

In general, a multidimensional MIMO system can provide two types of performance gains: the *space diversity* gain and the *spatial multiplexing* gain. A MIMO system with N_t transmit and N_r receive antennas can create $N_t N_r$ space diversity branches between the transmit and receive antenna ports. When the propagation channel is in deep fading, these branches can be exploited to improve system robustness. By transmitting and/or receiving replicated data symbols over different antennas, which is known as space diversity, the possibility of a transmission failure is significantly reduced because some symbol replica may undergo deep fades while others may not. The error probability of this space diversity system decreases exponentially by the number of combined diversity branches, *i.e.* , the *diversity order*. A classical example of an efficient space diversity is *space-time coding*, which has been applied in wireless communication systems [3, 4]. Under circumstances where the channel is not in a deep fade, MIMO systems can also be used to increase the data rate by means of spatial multiplexing techniques. MIMO systems over spatially uncorrelated channels can support $\min(N_t, N_r)$ independent spatial channels [5]. By dividing the transmission symbol stream into multiple parallel substreams and transmitting each substream via a separate spatial channel, the transmission data rate is increased by the number of spatial subchannels. Indeed, it has been theoretically proven that the ergodic channel capacity of a spatial multiplexing MIMO system increases linearly with the number of independent parallel spatial channels supported by the MIMO system, which is known as the *degree of freedom* [2]. The vertical Bell Laboratories layered space-time architecture (V-BLAST) is a famous example of spatial multiplexing [6]. Provided that the number of receive antennas is no less than the

number of transmit antennas, V-BLAST transmits parallel symbol streams over the transmit antennas, and the receive antennas are used for demultiplexing the different symbol streams at the receiver. The data rate of V-BLAST is therefore multiplied by the number of transmit antennas.

However, the space diversity gain and the spatial multiplexing gain of a MIMO system can not be maximized simultaneously. For example, a typical spatial multiplexing system provides no spatial diversity gain whereas a space-time code which achieves full space diversity reduces the achievable spatial multiplexing gain. Though spatial multiplexing is more attractive to obtain higher data rate than space diversity, the performance of a full spatial multiplexing system suffers from fading, particularly, in the low signal-to-noise (SNR) regime. Therefore, it is necessary in this case to reserve some of the available spatial resources for diversity to guarantee reliable transmission, which is known as *diversity-multiplexing tradeoff*. In [7], the optimal diversity-multiplexing tradeoff curves for some certain transmission schemes are derived, verifying that higher space diversity gain comes at the price of sacrificing spatial multiplexing. Spatial correlation is another negative factor which prevents from fully exploiting the theoretically promising advantages of MIMO systems, especially in the high SNR regime. Propagation channels are usually spatially correlated to various degrees because homogeneous scattering is an ideal and unrealistic assumption in most real-world channels. Furthermore, the physical dimension of handheld devices is often limited and results in high correlation between closely spaced antenna elements. Hence the number of available spatial resources is restricted by spatial correlation which is introduced both over the air and at the antenna side. In an extreme case, a "keyhole" correlated MIMO channel provides one degree of freedom [8], causing severe capacity losses in the high SNR regime comparing to spatially uncorrelated channels [9].

Having acknowledged that increasing the transmission reliability of MIMO systems by adding space diversity sacrifices the spatial multiplexing gain, a growing community of researchers have extended their scopes from only using the variation of fading channels to directly manipulating the antenna itself to provide diversity, which had been the most ignored part in MIMO technologies, until recently, for overcoming the challenges aforementioned. Space diversity mentioned above is an antenna diversity technique. Other antenna diversity techniques include *polarization diversity* and *pattern diversity*. Unlike space diversity which takes advantages of multipath fading in the space domain with separately spaced multi-element arrays, polarization diversity systems transmit signals with orthogonal polarizations of antennas, and pattern diversity provides orthogonality by producing spatially disjoint radiation patterns. For example, multi-mode antennas can generate pattern diversity by transmitting signals via orthogonal modes [10]. The multi-mode antenna MIMO produces

diversity without being separated by a physical distance and the system performance is comparable with conventional MIMO systems, which proves that space diversity can be replaced by pattern diversity. Therefore, it is possible to utilize pattern reconfigurable antennas in a spatial multiplexing MIMO system to achieve full spatial multiplexing gain while obtaining pattern diversity for reliable transmission.

This thesis is a contribution to the application of radiation pattern reconfigurable antennas in MIMO wireless communication systems. Reconfigurable antennas are switchable or tunable to produce a number of radiation patterns and provide pattern diversity. In the low SNR regime, the pattern diversity can provide additional diversity to guarantee reliable transmission. In the high SNR regime, the additional pattern diversity can be utilized to replace space diversity so that full spatial multiplexing gain is maintained without adding more antennas.

1.2 Objectives and Methodology

The general objective of this research is to analyze performances of MIMO systems with pattern reconfigurable antennas deployed at the receive side in wireless communications over flat or block fading channels. The methodology of this research is based on the analysis of system performance of MIMO with pattern reconfigurable antennas, assuming perfect channel state information (CSI) at the receiver side.

In the first part of this research, the system model of pattern selection MIMO (PS-MIMO) and the channel modeling with reconfigurable antennas are provided as the prerequisites for analyzing the system performance and designing selection algorithms for PS-MIMO.

The second part of this thesis investigates channel estimation techniques with reconfigurable antennas. Either full or partial channel state information (CSI) is necessary for analyzing system performances of PS-MIMO systems and designing pattern selection algorithms.

After obtaining channel parameters by estimation with reconfigurable antennas, the major part of this research then focuses on the design of selection algorithms and the analysis of system performances of PS-MIMO. The radiation pattern of a reconfigurable antenna can be electronically manipulated in real time. The PS-MIMO system selects a proper set of radiation patterns for the reconfigurable antennas to achieve certain kinds of performance gains. According to the selection method, there are two categories of PS-MIMO systems: the *statistical selection* and the *instantaneous selection*. The statistical pattern selection MIMO (SPS-MIMO) system configures the reconfigurable antennas based on a long-term channel

statistics. And statistical pattern selection algorithms should be designed according to long-term statistical performance criteria.

The instantaneous pattern selection MIMO (IPS-MIMO) system configures the reconfigurable antennas based on instantaneous full channel state information (CSI). And instantaneous pattern selection algorithms should be designed according to instantaneous performance criteria.

In summary, the specific objectives of this research include:

- A mathematical model of PS-MIMO systems and models of MIMO channels with reconfigurable antennas.
- Finding techniques to estimate channel parameters of MIMO channels modeled by the spatial channel model with reconfigurable antennas.
- Developing pattern selection algorithms and providing performance analysis for SPS-MIMO systems.
- Developing pattern selection algorithms and providing performance analysis for IPS-MIMO systems.

1.3 Contributions

This thesis is a contribution to the application of radiation pattern reconfigurable antennas in MIMO wireless communication systems. Our contributions in this thesis are listed as follows:

- We propose to use a pattern reconfigurable antenna array for estimating statistical parameters of spatial clustered channels. A novel channel model is proposed to remove the non-existent phantom clusters in the widely used Kronecker channel model. A MUSIC based direction of departure (DoD) estimation is proposed for mean angles of the clustered channel with pattern reconfigurable arrays. For the estimation of both the mean direction and the angular spread of the clustered channel, the covariance matching technique (COMET) is applied.
- We propose to use the statistical pattern selection (SPS) in MIMO systems over spatially correlated flat fading channels. An upperbound on the ergodic channel capacity of this SPS-MIMO system is calculated. Based on the upperbound, an exhaustive searching algorithm is proposed to find the radiation patterns of the reconfigurable antenna for

maximizing the ergodic channel capacity. A fast radiation pattern searching algorithm based on Newton's method is also proposed. The searching algorithms are validated with an actual pattern reconfigurable antenna, the composite right/left-handed leaky wave antenna (CRLH-LWA), as a demonstration.

- We propose to use the instantaneous pattern selection (IPS) in MIMO systems over spatially correlated flat fading channels. An accurate approximation to the ergodic channel capacity of IPS-OSTBC with arbitrarily correlated radiation patterns is proposed. A complexity reduced pattern selection algorithm for IPS-OSTBC and IPS-MIMO is proposed.

1.4 Organization of the Thesis

This thesis is divided into seven chapters. Chapter 1 is the introduction to this research and thesis, which provides an overview of the research background, objectives and contributions. The following part of this thesis is organized as follows.

In Chapter 2, a literature review is given concerning research results on reconfigurable antennas, pattern diversity MIMO systems and system performance analysis of instantaneous antenna selection for MIMO systems.

In Chapter 3, the reconfigurable antenna is briefly introduced and the system model of the PS-MIMO systems equipped with reconfigurable antennas is presented. General PS-MIMO channel models are presented in terms of both deterministic and stochastic approaches. The spatial cluster channel models for PS-MIMO are discussed for future evaluation. A spatially correlated MIMO channel model, the *sum-Kronecker mode* is proposed to generate channel matrices. This channel model is as easy to use as the Kronecker model but it is able to avoid artificial clusters. So it is particularly useful in verifying estimation algorithms for cluster parameters in multi-clustered MIMO channels.

In Chapter 4, a study of estimating the channel parameters of spatially clustered channels with a reconfigurable antenna array are presented. A subspace based method is examined for estimating the direction of arrivals (DoA) with reconfigurable antennas. A Capon-like spectrum estimator is proposed to jointly estimate the mean angle and angular spread of a clustered channel. The covariance matching technique for estimating the mean angle and angular spread is also discussed.

In Chapter 5, algorithms for maximizing the ergodic channel capacity of PS-MIMO systems with statistical pattern selection over spatially correlated Rayleigh fading channels are proposed. The ergodic channel capacity of the proposed selection algorithm is evaluated

by numerical simulations. Analysis of the ergodic channel capacity maximization problem for statistical selection is also included.

In Chapter 6, we focus on the instantaneous channel capacity performance of PS-MIMO systems with instantaneous pattern selection over spatially correlated Rayleigh fading channels. For every channel realization, the radiation patterns of the receiving antennas are selected to maximize the instantaneous channel capacity. The ergodic channel capacity of the instantaneous selection system is then studied based on an approximation of the capacity distribution. Algorithms aiming to select radiation patterns which maximizes the ergodic capacity of the instantaneous selection system are presented.

Finally, Chapter 7 concludes this thesis and discusses related future works.

CHAPTER 2

LITERATURE REVIEW

In this chapter, recent research results related to pattern diversity in MIMO systems are reviewed. The first section will give a brief introduction to the current progress in reconfigurable antennas. In the second section, we will present a literature survey on the application of radiation pattern reconfigurable antennas in MIMO communication systems. In the last section, we go over research results on antenna selection diversity in MIMO systems, a problem which exhibits some similarities with pattern diversity.

2.1 Reconfigurable Antennas

Radiation characteristics of antennas are traditionally assumed fixed at certain operating frequencies. Recently, microwave researchers have developed reconfigurable antennas to provide more possibilities. A reconfigurable antenna can intentionally alter its operating frequencies, impedance bandwidths, polarizations, and/or radiation patterns. Our research interests mainly focus on the application of radiation pattern reconfigurability in MIMO systems. Throughout this thesis, unless otherwise stated, we use the term "reconfigurable antenna" to refer to "radiation pattern reconfigurable antenna" for convenience.

Changing radiation patterns while keeping the operating frequency and bandwidth could greatly enhance system performances. Manipulating the radiation pattern of an antenna can be used to avoid interfering sources or improve transmission efficiency. The antenna radiation pattern is determined by the distribution of electric or magnetic currents on the radiating structure. Changes to the current distribution can be achieved by altering the physical or effective structure of the radiating structure or by changing the electrical characteristics of the radiating structure. The most common radiation pattern reconfiguration techniques are implemented by electric switches or variable reactive loading [11]. Depending on whether the tunable component of the reconfigurable antenna provides discrete or continuous changes, antenna reconfiguration techniques are classified into two categories: discrete tuning and continuous tuning. The discrete tuning provides a small number of radiation patterns while the continuous tuning can ideally excite infinite number of radiation patterns at the antenna port.

The discrete tuning is usually implemented by using active elements such as diodes or

field-effect transistors (FET) which switch between the "ON" state and "OFF" state. Piazza proposed to adjust the effective electric length of a dipole antenna with a PIN diode to switch between two distinct radiation patterns while keeping the operating frequency [12]. The radio-frequency microelectromechanical system (RF-MEMS) is another widely used switching component for radiation pattern reconfigurability. Petit designed a three-element parasitic-antenna array with two RF-MEMS switches which alter the length of the loading stubs to obtain reconfigurable radiation patterns [13]. In [14], Grau designed a pixel antenna which uses a multifunctional MEMS-reconfigurable radiator capable of producing up to five distinct radiation patterns.

The continuous tuning allows smooth changes in the antenna's radiation pattern. For instance, in 1978, Harrington proposed a parasitic dipole array in which the driven dipole element are surrounded by parasitic dipoles loaded with tunable reactances [15]. Varying the loading reactance of each parasitic element leads to changes to the apparent magnitude and phase of the signal on each array element and results in a directive beam in a desired direction. This electronically steerable parasitic radiator (ESPAR) antenna can provide continuous steerable radiation pattern [16]. However, limited by the element spacing and size, the ESPAR can not provide high-directive pattern and can not be easily used in MIMO systems. Another example of continuously tuned reconfigurable antennas is the composite right/left-handed leaky-wave antenna (CRLH-LWA). Caloz [17] proposed a CRLH-LWA design which consists of a periodic structure composed of cascaded CRLH microstrip unit cells with tunable varactors. The antenna can be continuously tuned to control the phase of the signal at each cell so that a directional radiation pattern is continuously steerable from backfire to endfire. Piazza in [18] proposed another CRLH-LWA structure of a compact size so that the antenna is more applicable in MIMO systems.

2.2 Radiation Pattern Diversity in MIMO Systems

Radiation pattern diversity in MIMO systems can improve the wireless communication performance in rich scattering environments. But system capacity and reliability suffers when the transmission channel is in deep fading or highly correlated. Since the propagation channel in the wireless medium is fixed by the given environment and out of control of the communication system, reconfiguring the radiation patterns of the antennas is an effective mechanism to change the propagation characteristics of the channel between the antenna ports at the transmitter and receiver side so that better performance can be achieved over the altered wireless channel. This is the fundamental idea of radiation pattern diversity.

It was proposed in [19] as a new approach to provide dynamic radiation pattern diversity

(DRPD).

Recently, polarization diversity, pattern diversity and multi-mode diversity have been studied to combat fading and improve system performances. [20] and [21] proposed to utilize different antenna radiation patterns in clustered MIMO channels to improve channel capacity by increasing the channel gain and/or reducing spatial correlation. But these schemes are unable to provide selection diversity. [22] proposed a real-time radiation pattern selection scenario for orthogonal space-time coding (OSTBC) systems. The authors proved that if P disjointed radiation patterns are used, the diversity order in terms of average error probability is multiplied by P fold. But this result is only valid for spatially uncorrelated MIMO channels.

Antennas are the key elements in wireless communication systems. Over the years, the operating characteristics of antennas such as their polarizations and radiation patterns have been assumed to be fixed at their operating frequencies. Though a phased array can produce a steerable radiation pattern, the operating characteristics of a single element in the array do not change. As discussed in Section 2.1, electronic engineers have recently developed reconfigurable antenna elements with one or some of their operating characteristics adjustable by mechanical or electrical method.

The major challenge of a wireless communication link is the uncertainty of the propagation environment which varies from time to time and from location to location. The varying nature of the wireless propagation environment is the key problem of wireless communications. MIMO systems can linearly increase the data rate by transmitting data streams over multiple antennas, i.e, spatial multiplexing. MIMO systems can also improve the link reliability by properly combining radio signals transmitted or received over different antennas, i.e, space diversity. However, it is not possible for a MIMO system to achieve maximum multplexing gain and full diversity at the same time with conventional static antennas. When the wireless channel undergoes strong fading, we have to sacrifice the multiplexing gain to provide more diversity. Furthermore, in indoor or urban wireless communication environments, the degree of freedom and diversity gain deteriorates due to the spatial correlation of the channel. And, because of the limited size of mobile terminals, closely spaced antennas make the MIMO channels even more correlated and therefore deteriorate system performances. Recently, several novel antennas providing DRPD have been designed, such as the CRLH-LWA with fully steerable directional radiation patterns and switchable micro-electromechanical systems (MEMS) antennas. For each antenna element, we can adjust its radiation pattern to fit the current instantaneous or long-term radio propagation channel characteristics and provide pattern diversity gain. As a consequence, we can replace space diversity by pattern diversity such that more spatial subchannels can be used to reliably transmit parallel data streams

and therefore increase the date rate. On the other hand, carefully adjusting the radiation patterns of different antennas may reduce channel correlation and improve multiplexing gain and diversity order. Therefore, it is proposed to deploy DRPD antennas in MIMO systems (DRPD-MIMO) over correlated channels such as indoor and urban environments.

The reconfigurability of antennas enables the capability of altering the propagation characteristics of the wireless channel between the transmitter and the receiver. Decades ago, wireless engineers began to use beamforming techniques to achieve similar features with antenna arrays consisting of monopoles or dipoles. However, a beamforming antenna array is not reconfigurable because its multiple antenna elements cannot change their operating characteristics.

The reconfigurability is most useful for devices with restricted space to install several antenna elements. A typical application is a single-element portable device, such as cell phones or laptops, which are limited both in size and battery power. A monopole or strip antenna is usually used with a fixed radiation pattern to provide omnidirectional coverage. In this case, if a reconfigurable antenna with its radiation pattern redirected to the direction of radio signals was used, the wireless device will then be able to use its battery power more efficiently.

In the uplink, it can either achieve higher data rate or improve the transmission reliability in poor propagation environments (deep fades) at no extra transmitting power. Or, the battery power assumption of the portable device can be significantly reduced without sacrificing transmission performances. In the downlink, it can also mitigate deep fades and interference from other users and therefore improve the signal-to-interference-plus-noise ratio (SINR).

In a multiple antenna scenario, radiation pattern reconfigurability introduces another degree of freedom which can be used to improve the diversity-multiplexing compromise. That is, the system can maintain its maximum spatial multiplexing gain given by the number of receive/transmit antennas, while increasing the diversity gain limited by the degree of reconfiguration provided by each antenna element.

In [23], it is suggested that by using reconfigurable directional antennas the MIMO channel capacity in indoor multipath environments can be improved by channel decorrelation as well as a directional gain. But these works are just showcases of exploiting the great potential of pattern diversity, and no quantitative performance analysis is given. In [20], the benefit of pattern diversity in a two-element circular patched antenna (CPA) array is analyzed. An upper bound of ergodic channel capacity is derived and the error performance of a practical system using Alamouti scheme is given.

It is shown in [24] that the capacity of MIMO systems can be increased over correlated fading channels by decorrelating with reconfigurable radiation patterns. It is in [25] that for the first time a theoretical analysis on the error performance gain offered by a reconfigurable MIMO system using Orthogonal Space-Time Block Codes (OSTBC) is derived. It is proved that with orthogonal radiation patterns the diversity order of the system is the product of the number of the transmit antennas, the number of the receive antennas and the number of available radiation pattern states. Furthermore, it was also observed that correlated radiation patterns degrades system performances comparing to systems with orthogonal radiation patterns. Channel estimation of the reconfigurable MIMO system is also discussed in [25].

However, recent researches of theoretical analysis on the performance gain of pattern diversity in MIMO systems is quite limited and how to select radiation patterns to maximize system performances is still an open problem.

2.3 Antenna Selection in MIMO Systems

In this section, we summarize existing literature on the application of antenna selection in MIMO systems. The radiation pattern selection is more complicated than antenna selection and these two selection schemes differ greatly for the antenna selection switches between the geometry locations of antenna elements while the radiation pattern selection switches between the radiation characteristics. However, it is still worthy of discussing the methodologies and system configurations of antenna selection.

Antenna selection in MIMO systems is proposed to reduce system cost by using fewer radio frequency (RF) chains than full MIMO systems. Antenna selection schemes for optimizing the capacity performance are proposed in [26–28]. In [26], the MIMO channel capacity of selecting a single receive antenna in MIMO systems under fading channels with correlation at the receiver side is considered. A closed-form expression for the outage probability and an upper bound for the ergodic capacity of such system is derived by analyzing the joint cumulative distribution function and the joint probability density function of the squared row norms of the channel matrix with moment methods. It is demonstrated that antenna selection based on maximizing the squared row norms of the channel matrix achieves a full diversity order that is similar to a full MIMO system without antenna selection. Antenna subset selection algorithms maximizing capacity of uncorrelated channels are discussed in [27] and [28].

[27] establishes the equivalence in diversity order between the full MIMO system and the antenna selection system by analyzing the outage characteristics. It is also proved in [27]

that the channel capacity is statistically lower bounded by the capacity of a set of parallel independent SIMO channels each with selection diversity. The proposed subset selection scheme achieves near optimal performance with low complexity. [28] derived an upper bound on the capacity based on the analysis of the joint statistics of the ordered SNR's, as the sum of the logarithms of ordered chi-square distributed variables based on the analysis of the joint statistics of the ordered SNR's. In [28], it is suggested that maximizing the rank and the singular values of the correlation matrix of the channel maximizes the capacity. The subset selection scheme proposed in [28] chooses two rows for the possible deletion whose correlation is the highest and delete the one with the lower power.

Low complexity antenna selection schemes aiming to capacity maximization in correlated MIMO channels are discussed in [29] and [30]. The proposed selection scheme in [29] is given based on the lower and upper bounds of the ergodic capacity with long-term channel statistics. The proposed selection algorithm applies a suboptimal sequential-selection approach instead of the exhaustive search. In [30] the low complexity selection scheme is proposed based on the theory of convex optimization and selection schemes for minimum mean square error (MMSE) and ordered successive interference cancellation (OSIC) V-BLAST receivers of spatial multiplexing MIMO systems are given.

Antenna selection schemes for improving system reliability are proposed in [24, 31–33]. In [31], the upper and lower bounds of the diversity order achieved by transmit antenna selection for spatial multiplexing systems in uncorrelated Rayleigh fading channels with linear receivers are given. [24] proposes an antenna selection scheme by maximizing instantaneous SNR. With this selection scheme the OSTBC-MIMO system achieves near optimal error rate performance in correlated Rayleigh channels with less complexity. [32] proposes a subset selection scheme to improve the array gain and adapting OSTBCs to any number of transmit antennas and to maximize the conditional SNR and minimize the instantaneous probability of error. [33] proposes transmit antenna selection and constellation selection for spatial multiplexing MIMO system for a given target data rate by maximizing the minimal post-processing SNR and maximizing the lower bound for a given outage data rate. In [34], antenna selection for spatial multiplexing multi-user MIMO systems in correlated spatial channels with linear and OSIC receivers are investigated. The selection algorithms are designed to maximize the sum rate or minimize the total power. Channel estimation issues for antenna selection are also considered and a training sequence signals in the preamble is proposed. [31] proposed a geometrical framework theoretically analyze the diversity order achieved by transmit antenna selection for separately encoded spatial multiplexing systems with linear and decision- feedback receivers. When two antennas are selected from the transmitter, the exact achievable diversity order is rigorously derived, which previously only appeared as conjectures based

on numerical results in the literature. If more than two antennas are selected, lower and upper bounds on the achievable diversity order are available. Furthermore, the same geometrical approach is used to evaluate the diversity-multiplexing trade-off curves for spatial multiplexing systems with transmit antenna selection.

CHAPTER 3

SYSTEM MODEL AND CHANNEL MODELS

In MIMO communications systems, the radio channel is one of the dominating factors which determine the characteristics of the entire system. Therefore, a proper channel model is a crucial precondition and guarantee to the system design. It helps to understand the system behavior and serves as a channel simulator so that system performances, including the channel capacity and the transmission error rate, can be reliably tested and fairly evaluated.

Wireless channels consists of the free space propagation environment and the antennas. Though the former has been addressed by a lot of published researches, the impact of the antenna part, apart from the antenna gain, is often ignored and the potential of the reconfigurability of antenna radiation characteristics usually neglected. Recent researches have discovered that deploying reconfigurable antennas in MIMO communication systems is a promising solution to the demand of high performance wireless communications over correlated channels on handhold devices where the antenna spacing is limited.

In this chapter, we first introduce the concept of antenna reconfigurability and the mathematical description of reconfigurable antennas and reconfigurable antenna arrays in Section 3.1. In Section 3.2, we propose the system model for a pattern-selection MIMO (PS-MIMO) wireless communication system and discuss its working mechanism. In the last section, we expand conventional MIMO channel modeling techniques to PS-MIMO channel modeling. In this section, a generic deterministic channel model with geometric parameters and a generic stochastic channel model for PS-MIMO systems are discussed. By assuming PS-MIMO over spatially clustered channels, we propose the Kronecker model and the sum-Kronecker model for PS-MIMO channels, both of which can be described by cluster statistics. The Kronecker model will be used for simulation and system performance analysis in future chapters. The sum-Kronecker model, which avoids spatial aliasing, will be used for simulation and analysis of channel estimation with PS-MIMO.

3.1 Reconfigurable Antennas for MIMO Systems

Each possible configuration with which a reconfigurable antenna can radiate distinct radiation patterns is called a *pattern state*. We denote the reconfiguration parameter by p, which can be either discrete or continuous, depending on whether it is switching-based or tuning-based.

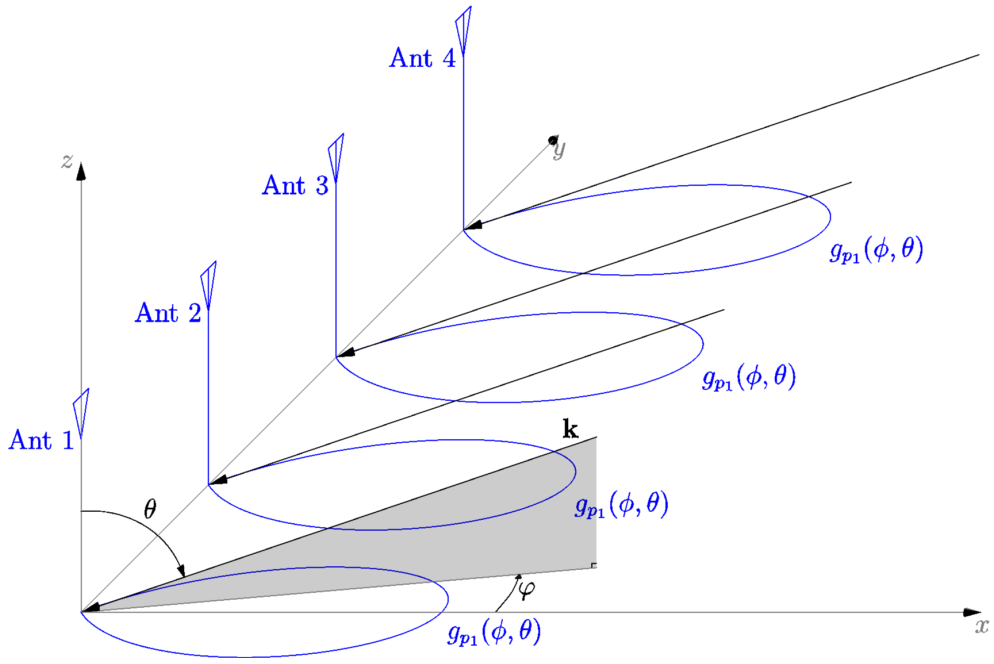

Figure 3.1 A 4-element reconfigurable antenna array is placed along the y-axis. When a plane wave with wavevector $\mathbf{k}(\phi,\theta)$ arrives at the array, the complex response of the n-th element at pattern state n_p is $g_{n_p}(\phi,\theta)$.

For the discrete case , without loss of generality, we assume that $p \in \{1,\ldots,P\}$ where P is the number of distinct pattern states to which the antenna can be configured. For the continuous case , the range of p is the direct product of the range of the reconfiguration parameter of each tunable element. However, we can convert the continuous case to the discrete case by making P samples from the reconfiguration parameter range so that the continuous case is reduced to the discrete case with P pattern states for selection. For conciseness, we abuse the use of the notation p and do not distinguish between the pattern state, the reconfiguration parameter and the numbered index of the reconfiguration parameter. With these notations, we denote the radiation pattern function of the reconfigurable antenna at the pattern state p by $g_p(\phi,\theta)$, where ϕ and θ are the azimuthal and elevation angle, respectively.

Consider an antenna array equipped with N reconfigurable antennas. Without loss of generality, we assume that radiation characteristics of the reconfigurable antennas in the array are identical and each antenna has P pattern states. We define the pattern vector of the array by

$$\mathbf{g}(\phi,\theta;\psi) = [g_{p_1}(\phi,\theta)\ g_{p_2}(\phi,\theta)\ \cdots\ g_{p_N}(\phi,\theta)]^T \tag{3.1}$$

where $p_n \in \{1,2,\ldots,P\}$ is the pattern state configured to the n-th antenna, $g_{p_n}(\phi,\theta)$ is the

3-dimensional complex radiation pattern. We use a N-digit and P-ary number

$$\psi = (p_1 p_2 \dots p_N)_P \tag{3.2}$$

to represent the radiation states configured at all the antennas in the array.

The array response of the reconfigurable array at the array state ψ to a plane radio wave at the solid angle (ϕ, θ) is referred to as the *array response vector*, denoted by $\mathbf{a}(\phi, \theta; \psi)$. The array response vector is given by the Hadamard product (element-wise product) of the *steering vector* $\mathbf{v}(\phi, \theta)$ and the pattern vector $\mathbf{g}(\phi, \theta; \psi)$:

$$\mathbf{a}(\phi, \theta; \psi) = \mathbf{v}(\phi, \theta) \odot \mathbf{g}(\phi, \theta; \psi). \tag{3.3}$$

The steering vector, which is given by

$$\mathbf{v}(\phi, \theta) = \left[e^{-j\mathbf{k}^T \mathbf{r}_1} \; e^{-j\mathbf{k}^T \mathbf{r}_2} \; \cdots \; e^{-j\mathbf{k}^T \mathbf{r}_N} \right]^T, \tag{3.4}$$

contains phases of signals excited by a plane radio wave from the direction (ϕ, θ) at the antenna ports. It is determined by the array geometry and the direction of the plane radio wave propagation. In Eq. (3.4), $\mathbf{r}_n = [x_n \, y_n \, z_n]^T$ is the *location vector* of antenna n ($n = 1, \cdots, N$) in Cartesian coordinates, and the *wavevector* $\mathbf{k}$ describes phase variation of the radio wave propagating along the direction (ϕ, θ)

$$\mathbf{k}(\phi, \theta) = \frac{2\pi}{\lambda} [\sin\theta \cos\phi \; \sin\theta \sin\phi \; \cos\theta]^T, \tag{3.5}$$

where λ is the wavelength of the propagating radio wave. The magnitude of the wavevector $k = |\mathbf{k}(\phi, \theta)| = 2\pi/\lambda$ is also known as the *wavenumber*. The inner product of the wavevector and the location vector of antenna n, $\mathbf{k}^T \mathbf{r}_n$, is the phase shift of the plane wave at the antenna relative to the origin of the coordinate system.

Fig. 3.1 illustrates an example of a 4-element reconfigurable antenna array with a plane wave impinging from the direction (ϕ, θ). The phase shift of the received signal at antenna n ($n = 1, 2, 3, 4$) is proportional to the projection of the corresponding antenna's location vector $\mathbf{r}_n$ upon the wave propagating direction *i.e.* $\mathbf{k}(\phi, \theta)^T \mathbf{r}_n$. The received amplitude at antenna n is weighted by $g_{p_n}(\phi, \theta)$, which is the corresponding 3-dimensional radiation pattern of the antenna.

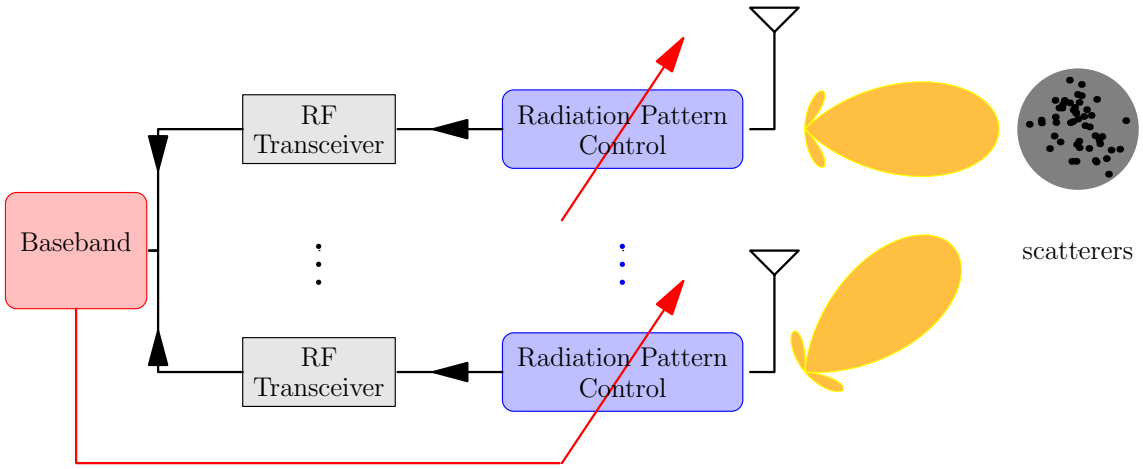

Figure 3.2 System model of PS-MIMO with reconfigurable antennas at the receiver side.

3.2 System Model of Pattern-Selection MIMO

Conventional MIMO systems are equipped with antennas which only provide fixed radiation patterns. A conventional MIMO system consisting of N_t transmit and N_r receive antennas is denoted by $[N_t, N_r]$. The input-output relation of the conventional MIMO system over block fading channels is given by

$$\mathbf{r} = \mathbf{H}\mathbf{s} + \mathbf{n} \tag{3.6}$$

where $\mathbf{r} \in \mathbb{C}^{N_r \times 1}$ is the received symbol vector and $\mathbf{s} \in \mathbb{C}^{N_t \times 1}$ is the transmitted symbol vector. $\mathbf{H} \in \mathbb{C}^{N_r \times N_t}$ is the MIMO channel transfer matrix, and $\mathbf{n} \in \mathbb{C}^{N_r \times 1}$ is the complex additive white Gaussian noise (AWGN) at the receiver.

Unlike conventional MIMO systems, a MIMO system equipped with pattern reconfigurable antennas at either or both the transmit and receive sides is defined by a *Pattern-Selection MIMO* (PS-MIMO) system. According to the deployed side(s) of the reconfigurable antennas, we classify PS-MIMO systems into three categories:

- Transmit pattern selection MIMO (TPS-MIMO), in which reconfigurable antennas are deployed at the transmit side only;
- Receive pattern selection MIMO (RPS-MIMO), in which reconfigurable antennas are deployed at the receive side only;
- Joint transmit and receive pattern selection MIMO (TRPS-MIMO), in which reconfigurable antennas are deployed at both the transmit and receive sides.

We use the following notation

$$[N_t|(P_{t,1}, P_{t,2}, \cdots, P_{t,N_t}); N_r|(P_{r,1}, P_{r,2}, \cdots, P_{r,N_r})]. \tag{3.7}$$

to represent a PS-MIMO system with N_t reconfigurable antennas at the transmitter and N_r reconfigurable antennas at the receiver.

The notation Eq. (3.7) means that the n_t-th ($n_t = 1, \ldots, N_t$) antenna in the transmit array has the capability to create P_{t,n_t} pattern states and the n_r-th ($n_r = 1, \ldots, N_r$) antenna in the receive array can create P_{r,n_r} pattern states. If the transmitter or the receiver uses identical reconfigurable antennas which has P_t or P_r pattern states, respectively, Eq. (3.7) is reduced to a simpler form given by

$$[N_t|P_t; N_r|P_r]. \tag{3.8}$$

With this notation, the $[N_t|1; N_r|1]$ PS-MIMO system is equivalent to the $[N_t; N_r]$ conventional MIMO system.

For a RPS-MIMO system, without loss of generality, it is convenient to assume that the reconfigurable antennas have identical radiation properties and each has P pattern states. We denote this RPS-MIMO system by $(N_t, N_r|P)$. Each combination of the pattern states of all reconfigurable receive antennas is called a *channel state*, denoted by ψ. For the sake of simplicity, we do not distinguish between the actual configuration of a channel state and the index of the channel state. In this case, we use a P-ary number with N_r digits to represent ψ by

$$\psi = (p_1 p_2 \cdots p_{N_r})_P \tag{3.9}$$

where p_{n_r} ($n_r \in \{1, 2, \ldots, N_r\}$) is the pattern state of the n_r-th receive antenna, *i.e.* , the index of the selected radiation pattern of receive antenna n. The universe set of the channel states of a PS-MIMO system is given by

$$\Psi = \{(p_1 p_2 \ldots p_{N_r})_P | p_1, p_2, \ldots, p_{N_r} \in \{1, 2, \ldots, P\}\}, \tag{3.10}$$

with its size $|\Psi| = P^{N_r}$.

With notations and assumptions introduced above, we can now present a general system model of RPS-MIMO systems:

$$\mathbf{r}(\psi) = \mathbf{H}(\psi)\mathbf{s} + \mathbf{n}(\psi), \qquad (\psi \in \Psi) \tag{3.11}$$

where $\mathbf{s}$ is the transmit symbol vector, ψ is a *channel state* selected from Ψ, and $\mathbf{H}(\psi)$, $\mathbf{r}(\psi)$ and $\mathbf{n}(\psi)$ are the channel transfer matrix, received vector and noise vector at the receiver corresponding to the configured channel state, respectively. It is straightforward to obtain similar models using a similar methodology for TPS-MIMO systems and TRPS-MIMO systems.

In Fig. 3.2, we illustrate a block diagram of TPS-MIMO system. Symbols for transmission are passed to the radio frequency circuits and transmitted to the free space by the reconfigurable antennas. The pattern states of the reconfigurable antennas are controlled by the baseband so that the radiation patterns are adapted to the instantaneous or long-term distribution of scatterers in the physical channel. The selection algorithm can be designed to maximize the instantaneous or ergodic channel capacity, to minimize the error rate or other criteria depending on system objectives.

Based on the channel state information (CSI) used by the selection algorithm, PS-MIMO systems can be classified into two categories:

- Instantaneous selection (IS): The selection algorithm switches the radiation patterns according to the instantaneous channel state information so that it achieves optimal performances at each channel snapshot.
- Statistical selection (SS): The selection algorithm determines the radiation patterns according to the long-term (statistical) channel state information so that it achieves better performance statistics (eg., average) over a large number of channel snapshots.

3.3 Modeling Pattern-Selection MIMO Channels

There are generally two major techniques to model multipath MIMO channels. One is the *deterministic* approach, which is also known as "ray-tracing". The deterministic approach models delays and complex gains of the propagating paths by parameters which describe the geometric positions of all antennas and scatterers in the propagation environment. By combining these path gains, we are able to generate channel matrices for further evaluation and simulations. The deterministic model is most useful for precisely evaluating system performances for a particular antenna system in a specific environment setup, without the need of performing measurement campaigns. The other is the *stochastic* approach, which generates channel matrix entries using predetermined statistics (eg., statistical distribution, mean and covariance) of sub-channel gains between antenna ports. The stochastic approach is faster and simpler in simulating channel matrices comparing to the deterministic approach but does not describe a specific environment. Some stochastic models are well structured and

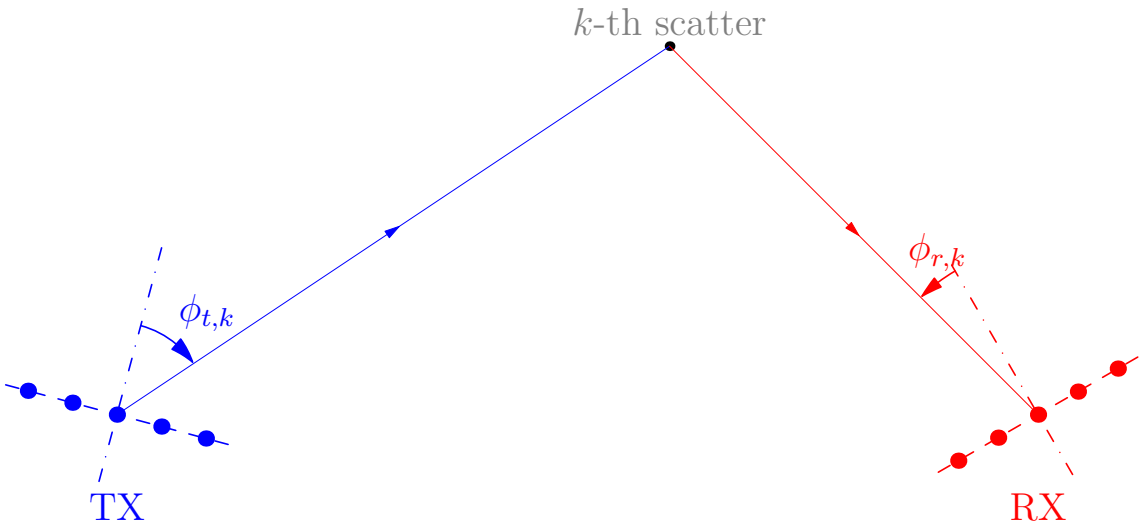

Figure 3.3 The top view of a MIMO channel in an indoor environment where multipath propagation in the elevation angle is assumed negligible. The multipath reflected by the k-th scatterer is shown in the figure, with $\phi_{t,k}$, the azimuth DoD, and $\phi_{r,k}$, the azimuth DoA, indicated, respectively.

tractable to obtain analytical results of system performances, which also enables insightful understanding of system designs.

Our thesis focuses on the analysis of pattern reconfigurable antennas in MIMO systems. Thus we need a channel model which is both geometrical and stochastic so that it can describe the spatial dispersion of the multipaths and is tractable to perform analytical analysis. In this section, firstly the *generic deterministic channel model* is introduced to model the channel directivity with directional channel response; secondly, the *generic stochastic channel model* is introduced to model the statistics of the channel matrices with the mean and auto/cross-correlation; thirdly, we introduce the *clustered channel model* to give a stochastic description of the MIMO channel with geometrical parameters, and discuss the relationship between the geometrical model and the stochastic model.

3.3.1 Deterministic Modeling

The most general deterministic model of MIMO channels is the *generic channel model* (GCM) proposed in [35]. The GCM distinguishes between the radio channel and the propagation channel. The latter is described by the *double-directional channel response*, excluding both the transmit and receive antennas, and the former is described by a non-directional channel response [35]. The GCM assumes K resolvable multipaths and describes how the multipaths, which are modeled by directions of departure (DoD) and directions of arrival (DoA), are

impacted by antenna configurations and the propagation channel separately. The effect of the propagation channel (the multipaths part) is described by the double-directional channel response, excluding the impact of both the transmit and receive antennas. The double-directional channel response is the superposition of the contributions of all multipath gains, which is given as following

$$h(\tau, \phi_r, \theta_r, \phi_t, \theta_t) = \sum_{k=1}^{K} \beta_k \delta(\tau - \tau_k)\delta(\phi_t - \phi_{t,k})\delta(\phi_r - \phi_{r,k})\delta(\theta_t - \theta_{t,k})\delta(\theta_r - \theta_{r,k}), \quad (3.12)$$

where $\tau, \phi_{t/r}, \theta_{t/r}$ are the delay, azimuth DoD/DoA, and elevation DoD/DoA, respectively, of the channel, β_k, τ_k, $\phi_{t/r,k}$ and $\theta_{t/r,k}$ are the complex gain, delay, azimuth DoD/DoA and elevation DoD/DoA, respectively, of the k-th multipath.

The impact of reconfigurable antenna arrays on impinging radio waves have been discussed in Section 3.1 and Section 3.2. Taking the antenna part into account, the channel matrix of a $(N_t|P_t, N_r|P_r)$ TRPS-MIMO system configured at the channel state (ψ_t, ψ_r) is modeled by concatenating the double channel response and the antennas:

$$\begin{aligned}\mathbf{H}(\tau; \psi_t, \psi_r) &= \int_{2\pi}\int_{2\pi}\int_{2\pi}\int_{2\pi} h(\tau, \phi_r, \theta_r, \phi_t, \theta_r)\mathbf{a}_r(\phi_r, \theta_r; \psi_r)\mathbf{a}_t(\phi_t, \theta_t; \psi_t)^T d\phi_t d\phi_r d\theta_t d\theta_r \\ &= \sum_{k=1}^{K} \beta_k \delta(\tau - \tau_k)\mathbf{a}_r(\theta_{r,k}, \phi_{r,k}; \psi_r)\mathbf{a}_t(\theta_{t,k}, \phi_{t,k}; \psi_t)^T, \end{aligned} \quad (3.13)$$

where ψ_t and ψ_r represent the reconfiguration parameters of the transmit and receive antenna array, $\mathbf{a}_t(\theta_t, \phi_t; \psi_t)$ and $\mathbf{a}_r(\theta_r, \phi_r; \psi_r)$ are the array response vectors of the reconfigurable transmit and receive array, with antenna geometry and radiation patterns included implicitly in the array response vectors as Eq. (3.3).

Throughout this thesis, our analysis focuses on the application of reconfigurable antennas in indoor propagation environments, where it is reasonable to assume that all radio waves propagate within the azimuthal plane and the elevation propagation is negligible, that is we will use the following assumption:

Assumption 3.1 (Azimuthal assumption)**.** *For indoor environments, all radio waves propagates in the azimuthal plane.*

The azimuthal assumption is verified by reported measurements that indoor multipath energy dispersion is very small in the vertical dimension and most of the energy is localized within the azimuthal plane. The reason is intuitive because the floor height is considerably smaller than the azimuthal size in most buildings [36]. In this case, the radiation pattern of a reconfigurable antenna at the pattern state p is written as $g_p(\phi)$. Fig. 3.3 illustrates the

generic spatial MIMO channel model in an indoor propagation environment. The multipath component corresponding to the k-th scatterer departs from the transmitter at azimuth angle $\phi_{t,k}$ and arrives at the receiver at azimuth angle $\phi_{r,k}$. In addition, we will also make the following assumption in the thesis regarding the independence of multipaths.

Assumption 3.2 (Uncorrelated scattering assumption)**.** *Radio waves that are coming at different directions are uncorrelated. [37]*

According to the azimuthal assumption and the uncorrelated scattering assumption, the channel matrix of a TRPS-MIMO configured at the channel state (ψ_t, ψ_r) in Eq. (3.13) reduces to

$$\mathbf{H}(\psi_t;\psi_r) = \sum_{k=1}^{K} \beta_k \mathbf{a}_r(\phi_{r,k};\psi_r)\mathbf{a}_t^T(\phi_{t,k};\psi_t), \quad \text{(where } \psi_t \in \Psi_t \text{ and } \psi_r \in \Psi_r\text{)} \tag{3.14}$$

For a $(N_t; N_r|P_r)$ RPS-MIMO system, the transmit array response is $\mathbf{a}_t(\phi_t)$ since the transmit antennas are non-reconfigurable. Therefore, the channel matrix of the RPS-MIMO in which the receive antenna array is configured to ψ_r is written as

$$\mathbf{H}(;\psi_r) = \sum_{k=1}^{K} \beta_k \mathbf{a}_r(\phi_{r,k};\psi_r)\mathbf{a}_t^T(\phi_{t,k};). \tag{3.15}$$

Similarly, the channel matrix of a $(N_t|P_t; N_r)$ TPS-MIMO system configured to ψ_t is

$$\mathbf{H}(\psi_t;) = \sum_{k=1}^{K} \beta_k \mathbf{a}_r(\phi_{r,k};)\mathbf{a}_t^T(\phi_{t,k};\psi_t). \tag{3.16}$$

Selecting from the Channel Generating Matrix

From Eq. (3.14) to Eq. (3.16), the channel matrix of the PS-MIMO system is generated with the selected array response vector(s). We will now consider a virtual MIMO system, in which each pattern state of the reconfigurable antenna assumes a distinct virtual antenna. That is we consider a virtual MIMO system with virtual antennas consisting of all possible pattern states of the reconfigurable antennas. The channel matrix of this virtual MIMO is denoted by $\mathbf{H}_G$. Similar to Eq. (3.14), the virtual channel matrix $\mathbf{H}_G$ of a TRPS-MIMO system modeled by the GCM is

$$\mathbf{H}_G = \sum_{k=1}^{K} \beta_k \tilde{\mathbf{a}}_r(\phi_{r,k})\tilde{\mathbf{a}}_t^T(\phi_{t,k}). \tag{3.17}$$

In this case, in order to obtain the real specific PS-MIMO channel matrix, we can generate $\mathbf{H}_G$ first and then select a submatrix of $\mathbf{H}_G$ according to the configured channel state of the PS-MIMO. $\mathbf{H}_G$ is therefore referred to as the *channel generating matrix* of a PS-MIMO channel snapshot.

For a TRPS-MIMO channel, $\mathbf{H}(\psi_t;\psi_r) \in \mathbb{C}^{N_r \times N_t}$ denotes the channel matrix of a channel snapshot at the channel state $(\psi_t;\psi_r)$. $\mathbf{H}(\psi_t;\psi_r)$ is generated by selecting a $N_r \times N_t$ submatrix from the generating channel matrix $\mathbf{H}_G$ according to the enumerating digits in ψ_t and ψ_r as defined in Eq. (3.9).

Selecting the array response of the PS-MIMO according to the array state is described as follows

$$\mathbf{a}_q(\phi_q;\psi_q) = \mathbf{S}_q(\psi_q)\tilde{\mathbf{a}}_q(\phi_q), \quad (q \in \{t,r\})$$

where $\tilde{\mathbf{a}}_q(\phi_q) \in \mathbb{C}^{P_q N_q}$ is the array response vector of the virtual MIMO system and $\mathbf{S}_q(\psi_q)$ is a $N_q \times P_q N_q$ selection matrix which selects N_q rows from $\tilde{\mathbf{a}}_q(\phi_q)$ by the indexing digits in ψ_q. We construct $\tilde{\mathbf{a}}_q(\phi_q)$ by

$$\tilde{\mathbf{a}}_q(\phi_q) = \mathrm{vec}\left(\begin{bmatrix} \mathbf{a}_q(\phi_q;1)^T \\ \mathbf{a}_q(\phi_q;2)^T \\ \vdots \\ \mathbf{a}_q(\phi_q;P_q)^T \end{bmatrix}\right), \qquad (q \in \{t,r\})$$

and construct $\mathbf{S}_q(\phi_q)$ by

$$\mathbf{S}_q(\psi_q) = \begin{bmatrix} \mathbf{e}_{p_1}^T & \mathbf{0} & \cdots & \mathbf{0} \\ \mathbf{0} & \mathbf{e}_{p_2}^T & \mathbf{0} & \vdots \\ \vdots & \mathbf{0} & \ddots & \mathbf{0} \\ \mathbf{0} & \cdots & \mathbf{0} & \mathbf{e}_{p_{N_q}}^T \end{bmatrix}, \qquad (q \in \{t,r\}) \tag{3.18}$$

where $\mathbf{e}_{p_{n_q}}$ is a standard P_q-dimensional orthogonal basis with 1 at the p_{n_q}-th dimension $(n_q = 1,\ldots,N_q)$. Therefore, the n_q-th row of $\mathbf{S}_q(\phi_q)$ extracts the $P_q(n_q-1)+p_{n_q}$-th row of $\tilde{\mathbf{a}}_q(\phi_q)$, which corresponds to pattern state p_{n_q} of the n_q-th antenna.

The channel matrix for a given channel state is straightforward to obtain by selecting the corresponding submatrix from the channel generating matrix $\mathbf{H}_G$. For a $(N_t|P_t;N_r|P_r)$ TRPS-MIMO system (double-sided) at the channel state $(\psi_t;\psi_r)$, the channel matrix is

selected by applying the selection matrix Eq. (3.18) to the channel generating matrix as

$$\mathbf{H}(\psi_t;\psi_r) = \mathbf{S}_r(\psi_r)\mathbf{H}_G\mathbf{S}_t(\psi_t)^T. \tag{3.19}$$

For illustration purpose, let's look at a $(N_t; N_r|P_r)$ RPS-MIMO system. The channel generating matrix for this system using the GCM is

$$\mathbf{H}_G = \sum_{k=1}^{K} \beta_k \tilde{\mathbf{a}}_r(\phi_{r,k})\mathbf{a}_t^T(\phi_{t,k}), \tag{3.20}$$

which is a $P_rN_r \times N_t$ matrix as follows

$$\mathbf{H}_G = \begin{bmatrix} H_G(1,1) & \cdots & H_G(1,N_t) \\ \vdots & \ddots & \vdots \\ H_G(P_r,1) & \cdots & H_G(P_r,N_t) \\ H_G(P_r+1,1) & \cdots & H_G(P_r+1,N_t) \\ \vdots & \ddots & \vdots \\ H_G(2P_r,1) & \cdots & H_G(2P_r,N_t) \\ \vdots & & \vdots \\ H_G(P_rN_r-P_r+1,1) & \cdots & H_G(P_rN_r-P_r+1,N_t) \\ \vdots & \ddots & \vdots \\ H_G(P_rN_r,1) & \cdots & H_G(P_rN_r,N_t) \end{bmatrix}. \tag{3.21}$$

$\mathbf{H}_G$ is constructed by sequentially stacking P_rN_r row vectors of dimension N_t, which correspond to channel coefficients between the transmit antennas and the receive antennas with all possible pattern states. $H_G(m,n)$, the (m,n)-th entry of $\mathbf{H}_G$, represents the complex gain from the n-th transmit antenna to the $\lceil \frac{m}{P_r} \rceil$-th reconfigurable receive antenna which is configured to the pattern state $(m-1 \mod P_r)+1$.

The channel matrix of the RPS-MIMO configured at the channel state $(;\psi_r)$ is generated by applying the selection matrix at the receiver side, i.e.,

$$\mathbf{H}(;\psi_r) = \mathbf{S}_r(\psi_r)\mathbf{H}_G. \tag{3.22}$$

For each channel snapshot, the RPS-MIMO selects N_tN_r subchannel coefficients out of $N_tN_rP_r$ channel coefficients candidates to form a channel matrix $\mathbf{H}(;\psi_r)$ at the channel state $(;\psi_r)$.

3.3.2 Stochastic Modeling

As discussed earlier, it is desirable to model the channel matrix entries with multivariate probability distribution for analytical performance assessment. Based on measurements and for simplicity, many MIMO channel models assume that the MIMO channel matrix follows a multivariate complex Gaussian distribution.

Stack columns of the channel matrix $\mathbf{H}_G \in \mathbb{C}^{N_r P \times N_t}$ and we get a PN_tN_r-dimensional complex vector

$$\mathbf{h}_G = \mathrm{vec}\left(\mathbf{H}_G\right). \tag{3.23}$$

The correlation matrix of $\mathbf{h}_G$ is defined by

$$\mathbf{R}_G = \mathbb{E}\left[\mathbf{h}_G \mathbf{h}_G^H\right], \tag{3.24}$$

which is also termed as correlation generating matrix of the channel generating matrix $\mathbf{H}_G$.

For Rayleigh fading channels, the probability distribution of the channel matrix is determined by the correlation (covariance) matrix $\mathbf{R}_G$ only, *i.e.*

$$\mathbf{h}_G \sim \mathcal{CN}(\mathbf{0}, \mathbf{R}_G). \tag{3.25}$$

The probability density function (PDF) of the zero-mean $\mathbf{h}_G$ is

$$f_{\mathbf{h}_G}(\mathbf{x}) = \frac{1}{\pi^{PN_tN_r} \det(\mathbf{R}_G)} e^{-\mathbf{x}^H \mathbf{R}_G^{-1} \mathbf{x}}. \tag{3.26}$$

where the correlation generating matrix $\mathbf{R}_G$ can be any semi-positive definite matrix.

We generate the Rayleigh faded channel matrix $\mathbf{H}$ by

$$\mathbf{H}_G = \mathrm{unvec}\left(\mathbf{R}_G^{1/2} \mathbf{w}\right) \tag{3.27}$$

where $\mathbf{w}$ is a complex zero-mean Gaussian independent identically distributed (i.i.d.) vector with unit variance and has the same dimension as $\mathbf{h}_G$, $\mathbf{R}_G^{1/2}$ is the matrix square root of $\mathbf{R}_G$, and $\mathrm{unvec}\left(\cdot\right)$ is an inverse operation of $\mathrm{vec}\left(\cdot\right)$ and transforms a vector into a matrix.

For a statistically modeled TRPS-MIMO Rayleigh fading channel, the channel matrix selected by the channel state $(\psi_t; \psi_r)$ is given from Eq. (3.19) and Eq. (3.27) by

$$\mathbf{H}(\psi_t; \psi_r) = \mathrm{unvec}\left(\mathbf{S}_t(\psi_t) \otimes \mathbf{S}_r(\psi_r)^T \cdot \mathbf{R}_G^{1/2} \mathbf{w}\right). \tag{3.28}$$

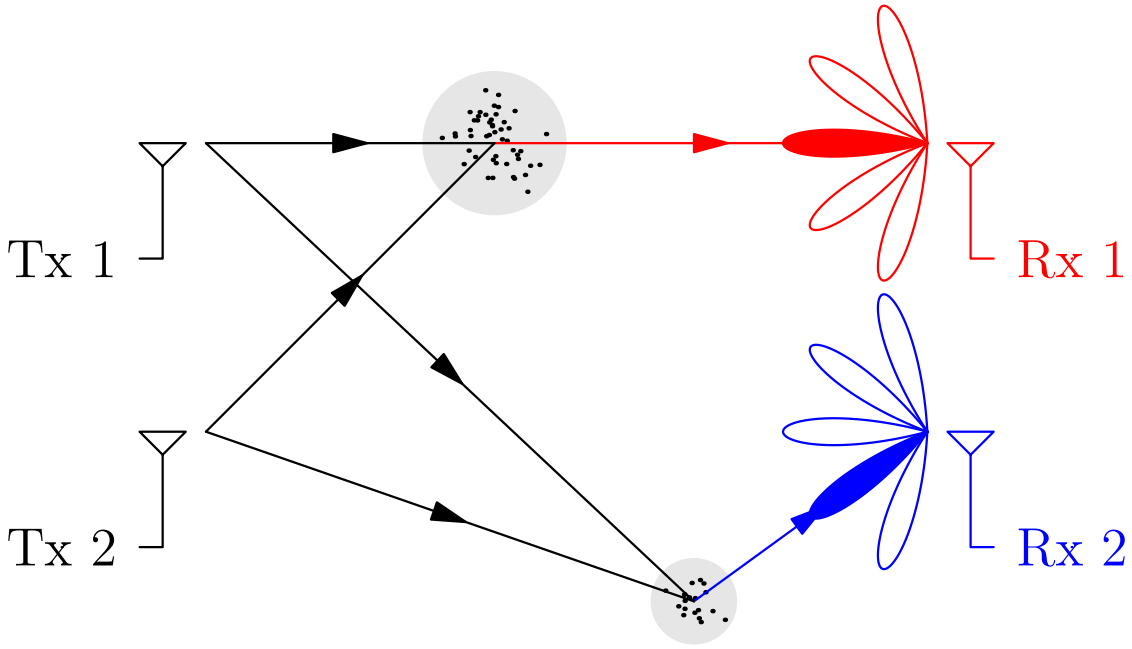

Figure 3.4 A cluster-based channel. Clusters are decomposed into a number of resolvable multipath components and can be viewed differently at either link-end.

In this case, modeling the Rayleigh faded channel $\mathbf{H}$ from the stochastic perspective is equivalent to modeling the statistics of the correlation generating matrix $\mathbf{R}_G$. Applying some further assumptions to the structure of the total correlation matrix, $\mathbf{R}_G$, usually lead to a simpler expression for $\mathbf{H}_G$. The first proposed stochastic MIMO channel model simply assumes $\mathbf{R}_G = \mathbf{I}_{N_t N_r}$,*i.e.* , uncorrelated paths among antennas and reconfiguration states. Another popular stochastic model is the Kronecker model, assuming separable correlation between the transmitter and the receiver. Other models, such as the Weichselberger model and the virtual channel representation, use more complicated correlation structures.

3.3.3 Clustered Channel Models

The GCM does not indicate how to compute multipath component parameters (the gain, delay, DoA and DoD of the subpath). They can be numerically calculated by ray-tracing techniques with electromagnetic (EM) methods such as the finite-difference time domain (FDTD) method and the method of moments (MoM). EM methods require complete description of all scatterers and antenna elements in the propagation environments, including their geometries and EM properties. The ray-tracing model presents physical aspects of a real-world MIMO channel. Because of its deterministic nature and heavy computational burden, the ray-tracing model is not suitable for system level evaluation. To overcome this

disadvantage, clustered channel models have been proposed and will now be considered.

Unlike ray-tracing models, cluster models do not characterize the channel by modeling the behavior of each multipath. Instead, multipath components are grouped into clusters according to their stochastic spatial similarity. Within each cluster, the DoD's and DoA's of intra-cluster multipath components are considered identically distributed and characterized by the mean angle, the angular spread and the power strength of the cluster.

Clustered channel models describe MIMO channels from a perspective which is geometrical as well as statistical. First, cluster models are statistical because the multipath components are characterized by probability distributions. Second, cluster models are also geometrical and reflect real channels since the parameters of the probability distributions are extracted from measured data.

The first clustered channel model is the Saleh-Valenzuela model (SVM) which groups multipath component in clusters by time arrivals. Clustering in the angular domain both at the transmit and receive side is introduced by the extended SVM (E-SVM) [38] [39]. These clustered channel models assume that multipath component parameters at different directions are independent of each other and can be generated by certain probability distributions. The random cluster model (RCM) use a joint multivariate probability density function to characterize the channel statistics [40]. Among these models, the RCM is the most accurate but complex one.

Bridging the Gap

It would be desirable to describe the statistics of subchannel gains between antenna ports with the distribution of multipath parameters. In order to bridge this gap, the *clustered MIMO channel models* is proposed with assumptions that the multipath parameters follow some certain distributions. The clustered channel model was first proposed by Saleh and Valenzuela who observed that multipaths can be grouped into clusters by similar time delay [41]. It was extended by Spencer to the space domain at the receiver [38], and Czink verifies that spatial clustering also applies at the transmitter side [39].

For a narrowband $(N_t, P_t; N_r, P_r)$ PS-MIMO system in the indoor environment, we derive the generating channel matrix $\mathbf{H}_G \in \mathbb{C}^{N_r P_r \times N_t P_t}$ based on Eq. (3.14). We can extend the expression with radiation patterns of antenna elements taken into account and rewrite the channel matrix as

$$\mathbf{H}_G = \frac{1}{\sqrt{K}} \sum_{k=1}^{K} \beta_k \tilde{\mathbf{a}}_r(\phi_{r,k}) \tilde{\mathbf{a}}_t^T(\phi_{t,k}). \tag{3.29}$$

Over Rayleigh narrowband fading channels, the channel generating matrix is statistically described by

$$\mathbf{H}_G \sim \mathcal{CN}(\mathbf{0}, \mathbf{R}_G).$$

In order to establish the relationship between the geometrical description and the stochastic description, the multipath component parameters β_k, $\phi_{t,k}$ and $\phi_{r,k}$ are assumed random variables which follow some given probability distributions. In this case, the correlation generating matrix $\mathbf{R}_G$ is determined by the statistics of the multipath components as follows

$$\begin{aligned}
\mathbf{R}_G &= \mathbb{E}\Big[\mathbf{h}_G \mathbf{h}_G^H\Big] \\
&= \mathbb{E}\left[\frac{1}{K}\mathrm{vec}\left(\sum_{k=1}^{K}\beta_k \tilde{\mathbf{a}}_r(\phi_{r,k})\tilde{\mathbf{a}}_t(\phi_{t,k})^T\right)\mathrm{vec}\left(\sum_{k'=1}^{K}\beta_{k'} \tilde{\mathbf{a}}_r(\phi_{r,k'})\tilde{\mathbf{a}}_t(\phi_{t,k'})^T\right)^H\right] \\
&= \mathbb{E}\left[\frac{1}{K}\sum_{k=1}^{K}\sum_{k'=1}^{K}\beta_k\beta_{k'}^*[\tilde{\mathbf{a}}_t(\phi_{t,k})\otimes\tilde{\mathbf{a}}_r(\phi_{r,k})][\tilde{\mathbf{a}}_t(\phi_{t,k'})^H\otimes\tilde{\mathbf{a}}_r(\phi_{r,k'})^H]\right].
\end{aligned} \tag{3.30}$$

Assuming the multipath component gains β_l are independent, we rewrite $\mathbf{R}_G$ as

$$\begin{aligned}
\mathbf{R}_G &= \mathbb{E}\left[\frac{1}{K}\sum_{k=1}^{K}|\beta_k|^2[\tilde{\mathbf{a}}_t(\phi_{t,k})\otimes\tilde{\mathbf{a}}_r(\phi_{r,k})][\tilde{\mathbf{a}}_t(\phi_{t,k})^H\otimes\tilde{\mathbf{a}}_r(\phi_{r,k})^H]\right] \\
&= \mathbb{E}\left[\frac{1}{K}\sum_{k=1}^{K}|\beta_k|^2[\tilde{\mathbf{a}}_t(\phi_{t,k})\tilde{\mathbf{a}}_t(\phi_{t,k})^H]\otimes[\tilde{\mathbf{a}}_r(\phi_{r,k})\tilde{\mathbf{a}}_r(\phi_{r,k})^H]\right].
\end{aligned} \tag{3.31}$$

The last equation of Eq. (3.31) is obtained by the mixed-product property of the Kronecker product. We assume that the complex path gains have zero mean and unit variance. When K, the number of the multipath components, are large enough, Eq. (3.31) becomes a double integral which is written as

$$\mathbf{R}_G = \int_{2\pi}\int_{2\pi} PAS(\phi_t,\phi_r)\cdot\Big[\tilde{\mathbf{a}}_t(\phi_t)\tilde{\mathbf{a}}_t^H(\phi_t)\Big]\otimes\Big[\tilde{\mathbf{a}}_r(\phi_r)\tilde{\mathbf{a}}_r^H(\phi_r)\Big]\,d\phi_t d\phi_r \tag{3.32}$$

where $PAS(\phi_t,\phi_r)$ is known as the double-side *power angular spectrum* (PAS), which is the joint PDF of the DoD and the DoA, satisfying

$$\int_{2\pi}\int_{2\pi} PAS(\phi_t,\phi_r)\,d\phi_t d\phi_r = \lim_{K\to\infty}\mathbb{E}\left[\frac{1}{K}\sum_{k=1}^{K}|\beta_k|^2\right] = 1.$$

Thus, the relationship between the geometric description and the stochastic description is established if and only if the double-side PAS is known.

Clustered Channels

PAS, the DoA-DoD joint power dispersion, can be attributed to the geometric distribution of the scatterers in the propagation environment. [38] and [39] found that the power of multipath components is distributed in clusters, both in the delay domain and in the angular domain. Based on the narrowband asumption and the azimuth assumption, the temporal multipaths are unresolvable and the spatial dispersion along the elevation direction angle is neglected. For a L-cluster multipath channel with K subpaths in each cluster, the double-directional channel response of Eq. (3.12) is rewritten as the weighted sum of the double-directional channel response of each individual cluster [42]

$$h(\phi_t, \phi_r) = c \sum_{l=1}^{L} \sqrt{w_l} h_l(\phi_t, \phi_r) \tag{3.33}$$

where c is a constant power factor, w_l is the power weight of the l-th cluster which satisfy $\sum_{l=1}^{L} w_l = 1$. The double-directional channel response of cluster l

$$h_l(\phi_t, \phi_r) \;=\; \frac{1}{\sqrt{K}} \sum_{k=1}^{K} \beta_k^{(l)} \delta(\phi_t - \phi_{t,k}^{(l)}) \delta(\phi_r - \phi_{r,k}^{(l)}), \tag{3.34}$$

where $\beta_k^{(l)}$, $\phi_{t,k}^{(l)}$ and $\phi_{r,k}^{(l)}$ are the normalized complex gain, the DoD and the DoA at the k-th subpath of the l-th cluster, respectively.

Kronecker Model of PS-MIMO Channels

Recent indoor channel measurement [38] by Spencer measured the PAS's at the transmit and receive side separately so that the separable assumption was inherently assumed. The measurement demonstrated that the marginal probability distribution of the DoD's/DoA's within a cluster can be closely modeled by the Laplace distribution, which is given by

$$f_{\mathcal{L}}(\phi; \bar{\phi}, \sigma) = \begin{cases} \frac{\beta}{\sqrt{2}\sigma} e^{-\sqrt{2}|\phi - \bar{\phi}|/\sigma} & \text{if } \phi \in [-\pi, \pi), \\ 0 & \text{others.} \end{cases} \tag{3.35}$$

where ϕ is the DoA/DoD of the random paths over azimuth plane, ϕ_c is the mean DoA/DoD of the cluster, σ_c is the standard deviation of the PAS, i.e., the angle spread (AS) of the cluster, and $\beta = 1/\left(1 - e^{-\sqrt{2}\pi/\sigma_c}\right)$ normalizes the PAS so that $\int_{-\pi}^{\pi} f_{\mathcal{L}}(\phi; \bar{\phi}, \sigma) d\phi = 1$.

For a spatial channel with L clusters, the multipath components of each cluster are characterized by the same type of probability distribution. Regarding the multipath component directions within the l-th cluster, [38] verified that the DoD's $\phi_{t,k}^{(l)}$ and DoA's $\phi_{r,k}^{(l)}$ are

distributed around the mean DoD $\bar{\phi}_t^{(l)}$ and the mean DoA $\bar{\phi}_r^{(l)}$ of the l-th cluster. In [38], the PAS at the transmitter and receiver side are the weighted sums of Eq. (3.35), *i.e.*

$$PAS_q(\phi_q) = \sum_{l=1}^{L} p^{(l)} f_{\mathcal{L}}(\phi; \bar{\phi}_q^{(l)}, \bar{\sigma}_q^{(l)}), \qquad (q \in \{t, r\}) \tag{3.36}$$

where the $\bar{\phi}_q^{(l)}, \sigma_q^{(l)}$, and $p^{(l)}$ are the mean angle, angular spread and normalized power of the l-th cluster, respectively.

Since the DoD's are assumed independent of the DoA's, the joint power azimuth spectrum $PAS(\phi_t, \phi_r)$ is separable as

$$PAS(\phi_t, \phi_r) = PAS_t(\phi_t) PAS_r(\phi_r), \tag{3.37}$$

where $PAS_t(\phi_t)$ and $PAS_r(\phi_r)$ are the marginal PAS observed at the transmitter and receiver side, respectively. The separable assumption leads to a Kronecker product structure of the channel correlation matrix. Substituting Eq. (3.37) into Eq. (3.32), we can now re-write the correlation generating matrix Eq. (3.32) of the full virtual MIMO system in the form of a Kronecker product as

$$\begin{aligned} \mathbf{R}_G &= \left[\int_{2\pi} \int_{2\pi} \tilde{\mathbf{a}}_t(\phi_t) \tilde{\mathbf{a}}_t^H(\phi_t) PAS_t(\phi_t) d\phi_t \right] \otimes \left[\int_{2\pi} \int_{2\pi} \tilde{\mathbf{a}}_r(\phi_r) \tilde{\mathbf{a}}_r^H(\phi_r) PAS_r(\phi_r) d\phi_r \right] \\ &= \tilde{\mathbf{R}}_t \otimes \tilde{\mathbf{R}}_r, \end{aligned} \tag{3.38}$$

where

$$\begin{aligned} \tilde{\mathbf{R}}_t &= \int_{2\pi} \int_{2\pi} \tilde{\mathbf{a}}_t(\phi_t) \tilde{\mathbf{a}}_t^H(\phi_t) PAS_t(\phi_t) d\phi_t \\ \tilde{\mathbf{R}}_r &= \int_{2\pi} \int_{2\pi} \tilde{\mathbf{a}}_r(\phi_r) \tilde{\mathbf{a}}_r^H(\phi_r) PAS_r(\phi_r) d\phi_r \end{aligned} \tag{3.39}$$

are the normalized covariance matrices at the transmit and receive side, respectively.

We can now generate channel matrices for TRPS-MIMO systems using the Kronecker model. First we obtain the correlation generating matrix $\mathbf{R}_G$ of the Kronecker model by Eq. (3.38) with given cluster parameters. Then we get the channel generating matrix by

$$\mathbf{H}_G = \tilde{\mathbf{R}}_r^{1/2} \mathbf{W}_G \tilde{\mathbf{R}}_r^{T/2} = \text{unvec}\left(\left(\tilde{\mathbf{R}}_t \otimes \tilde{\mathbf{R}}_r \right)^{1/2} \mathbf{w}_G \right). \tag{3.40}$$

In the next, we select the Kronecker modeled TPRS-MIMO channel matrix by Eq. (3.19). And for RPS-MIMO channels used in future chapters, we modify the correlation generating matrix and the channel generating matrix accordingly, and select the channel matrix by

Eq. (3.22).

Sum-Kronecker Model of PS-MIMO Channels

The Kronecker model assumes that the multipath DoD's and DoA's are independent so that the joint PAS of the Kronecker model is the product of the marginal PAS's at the transmit side and at the receive side. This assumption means that each multipath arriving at a specific cluster at the transmitter side is independently reflected to any other cluster seen by the receiver side. However, in real scattering environments, the DoD and DoA of each multipath is associated with a specific scatterer, contradicting the independence assumption presumed by the Kronecker model. This deficiency of the Kronecker model has been observed in [43] and it was shown that the Kronecker model produces non-existent phantom clusters which lies at the intersections of the DoD's and DoA's of real clusters by forcing the joint PAS to be separable. Fig. 3.5 illustrates *the joint Capon spectrum*[1] of a two-cluster channel observed by a 4×4 MIMO system. The joint spectrum shown in Fig. 3.5(a) is estimated by the Kronecker model, which introduces two phantom clusters. As discussed in [43], it has been found that the Kronecker model tends to underestimate the true channel capacity and overestimate the diversity order. The reason is that the Kronecker model introduces non-existent clusters and multipaths. Though the Kronecker model has these deficiencies, it is still favored by many researchers because of the tractability of the Kronecker product structure. In our thesis, we also accept the Kronecker model in cases of analyzing the system performances of channel capacity and detection error rates.

As aforementioned, the resulted modeling error is an alarm against assuming the Kronecker model in evaluating channel capacity and detection error rate for high resolution MIMO systems, including high dimensional antenna arrays and reconfigurable MIMO with highly directive radiation patterns. For a PS-MIMO system equipped with reconfigurable antennas at both sides, the problem becomes even worse. If the Kronecker model is used in simulations, when the reconfigurable transmit antennas and the reconfigurable receive antennas are steered to a phantom cluster, it will definitely result in a transmission failure. For this reason, we propose a novel channel model, the *sum-Kronecker model*, which complies

[1]The joint DoD-DoA Capon spectrum of a MIMO system over Rayleigh fading channels with respect to the correlation matrix $\mathbf{R}$ is defined by

$$P_{Capon}(\phi_t, \phi_r; \mathbf{R}) = \frac{1}{(\mathbf{a}_t(\phi_t) \otimes \mathbf{a}_r(\phi_r))^H \mathbf{R}^{-1} (\mathbf{a}_t(\phi_t) \otimes \mathbf{a}_r(\phi_r))},$$

where $\mathbf{R}$ is positive definite.

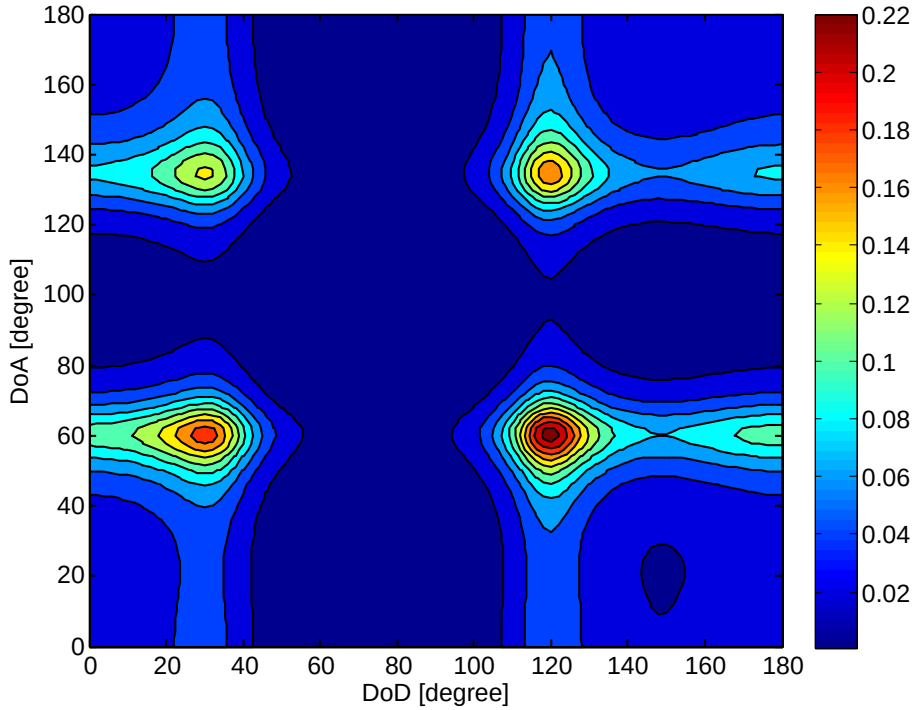

(a) Joint DoD-DoA Capon spectrum generated by the Kronecker model. The Kronecker model introduces two phantom clusters at $(30°, 60°)$ and $(120°, 135°)$, which are the intersections of the real clusters.

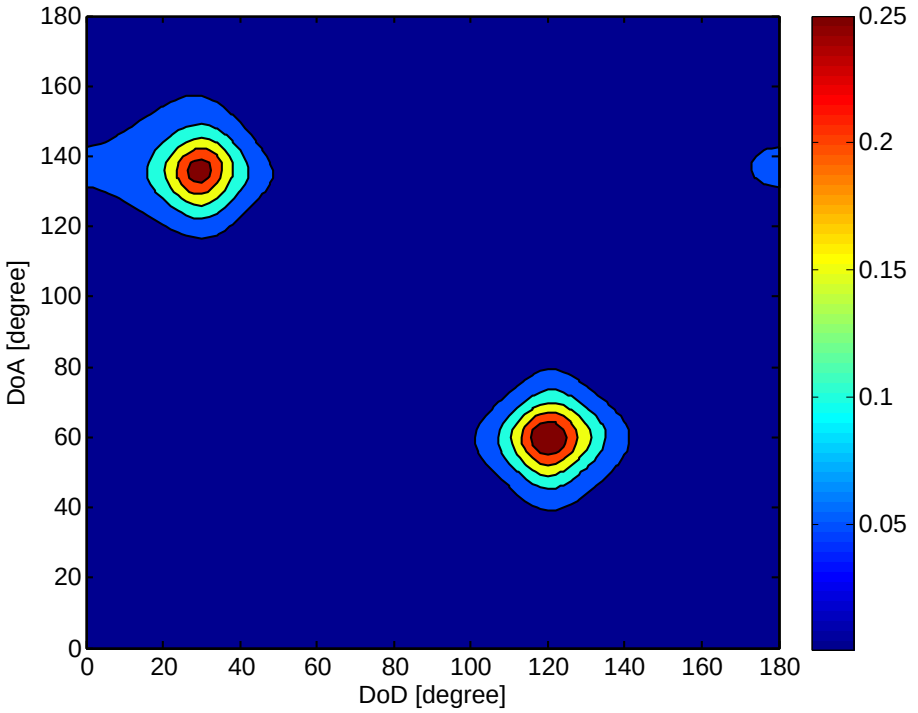

(b) Joint DoD-DoA Capon spectrum generated by the sum-Kronecker model.

Figure 3.5 A two-cluster channel with the first cluster at $(30°, 135°)$ and the second cluster at $(120°, 60°)$. Both clusters have the same power. The angular spread of each cluster at either the TX or the RX side is $10°$. These two subfigures illustrate the joint Capon spectrum simulated by a 4×4 MIMO system with half-wavelength spaced ULA at both sides.

with the cluster positions of the joint PAS. Recall that the joint correlation matrix is

$$\mathbf{R}_G = \int_{2\pi}\int_{2\pi} PAS(\phi_t, \phi_r) \cdot \left[\tilde{\mathbf{a}}_t(\phi_t)\tilde{\mathbf{a}}_t^H(\phi_t)\right] \otimes \left[\tilde{\mathbf{a}}_r(\phi_r)\tilde{\mathbf{a}}_r^H(\phi_r)\right] d\phi_t d\phi_r.$$

Unlike the Kronecker model which applies the separable assumption to the multipath DoD's and DoA's globally, we restrict the separable assumption for the intra-cluster DoD's and DoA's to avoid phantom clusters. We assume that the joint DoD-DoA power angular spectrum $PAS(\phi_t, \phi_r)$ of a L-cluster channel is the weighted superposition as follows

$$PAS(\phi_t, \phi_r) = \sum_{l=1}^{L} p^{(l)} PAS^{(l)}(\phi_t, \phi_r), \tag{3.41}$$

where $PAS^{(l)}(\phi_t, \phi_r)$ is the normalized joint PAS of the l-th cluster. Similar to the Kronecker model, we assume that the multipaths within each cluster are independent and also follow the Laplace distribution:

$$PAS^{(l)}(\phi_t, \phi_r) = f_{\mathcal{L}}(\phi_t; \bar{\phi}_t^{(l)}, \sigma_t^{(l)}) f_{\mathcal{L}}(\phi_r; \bar{\phi}_r^{(l)}, \sigma_r^{(l)}), \tag{3.42}$$

where $\bar{\phi}_t^{(l)}$ and $\sigma_t^{(l)}$ are the mean angle and angular spread of the l-th cluster at the transmit side, and $\bar{\phi}_r^{(l)}$ and $\sigma_r^{(l)}$ are the mean angle and angular spread of the l-th cluster at the receive side.

$$\mathbf{H}_G = \text{unvec}\left(\left(\sum_{l=1}^{L} p^{(l)} \mathbf{R}_t^{(l)} \otimes \mathbf{R}_r^{(l)}\right)^{1/2} \mathbf{w}\right), \tag{3.43}$$

or

$$\mathbf{H}_G = \sum_{l=1}^{L} p^{(l)} (\mathbf{R}_r^{(l)})^{1/2} \mathbf{W}_l (\mathbf{R}_r^{(l)})^{T/2}. \tag{3.44}$$

In the next, we select the TPRS-MIMO channel matrix from the channel generating matrix of the sum-Kronecker model by Eq. (3.19). And for RPS-MIMO channels used in future chapters, we modify the correlation generating matrix and the channel generating matrix accordingly, and select the channel matrix with the Kronecker model by Eq. (3.22).

The sum-Kronecker model is the limit of the multipath model in rich scattering environments with large number of scatterers. And it also well approximates the curve of the multipath model when the number of the scatterers is as low as 20. It is also worth mentioning that the proposed sum-Kronecker model is different from the Kronecker model constructed

by Weichselberger [44]. Though both channel models expand the correlation matrix into a sum of a series of Kronecker products, the Kronecker modes of Weichselberger's model decompose the correlation matrix in the eigenspace while the sum-Kronecker model proposed in this thesis decomposes the joint correlation in the angular domain.

3.4 Chapter Summary

In this chapter, we have presented the fundamentals of PS-MIMO communication systems with pattern reconfigurable antennas. The reconfigurability of antenna radiation patterns plays a significant role in optimizing capacity and reliability of the system.

A short introduction to reconfigurable antennas and reconfigurable antenna arrays have been included in this chapter. The mathematical representations of the pattern reconfigurable antenna and the reconfigurable antenna array defined in Eq. (3.1) and Eq. (3.3) will be used throughout this thesis. The system model of PS-MIMO has been introduced. Concerning channel modeling for PS-MIMO, two PS-MIMO channel models based on spatial clustering have been described in this chapter. The Kronecker PS-MIMO channel model will be used in Chapter 5, Chapter 6 to study the channel capacity and error rate performances of PS-MIMO systems. The sum-Kronecker PS-MIMO channel model will be used in Chapter 4 to study the estimation of the channel cluster parameters with reconfigurable antenna arrays.

CHAPTER 4

ESTIMATING PARAMETERS OF CLUSTER CHANNELS FOR RECONFIGURABLE ANTENNA ARRAYS

In Chapter 5 and Chapter 6, we will quantitatively analyze the capacity or reliability performance of PS-MIMO systems based on the knowledge of the spatial channels and the reconfigurability of the dynamic antenna elements. For the IPS-MIMO, full channel state information, i.e., the channel matrices for every possible radiation pattern configuration, are required. For the SPS-MIMO, the statistics of the MIMO channels for every possible pattern configuration are required. Therefore, estimating channel parameters of PS-MIMO channels is crucial. In this chapter, we focus on how to estimate the long-term statistics of the spatial channel, i.e., the mean angles and angular spreads of the spatial clusters. The pattern state is selected based on long-term statistics such as the covariance matrix. We propose to estimate the receiver side PAS of the propagation paths instead of to estimate covariance matrices $\mathbf{R}(\psi)$ for all possible channel state configurations ψ. In addition, we propose to investigate if reconfigurable array systems can improve the estimation accuracy comparing to conventional systems. When the number of radiation patterns is too large, estimating all possible instantaneous channel realizations is very time consuming and not applicable, because we have to correlate received signals from all antenna ports with all possible radiation patterns. In order to overcome this difficulty, we propose that we estimate the power angular spectrum (PAS) of the propagation paths instead of estimating the covariance matrices $\mathbf{R}(\psi)$ (where $\psi \in \Psi$). This proposal is based on the observation that the covariance matrix $\mathbf{R}$ is determined by radiation patterns, antenna spacing, and PAS.

The problem of estimating all $\mathbf{R}(\psi)$ is converted to estimating $PAS(\phi)$. Since the PS-MIMO system works in the context of clustered channels, $PAS(\phi)$ can thus be parameterized as $PAS(\phi;\eta)$, where $\eta = \{\phi_c, \sigma_c\}$, ϕ_c are the mean angles of the clusters and σ_c is the angular spreads of the clusters. The parameter vector η can be estimated based on the covariance matrix of a given radiation pattern configuration ψ. Though there exists many well developed estimation theory for array processing, they are all based on omni-directional antennas. In our research, we propose to extend estimation theory to DRPD-MIMO systems and analyze its estimation accuracy. Here we give an illustrative analysis about the estimation accuracy with DRPD-MIMO. The accuracy of estimating with a given estimation technique can be evaluated by the Cramer-Rao lower bound (CRB). The CRB is given by the inverse of Fisher

Information Matrix (FIM). Considering L pattern configurations we have covariance matrices for each independent estimation with different pattern configurations, i.e, $\mathbf{R}(\psi(l))$ (where $l = 1, \cdots, L$). For the covariance matching estimation technique with pattern configuration psi l , the (m,n)-th element of the inverse of the corresponding CRB where N is the length of the received signal sequence for each estimation. The covariance matrix of the total estimation with L pattern configurations By selecting proper Ψ, it is possible achieving higher estimation accuracy with DRPD-MIMO than that with conventional MIMO.

Generally, the angular resolution of a scanning beam is determined by the antenna beam width. When multiple waves are incident within an angular range narrower than the scanning antenna beamwidth, it is difficult to separate the incident waves. In the case that the difference in the distances between the targets is larger than the range resolution, which is governed by the transmission bandwidth, the mixed signals can be separated. In this situation, it is important to perform DOA estimation by improving the angular resolution. When multiple received signals can be derived from an array antenna, as in the case of beamforming, there are DOA estimation methods based on the superresolution algorithm, such as MUSIC (multiple signal classification), which can estimate the DOAs of multiple waves closing less than the beamwidth. In scanning beams, the antenna gain of the incident wave is uniquely determined according to the beam direction. Thus, a DOA estimation algorithm can be considered in which the incident waves are derived with multiple beams whose directions are different, and the corresponding antenna gains are used as the feature parameters of the incident angle.

4.1 Data Model

Most conventional direction finding algorithms have been developed for point sources. However, in indoor wireless communication scenarios introduced in Chapter 3, the scatters in the propagation environment are geometrically distributed in groups (clusters). For instance, angular spreads up to 15° have been observed in an indoor measurement campaign [Laplacian distribution]. Therefore, the source can no longer be modeled using the point assumption.

Multipath propagation in indoor environments leads to energy dispersion in the spatial domain. Depending on the nature of the reflection and scattering in the propagation environment, signal components arriving from different directions exhibit varying degrees of correlation, ranging from totally uncorrelated (incoherent) to fully correlated (coherent) cases [45]. A source can be viewed as coherently distributed (CD) if the signal components arriving from different directions are replicas of the same signal. To the contrary, sources are called incoherently distributed (ID) if all signals from different directions are uncorrelated.

Indeed, if the channel coherency time is much smaller than the observation period, then the ID model is relevant. In the opposite case, the CD model or a partially coherent model can be used. In this chapter, we consider narrowband signals propagating over clustered channels and observed by a reconfigurable antenna array. Under stationary conditions, the signal components reflected from different differ parts of the object differ by a deterministic phase component that depends on the reflection coefficients of the surface elements, the difference in travel times, and the frequency of the incident wave [45].

In some cases, the signal rays arriving from different directions can be assumed uncorrelated. For example, in the transmission of the radio-waves through tropospheric scatter links, the signal rays reflected from different layers of the troposphere have uncorrelated phases. A similar effect is observed when the signal rays are the reflections from different parts of a rough surface. According to the *Rayleigh roughness criterion*, a surface is rough enough if $h \sin \phi > \lambda/8$, where h is the height of the roughness in the surface, ϕ is the reflection angle measured from the normal, and λ is the wavelength of the propagating radio wave [45, 46]. In this chapter, we only consider ID cases.

Consider the signal model of conventional non-reconfigurable systems

$$\mathbf{r} = \mathbf{H}\mathbf{s} + \mathbf{n}, \tag{4.1}$$

where $\mathbf{r} \in \mathbb{C}^N$ is the complex symbol vector of dimension N_r observed by the antenna array. The model requires a narrowband signal. The propagation delays between antenna elements in the array may be modeled as phase shifts provided the bandwidth of the signal is sufficiently small.

In the following, the signal model for conventional antenna array systems in Eq. (4.1) is extended for reconfigurable array systems by importing the time-varying array responses. We assume that during the observation period the reconfigurable array is switched to P distinguish array states $\psi_1, \psi_2, \cdots, \psi_P$, and each array state lasts for N symbols long, where N satisfies $NP = N$. For array state ψ_p, the observation symbol vector is

$$\mathbf{r}(t) = \mathbf{H}(\psi(t))\mathbf{s}(t) + \mathbf{n}(t), \tag{4.2}$$

where $\mathbf{H}(\psi(t))$ is the channel matrix which is a function of the time-switching array state $\psi(t)$.

Stacking all the obvserved signal vectors in a single vector, i.e.,

$$\begin{aligned}\bar{\mathbf{r}} &= [\mathbf{r}_1^T\, \mathbf{r}_2^T \cdots \mathbf{r}_P^T\,]^T \\ \bar{\mathbf{s}} &= [\mathbf{s}_1^T\, \mathbf{s}_2^T \cdots \mathbf{s}_P^T\,]^T \\ \bar{\mathbf{n}} &= [\mathbf{n}_1^T\, \mathbf{n}_2^T \cdots \mathbf{n}_P^T\,]^T,\end{aligned}$$

and

$$\mathbf{H} = \text{diag}\{\mathbf{H}(\psi_1), \mathbf{H}(\psi_2), \cdots, \mathbf{H}(\psi_P)\}. \tag{4.3}$$

The signal model can be presented by

$$\begin{bmatrix} \mathbf{r}(t_1) \\ \mathbf{r}(t_2) \\ \vdots \\ \mathbf{r}(t_P) \end{bmatrix} = \begin{bmatrix} \mathbf{H}(\psi_1) & & & \\ & \mathbf{H}(\psi_2) & & \\ & & \ddots & \\ & & & \mathbf{H}(\psi_P) \end{bmatrix} \begin{bmatrix} \mathbf{s}(t_1) \\ \mathbf{s}(t_2) \\ \vdots \\ \mathbf{s}(t_P) \end{bmatrix} + \begin{bmatrix} \mathbf{n}(t_1) \\ \mathbf{n}(t_2) \\ \vdots \\ \mathbf{n}(t_P). \end{bmatrix} \tag{4.4}$$

Or, in a compact expression by

$$\bar{\mathbf{r}} = \mathbf{H}\bar{\mathbf{s}} + \bar{\mathbf{n}}. \tag{4.5}$$

Assume that $\mathbf{s}_k$ are i.i.d. complex Gaussian vectors and are uncorrelated with each other:

$$\mathbb{E}\left[\mathbf{s}_k \mathbf{s}_j^H\right] = E_s \delta(k-j)\mathbf{I}, \tag{4.6}$$

where E_s is the symbol power.

4.2 Spectrum Methods for Reconfigurable Antenna Arrays

4.2.1 Conventional Capon Estimation of DoA

In 1969, Jack Capon introduced a high-resolution spatial spectrum estimation method [47] which is in this chapter referred to as *the conventional Capon estimator*. The conventional Capon estimator can be considered as a spatial filter which can distortionlessly pass the signal from the array steering direction while maximally rejecting signals from other directions. For narrowband plane waves, the optimal array weights can be estimated by solving the

optimization problem

$$\min_{\mathbf{w}} \mathbf{w}^H \mathbf{R}_r \mathbf{w} \quad \text{s.t. } \mathbf{w}^H \mathbf{a} = 1 \tag{4.7}$$

The solution to Eq. (4.7) is given by

$$\mathbf{w}_C(\phi) = \frac{\mathbf{R}_r^{-1}\mathbf{a}(\phi)}{\mathbf{a}(\phi)^H \mathbf{R}_r^{-1}\mathbf{a}(\phi)}. \tag{4.8}$$

The conventional Capon pseudo-spectrum is defined as

$$P_C(\phi) = \mathbf{w}_C^H(\phi)\mathbf{R}_r\mathbf{w}_C(\phi) = \frac{1}{\mathbf{a}(\phi)^H \mathbf{R}_r^{-1}\mathbf{a}(\phi)}. \tag{4.9}$$

It is clear that if the energy of the i-th point source impinges from a direction ϕ', then $P_C(\phi)$ is expected to have a separate peak at $\phi = \phi'$. Hence, the DoA of the point source can be estimated from the highest maxima of Eq. (4.9), which can be obtained by means of a one-dimensional spectral search.

4.2.2 Generalized Capon Estimation of DoA and Angular Spread

To estimate the parameters of ID sources with reconfigurable antenna array, Eq. (4.7) can be generalized as

$$\min_{\mathbf{w}} \mathbf{w}^H \mathbf{R}_r(\Psi) \mathbf{w} \quad \text{s.t. } \mathbf{w}^H \mathbf{R}_s(\mathbf{\Theta}) \mathbf{w} = 1 \tag{4.10}$$

where

$$\mathbf{R}_s(\mathbf{\Theta}) = \int_{2\pi} PAS_r(\phi_r; \mathbf{\Theta}) \mathbf{a}_r(\phi_r) \mathbf{a}_r^H(\phi_r) d\phi_r \tag{4.11}$$

is the normalized covariance matrix of the ID source with the parameter vector. The generalized Capon spatial filter maintains distortionless spatial response to a hypothetical source with the vector parameter while maximally rejecting the contribution of any other sources.

The solution is given in [48] by using the method of Lagrangian multipliers. The Lagrangian function of the optimization problem Eq. (4.10) is

$$L(\mathbf{w}, \lambda) = \mathbf{w}^H \mathbf{R}_r(\Psi)\mathbf{w} + \lambda(1 - \mathbf{w}^H \mathbf{R}_s(\eta)\mathbf{w}). \tag{4.12}$$

Let $\frac{\partial L}{\partial \mathbf{w}^*} = 0$ and we have

$$\mathbf{R}_r(\Psi)\mathbf{w} = \lambda \mathbf{R}_s(\eta)\mathbf{w}. \tag{4.13}$$

Eq. (4.13) indicates that the Lagrangian multiplier λ is a generalized eigenvalue of the matrix pencil $\{\mathbf{R}_r(\Psi), \mathbf{R}_s(\eta)\}$. It is obtained as $\lambda = \mathbf{w}^H \mathbf{R}_r \mathbf{w}$ by left-multiplying $\mathbf{w}^H$ to Eq. (4.13) and making use of the constraint $\mathbf{w}^H \mathbf{R}_s(\eta)\mathbf{w} = 1$. Since both $\mathbf{R}_r(\Psi)$ and $\mathbf{R}_s(\eta)$ are Hermitian matrices, λ is a real valued number. In this case, the optimization problem Eq. (4.10) is equivalent to

$$\min_{\mathbf{w}} \mathbf{w}^H \mathbf{R}_r(\Psi)\mathbf{w} = \lambda_{min}\{\mathbf{R}_r(\Psi), \mathbf{R}_s(\eta)\}, \tag{4.14}$$

where $\lambda_{min}\{\mathbf{R}_r(\Psi), \mathbf{R}_s(\eta)\}$ is the minimum generalized eigenvalue of the matrix pencil.

The generalized Capon pseudo spectrum for the reconfigurable array is given by

$$P_{GC}(\eta) = \lambda_{min}\{\mathbf{R}_r(\Psi), \mathbf{R}_s(\eta)\} = \frac{1}{\mu_{max}\{\mathbf{R}_x^{-1}(\Psi)\mathbf{R}_s(\eta)\}}, \tag{4.15}$$

where $\mu_{max}\{\cdot\}$ is the maximum eigenvalue of a matrix. For a N_c-cluster channel, the PAS parameter vector η can be estimated by finding the locations of N_c main peaks over the pseudo spectrum $P_{GC}(\eta)$ calculated according to Eq. (4.15).

The conventional Capon estimator is a non-parametric estimator whereas the generalized Capon estimator is parametric. Therefore the generalized Capon estimation requires *a priori* knowledge of the shape of the scatter distribution. To find the estimates of the parameters of the PAS, a q-dimensional search is required where q is the number of the PAS parameters, including cluster powers, mean angles and angular spreads. If the scatters within each cluster follow the same shape of distribution, the cluster parameters can be found by performing a 3-dimensional search, where q is the number of the parameters of the distribution. As a special case, if the scatter distribution within each cluster has the same shape and the same power, the mean angles and angular spreads can be found by performing a 2-dimensional search.

4.2.3 Simulation

In this section, we use theoretical radiation patterns of a CRLH-LWA to illustrate the generalized Capon estimator for reconfigurable array. The azimuth radiation pattern of CRLH-LWA

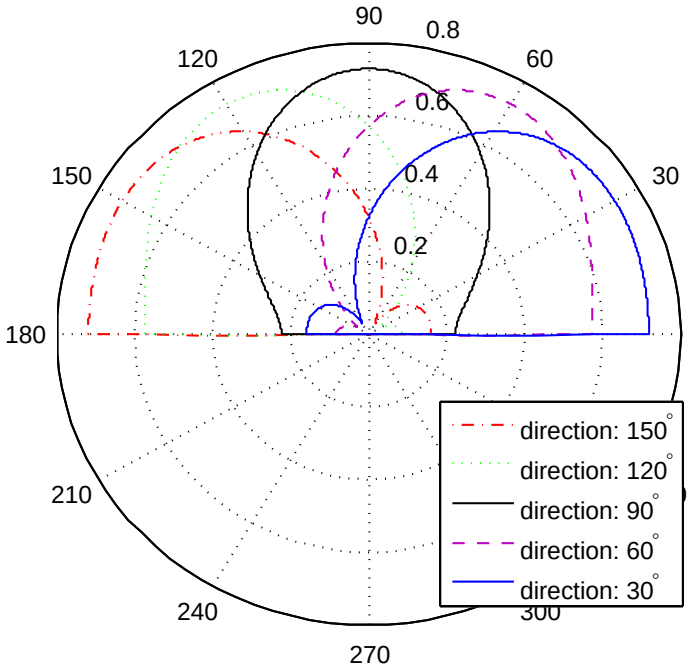

Figure 4.1 Radiation patterns of a reconfigurable CRLH-LWA with 5 pattern states at the antenna.

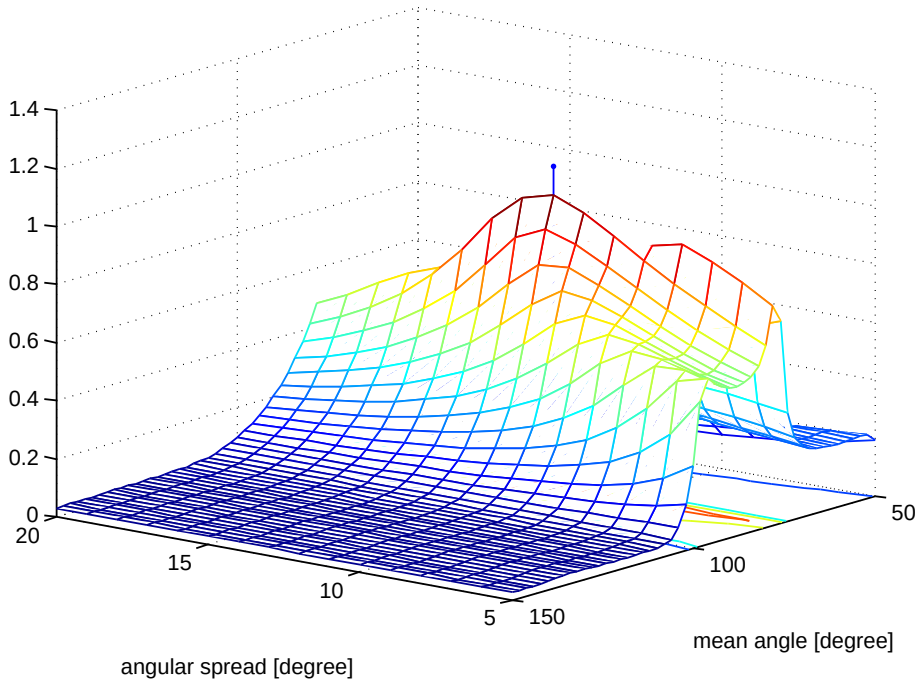

Figure 4.2 The theoretical pseudo spectrum of the generalized Capon estimator for the mean angle and angular spread of a 1-cluster channel. The mean angle $\phi_c = 80°$. The angular spread $\sigma_c = 12°$. SNR $\gamma = 10$ dB.

is given by the array factor approach in [17]

$$g(\phi) = \sum_{n=1}^{N} I_0 e^{-\alpha(n-1)d + j(n-1)k_0 d(\sin\phi - \sin\phi_0)} \tag{4.16}$$

where N is the number of cells of the CRLH-LWA.

In our simulation, we use a 10-cell CRLH-LWA to generate 5 discrete radiation patterns as shown in Fig. 4.1. The beam directions are 30°, 60°, 90°, 120° and 150°, respectively. Assuming a single-cluster spatial channel with the mean angle $\phi_c = 80°$, the angular spread $\sigma_c = 12°$ and the SNR $\gamma = 10$ dB. We compute the theoretical pseudo spectrum of the generalized Capon estimator by Eq. (4.15) for this channel as shown by Fig. 4.2. The pseudo spectrum indicates that the generalized Capon estimator works properly.

4.3 Covariance Matching Estimation Techniques for Reconfigurable Antenna Array

Parameter estimation of a cluster MIMO channel, i.e., estimating the mean angles of the cluster and the angle spread are essential for maximizing the channel capacity for a MIMO system with dynamic radiation pattern antennas. Many algorithms for sensor array processing have been proposed in recent years for DoA estimation as well as joint DoA and angle spread estimation of dispersed sources. These algorithms include maximum likelihood (ML) estimation, subspace methods such as multiple signal classification (MUSIC) and multidimensional MUSIC, rotational invariance methods such as ESPRIT, and covariance matching estimation techniques (COMET) , i.e. subspace fitting, and its variation with extended invariance principle. In our research, we use one or more antenna elements with dynamic radiation patterns to estimate parameters of clustered wireless channel. The Cramer-Rau lower bound (CRB) of the estimation with DRPD is derived. The results indicated that parameter estimation of clustered channels utilizing dynamic radiation pattern diversity offers great performance enhancement comparing to traditional ULA sensor processing techniques. COMET method is used in estimating the cluster parameters with dynamic radiation pattern antennas based on correlation coefficients of each radiation pattern steered.

Denote estimation vector $\eta = \{\phi_c, \sigma_c, \sigma_n^2\}$, where ϕ_c is the mean angle of the cluster, σ_c is the angle spread of the cluster, and σ_n^2 is the noise variance. It is verified by experiments that PAS fits most to Laplacian distribution, i.e.,

$$PAS(\phi_c, \sigma_c, \sigma_n) = \frac{1}{\sqrt{2}\sigma_c} e^{-\sqrt{2}|\phi - \phi_c|/\sigma_c} \tag{4.17}$$

Assume that an antenna element with N steerable patterns is deployed. And assume that all possible radiation patterns are uncorrelated with each other. The covariance matrix $\mathbf{R}$ of the signals received by all the pattern states is diagonal, i.e.,

$$\mathbf{R} = \text{diag}\{r_1, \cdots, r_N\}. \tag{4.18}$$

Given radiation patterns $g_n(\phi)$ where $n = 1, \cdots, N$, we have

$$r_n(\eta) = \int_{2\pi} |g_n(\eta)|^2 PAS(\phi; \phi_c, \sigma_c) d\phi + \sigma_n^2. \tag{4.19}$$

Expand $|g_n(\phi)|^2$ and $PAS(\phi; \phi_c, \sigma_c)$ into Fourier series as

$$|g_n(\phi)|^2 = \sum_k G_{n,k} e^{jk\phi} \tag{4.20}$$

$$PAS(\phi; \phi_c, \sigma_c) = \sum_k P_k(\phi_c, \sigma_c) e^{jk\eta} \tag{4.21}$$

where G_k depends on the pattern selected, and

$$P_k(\phi_c, \sigma_c) = \frac{e^{-jk\phi_c}}{2\pi(1 + k^2\sigma_c^2/2)}. \tag{4.22}$$

Thus we have

$$r_n(\eta) = \sum_k (G_n * \frac{\partial P}{\partial \eta_i})_k e^{jk\phi} \tag{4.23}$$

where $*$ is the discrete convolution operator. The CRB matrix $\mathbf{B}$ is the inverse of the Fisher information matrix, i.e.,

$$\begin{aligned} (\mathbf{B}^{-1})_{ij} &= \text{tr}\left(\mathbf{R}^{-1}\frac{\partial \mathbf{R}}{\partial \eta_i}\mathbf{R}^{-1}\frac{\partial \mathbf{R}}{\partial \eta_j}\right) \\ &= \frac{1}{N}\sum_{n=1}^{N} r_n^{-2}\frac{\partial \mathbf{r}}{\partial \eta_i}\frac{\partial \mathbf{r}}{\partial \eta_j} \end{aligned} \tag{4.24}$$

where

$$\frac{\partial r_n}{\partial \eta_i} = \frac{1}{N}\sum_k (G_n * \frac{\partial P}{\partial \eta_i})_k e^{jk\phi} \tag{4.25}$$

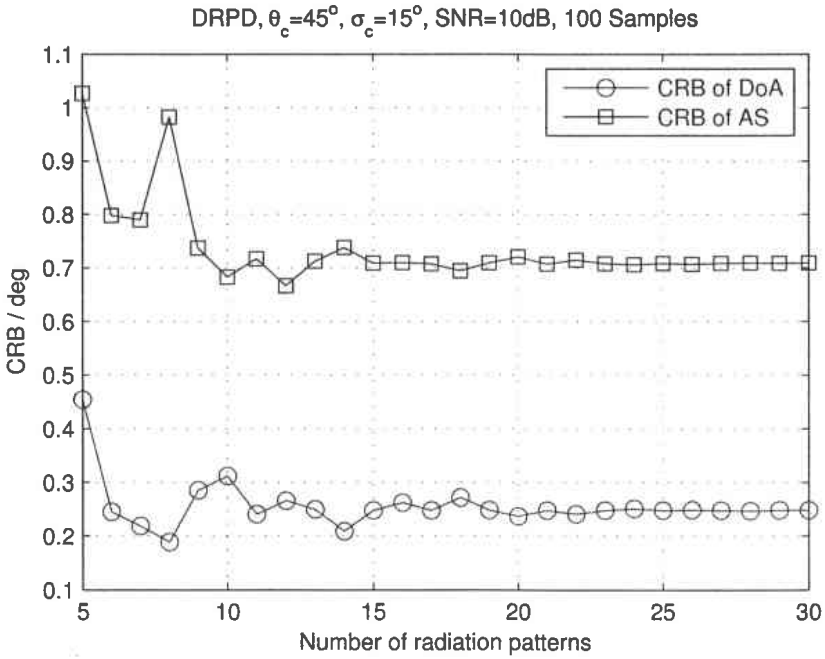

Figure 4.3 Cramer-Rao bound of the mean angle and angular spread of a cluster with a single reconfigurable antenna which has the beamwidth of 60°.

and

$$\begin{aligned}
\frac{\partial P_k}{\partial \phi_c} &= -\frac{jke^{-jk\phi_c}}{2\pi(1+k^2\sigma_c^2/2)}, \\
\frac{\partial P_k}{\partial \sigma_c} &= -\frac{\sigma_c k^2 e^{-jk\phi_c}}{2\pi(1+k^2\sigma_c^2/2)}, \\
\frac{\partial P_k}{\partial \phi_n^2} &= 0.
\end{aligned} \tag{4.26}$$

In the following, we illustrate the numerical simulation of the CRB of the mean DoA and the AS of a single-cluster spatial channel estimated with a single reconfigurable antenna using the COMET. The mean angle of the cluster is $\phi_c = 45°$, the angular spread is $\sigma_c = 15°$ and the SNR is 10 dB. The radiation patterns are selected from a rotating directional antenna with identical beamwidth of 60° and the beam directions uniformly separated from 0° to 180° by the number of radiation patterns. Fig. 4.3 illustrates the CRB curves of the mean angle and the angular spread versus the number of radiation patterns. Notice that the conventional COMET estimator using an antenna array requires at least 2 antenna elements for estimating the mean angle and angular spread of a single cluster, while the proposed COMET estimator with reconfigurable antenna only requires a single antenna with multiple

radiation patterns. This suggests that a pattern reconfigurable antenna can be used to replace an antenna array for the PAS estimation. Furthermore, the simulated results indicate that the COMET estimator is less accurate in estimating the angular spread than estimating the mean angle.

4.4 Chapter Summary

In this chapter, a Capon-like estimator and a COMET estimator for jointly estimating the mean angle and angular spread of spatial channels using reconfigurable antennas are proposed. The estimation performance of the proposed method is evaluated by numerical simulation. We conclude that a single reconfigurable antenna which provides multiple radiation pattern states can be used to replace the conventional antenna array for estimating the long-term statistics of the spatial channel.

CHAPTER 5

PS-MIMO SYSTEMS WITH STATISTICAL SELECTION

In wireless communications, multiple-input multiple-output (MIMO) is a promising solution to provide wireless links with high data rate and reliability. It is well-known that the channel capacity of a MIMO system increases linearly in uncorrelated channels [49]. But this result is not guaranteed in real propagation environment because of the existence of spatial correlation [50]. The spatial correlation is affected by the propagation environment as well as antenna characteristics, such as antenna spacing and radiation patterns. In previous years, polarization and pattern diversity have been studied to combat spatial correlation and improve MIMO channel capacity. The CRLH-LWA was proposed in [19] as a new approach to provide dynamic radiation pattern diversity.

In this chapter we investigate the use of the CRLH-LWA in an PS-MIMO system where the radiation patterns are selected based on the statistical properties of the environment. Theoretical and simulation results are presented and illustrate the significant power gain and decorrelation gain provided by SPS-MIMO as compared to conventional MIMO systems with omni-directional antennas. We first present the radiation patterns models for the CRLH-LWA. Next, we derive a tight upper bound of the ergodic capacity of the MIMO channel which can be maximized by properly choosing the radiation patterns. The capacity gain offered by dynamic radiation patterns is then compared to MIMO systems deploying omni-directional antennas. Finally, we propose methods to find the proper radiation patterns that maximize channel capacity of a $(2, 2)$ MIMO system.[1]

5.1 Dynamic Radiation Pattern and CRLH-Leaky-Wave Antenna

The spatial clustered channel presented in Section 3.3.3 indicates that power transmitted over the propagation environment is concentrated within clusters over the azimuth plane. In this case, antennas with omni-directional radiation pattern are not as effective to send and gather signal power as antennas with directional radiation patterns aiming to the clusters. To adapt to different propagation environments, it is advisable to use dynamic radiation patterns with adjustable direction and beamwidth.

[1]Part of the work presented in this chapter was published in: X. Li and J.-F. Frigon, "Capacity analysis of MIMO systems with dynamic radiation pattern diversity." in *Proc. IEEE VTS Vehicular Technology Conference (VTC'09 Spring)*, Barcelona, Spain, Apr. 2009, pp. 1–5.

We propose to use a PS-MIMO system with a novel CRLH leaky-wave antenna designed to provide dynamic radiation pattern diversity [17, 19]. The direction of the CRLH-LWA can be swept from backfire to endfire on-the-fly by changing the varactor voltages. The beamwidth is relative to the number of cells used. That is, the more cells used in the structure, the narrower beam we have. Unlike smart antennas or phased antenna arrays, the CRLH-LWA provides dynamic radiation pattern with only one antenna element. This feature is extremely beneficial for handsets whose size is too limited to deploy multiple antennas.

The radiation pattern of the CRLH-LWA over the azimuth plane is given by the *array factor approach* [17]

$$g_{LWA}(\phi) = \sum_{n=1}^{N_c} I_0 e^{-\alpha(n-1)p + j(n-1)k_0 p(\sin\phi - \sin\phi_0)} \tag{5.1}$$

where N_c is the cell number, α is the leakage factor, p is the period of the structure, k_0 is the free space wavenumber, and ϕ_0 is the radiation angle.

The expression of the CRLH-LWA dynamic radiation patterns is too complex for mathematical analysis. Thus, we propose an artificial rectangular radiation pattern $g(\phi)$ as a proper abstraction to capture the direction steerability and beamwidth characteristics of dynamic radiation patterns:

$$g(\phi) = \begin{cases} \sqrt{\pi/B}, & \phi_0 - B \le \phi < \phi_0 + B \\ 0, & \text{otherwise.} \end{cases} \tag{5.2}$$

$g(\phi)$ is steered to direction ϕ_0 with symmetric beamwidth $2B$. Since the radiation pattern of the omni-directional antenna $g^o(\phi) = 1$, $-\pi \le \phi < \pi$, $g(\phi)$ is chosen so that its square integration is normalized to 2π. In the next section, we will theoretically analyze the effects on the channel capacity of the dynamic radiation patterns steerable direction and beamwidth for the multiple antennas based on this artificial pattern. The actual CRLH-LWA radiation pattern models will be used in the simulations presented in Section 5.4.

5.2 Capacity of Clustered MIMO Channels with Dynamic Radiation Patterns

In this section, we first analyze the ergodic channel capacity of MIMO systems with dynamic radiation patterns. Then we present a systematic approach to maximize the ergodic channel capacity by properly selecting radiation patterns and mathematically derive the capacity gain.

5.2.1 Ergodic Capacity of Kronecker Model

For MIMO channels, the spatial correlation between signals received by different antennas is an essential factor determining the channel capacity. Here we give an expression of the spatial correlation for MIMO clustered channels with dynamic radiation patterns. Then, we examine how the dynamic radiation pattern affects the correlation and the channel capacity.

If the channel information is unknown to the transmitter, the ergodic channel capacity is given by [49]

$$\bar{C} = \mathbb{E}[\log_2 \det(\mathbf{I} + \rho \mathbf{H}\mathbf{H}^*)], \tag{5.3}$$

where $\rho \triangleq \gamma/N_t$ is the signal-to-noise ratio (SNR) averaged over transmit antennas. [9] derived a tight ergodic capacity upper bound of MIMO channels with Kronecker product structured covariance, i.e., $\mathbf{H} \sim \mathcal{CN}(\mathbf{0}, \mathbf{R}_t \otimes \mathbf{R}_r)$.

According to [9], the ergodic capacity of this correlated MIMO channel is tightly upper bounded by

$$\begin{aligned} C &\leq \log_2 \left[\sum_{k=0}^{\min\{N_t,N_r\}} k! \rho^k \sum_{1 \leq i_1 < \cdots < i_k \leq N_t} \det\left(\mathbf{R}_{t,i_1,\cdots,i_k}^{i_1,\cdots,i_k}\right) \sum_{1 \leq u_1 < \cdots < u_k \leq N_r} \det\left(\mathbf{R}_{r,u_1,\cdots,u_k}^{u_1,\cdots,u_k}\right) \right] \\ &\triangleq \bar{C}_{ub} \end{aligned} \tag{5.4}$$

where $\mathbf{R}_{r,u_1,\cdots,u_k}^{u_1,\cdots,u_k}$ is the $k \times k$ sub-matrix of $\mathbf{R}_r$ on the $u_1, \cdots, u_k$-th rows and $u_1, \cdots, u_k$-th columns, and $\mathbf{R}_{t,i_1,\cdots,i_k}^{i_1,\cdots,i_k}$ is the $k \times k$ sub-matrix of $\mathbf{R}_t$ on the $i_1, \cdots, i_k$-th rows and $i_1, \cdots, i_k$-th columns, respectively.

At high SNR, we have an asymptotic approximation to the capacity upper bound when $N_t = N_r = N$,

$$\bar{C}_{ub} \approx \log_2 N! + N \log_2 \rho + \log_2 \det(\mathbf{R}_t) + \log_2 \det(\mathbf{R}_r) \tag{5.5}$$

We can see that at high SNR, the spatial correlation matrices at transmitter and receiver side have separable influence on the channel capacity. We assume that around the transmitter, the scatters are uniformly distributed, and the ULA is spaced by half wavelength with omni-directional antennas. So the channel at the transmitter side is almost fully decorrelated, i.e., $\mathbf{R}_t \approx \mathbf{I}$. This makes the correlation at the transmitter and receiver side separable. This

simplifies Eq. (5.3) to

$$\begin{aligned}\bar{C} &\leq \log_2 \left[\sum_{k=0}^{N} \frac{N!\rho^k}{(N-k)!} \sum_{1 \leq i_1 < \cdots < i_k \leq N} \det\left(\mathbf{R}_{i_1,\cdots,i_k}^{i_1,\cdots,i_k}\right) \right] \\ &\triangleq \bar{C}_{ub}, \end{aligned} \tag{5.6}$$

and its asymptotic approximation at high SNR is

$$\bar{C}_{ub}(\mathbf{R}) \approx \log_2 N! + N \log_2 \rho + \log_2 \det(\mathbf{R}). \tag{5.7}$$

5.2.2 Ergodic Capacity Gain of SPS-MIMO

In this section, we evaluate the capacity performance of the SPS-MIMO system over the conventional MIMO system equipped with omni-directional antennas.

We denote the channel covariance matrix of a MIMO system using omni-directional antennas with the same channel cluster parameters and antenna configuration by $\mathbf{R}^o$. Based on the asymptotic ergodic MIMO channel capacity Eq. (5.7), we approximate the gain of the ergodic channel capacity of the SPS-MIMO over the conventional MIMO by

$$\begin{aligned}\Delta\bar{C} &= \bar{C}(\mathbf{R}) - \bar{C}(\mathbf{R}^o) \\ &\approx \bar{C}_{ub}(\mathbf{R}) - \bar{C}_{ub}(\mathbf{R}^o) \\ &= \log_2 \frac{\det \mathbf{R}}{\det \mathbf{R}^o}. \end{aligned} \tag{5.8}$$

We assume that the antenna spacing of the conventional MIMO is the same as that of the SPS-MIMO. According to the previous analysis, the ergodic capacity upper bound is a function of the spatial correlation matrices. Since the spatial correlation matrices can be adjusted by deploying dynamic radiation patterns, the channel capacity can be maximized by properly choosing the radiation patterns.

We use the asymptotic approximation of the capacity upper bound Eq. (5.7) as the objective function to maximize. In order to maximize Eq. (5.7), we need to find a set of radiation patterns for the antennas, i.e.,

$$\arg \max_{\{g_n\}_{n=1}^{N}} \det(\mathbf{R}), \tag{5.9}$$

where g_n $(n = 1, \cdots, N)$ is the dynamic radiation pattern of the n-th antenna.

We will now focus our analysis on the single cluster case with $N_t = N_r = N = 2$. We use the abstract dynamic radiation pattern given in Eq. (5.2) to study how the steerable direction and beamwidth affect the channel capacity. We have

$$\det(\mathbf{R}) = r_{11}r_{22} - r_{12}r_{21}. \tag{5.10}$$

The auto-correlation coefficients are given by

$$r_{nn} = \frac{\beta\pi}{\sqrt{2}B\sigma_c}\int_{\phi_n-B}^{\phi_n+B} e^{-\sqrt{2}|\phi-\phi_c|/\sigma_c}d\phi, \quad n = 1, 2, \tag{5.11}$$

and the cross-correlation coefficients by

$$r_{12} = r_{21}^* = \begin{cases} \frac{\pi}{B}\int_{\min(\phi_1,\phi_2)-B}^{\max(\phi_1,\phi_2)+B} e^{-j2\pi d\sin\phi}PAS(\phi)d\phi & \text{if } |\phi_1 - \phi_2| \le 2B, \\ 0 & \text{otherwise,} \end{cases} \tag{5.12}$$

where ϕ_1 and ϕ_2 are the radiation pattern directions of the n-th antenna. The optimal $\hat{\phi}_{1,2}$ maximizing $\det(\mathbf{R})$ given fixed beamwidth B can be found by using numerical optimization methods.

We denote $\mathbf{R}^o = \{r_{nm}^o\}^{2\times 2}$ as the channel covariance matrix using omni-directional antennas with the same channel cluster parameters and antenna configuration as those of $\mathbf{R}$. Note that

$$\det(\mathbf{R}) = r_{11}r_{22} \cdot (1 - r_{12}r_{21}/r_{11}r_{22}). \tag{5.13}$$

We define

$$G_p \triangleq \frac{r_{11}r_{22}}{r_{11}^o r_{22}^o} = r_{11}r_{22} \tag{5.14}$$

as the *capacity power gain*, and

$$G_d \triangleq \frac{1 - r_{12}r_{21}/r_{11}r_{22}}{1 - r_{12}^o r_{21}^o/r_{11}^o r_{22}^o} = \frac{1 - r_{12}r_{21}/r_{11}r_{22}}{1 - r_{12}^o r_{21}^o} \tag{5.15}$$

as the *capacity decorrelation gain*. Thus $\det(\mathbf{R}) = G_pG_d \cdot \det(\mathbf{R}^o)$, where G_p and G_d indicate the capacity gain comparing to that of the half-wavelength ULA because of power concentration and channel decorrelation, respectively. For radiation patterns with wide beamwidth, G_p can be approximated by

$$G_p \approx \left(\frac{\pi}{B}\right)^2. \tag{5.16}$$

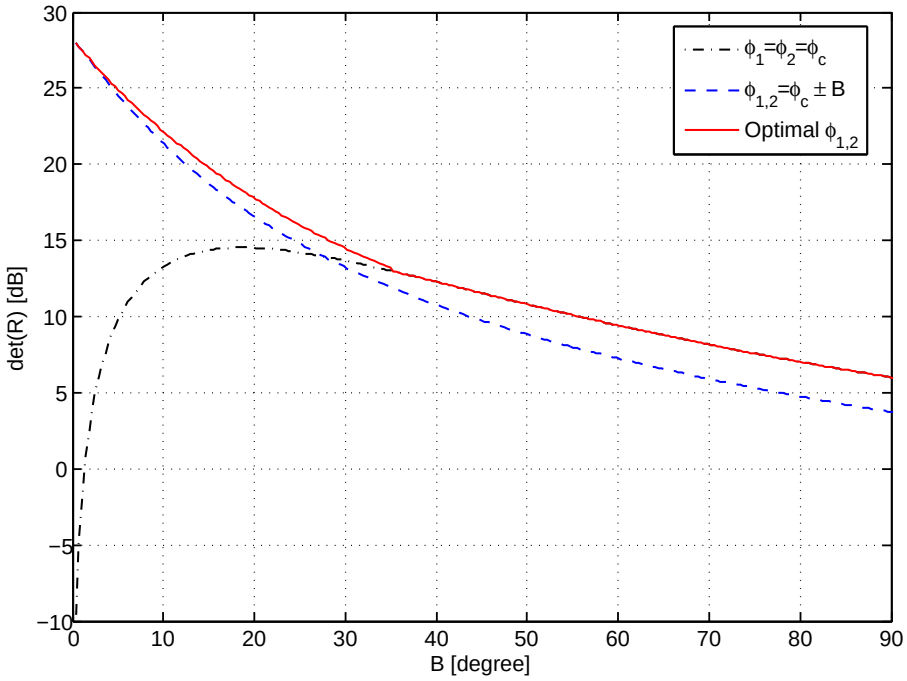

Figure 5.1 The determinant of a $(2, 2)$ MIMO channel correlation matrix $\mathbf{R}$, given different radiation pattern directions when the beamwidth of the abstract radiation pattern varies from 0 to 180 degrees. The solid line is the case when the directions are optimized. The dotted line is the case when both directions aim to the mean angle of the cluster. The dashed line is the case with full radiation pattern decorrelation. The cluster parameters are $\phi_c = 0°$ and $\sigma_c = 15°$. Half-wavelength ULA is deployed.

For an extremely narrow beamwidth, G_p is maximized as

$$\max G_p = \lim_{B\to 0} \lim_{\phi_{1,2}\to\phi_c} r_{11}r_{22} = \left(\frac{\beta\pi}{\sigma_c/\sqrt{2}}\right)^2. \tag{5.17}$$

We can see that the capacity power gain increases when the beamwidth of the antenna or the angle spread of the cluster decreases. According to Fig. 5.1, if the beamwidth is relatively wide, just aiming the two beams to the mean angle of the cluster can be a near optimal solution that maximize the determinant and the capacity, because G_d remains near 1 for wide beamwidth. If the beamwidth is narrow, steering the patterns to the same direction will introduce high correlation between antennas and thus deteriorates the capacity performance. Steering the two beams to directions slightly deviating from the mean angle will reduce the correlation while still benefiting from high power gain. Fig. 5.2 is another example of the power gain. The figures show that the power gain is maximized when the radiation pattern beam is directed to the maximum of the PAS.

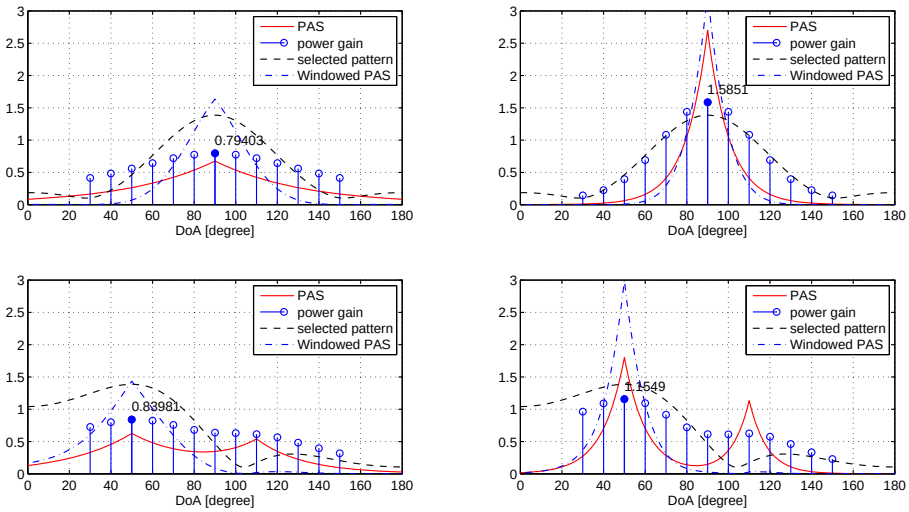

Figure 5.2 Impact of the power gain of a SPS-SISO system in 4 different spatial clustered channels.

5.3 Finding the Optimal Configuration

The ideas of how to develop a merit function to measure the performance gain introduced by pattern diversity are well discussed in the previous two sections. In the previous section, we have discussed how to select a proper radiation pattern state to fully and efficiently exploit the capacity gain or error performance gain introduced by radiation pattern diversity when the merit function is known.

A straightforward approach to solve problem Eq. (5.9) is to carry an exhaustive search over all possible radiation pattern states. Obviously, the exhaustive search is too computationally expensive and is only useful for PS-MIMO systems with very few antennas and radiation patterns. But it is still an acceptable approach to provide illustrative results in the preliminary stage of our research.

Another approach is to develop alternative merit functions which are suitable to apply mathematical optimization theory. For radiation patterns of reconfigurable antennas which are continuously tunable, we propose to use Newton's method to find the optimal radiation pattern configuration. For example, for the CRLH-LWA patterns described in Eq. (5.1) and the hypothetical patterns described in Eq. (5.2), the determinant merit function is continuous and partially differentiable with respect to the directions of the reconfigurable antennas at the receiver, which guarantees the convergence of Newton's method. The partial derivatives are given by

$$\frac{\partial \det \mathbf{R}}{\partial \phi_n} = \frac{\partial r_{nn}}{\partial \phi_n} - \frac{\partial \mathbf{r}_{n^-}}{\partial \phi_n} \mathbf{R}_{n^-}^{-1} \frac{\partial \mathbf{r}_{n^-}}{\partial \phi_n}, \tag{5.18}$$

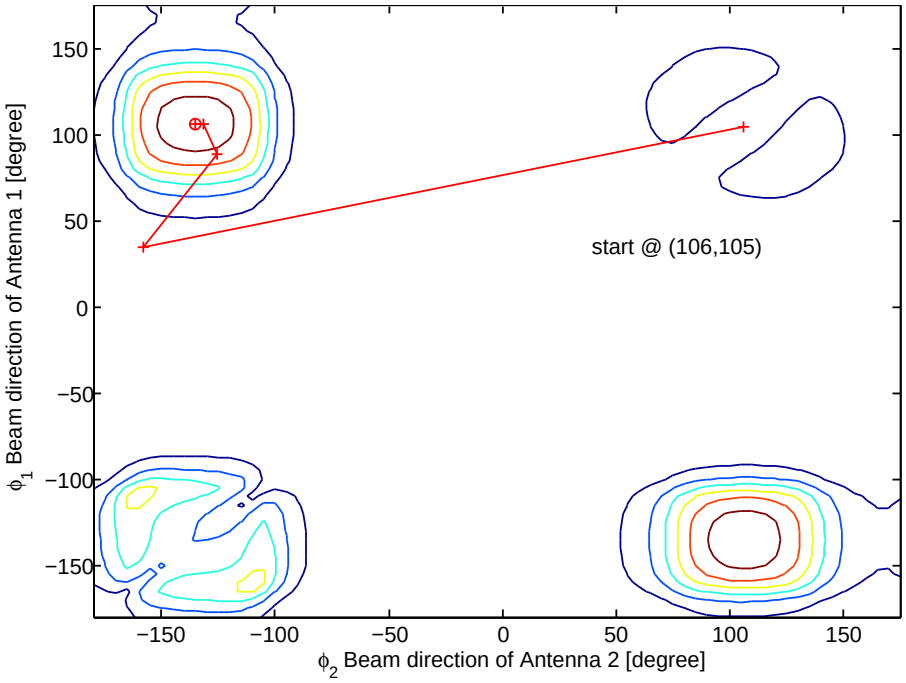

Figure 5.3 Search the radiation pattern state maximizing the capacity merit function with Newton's method.

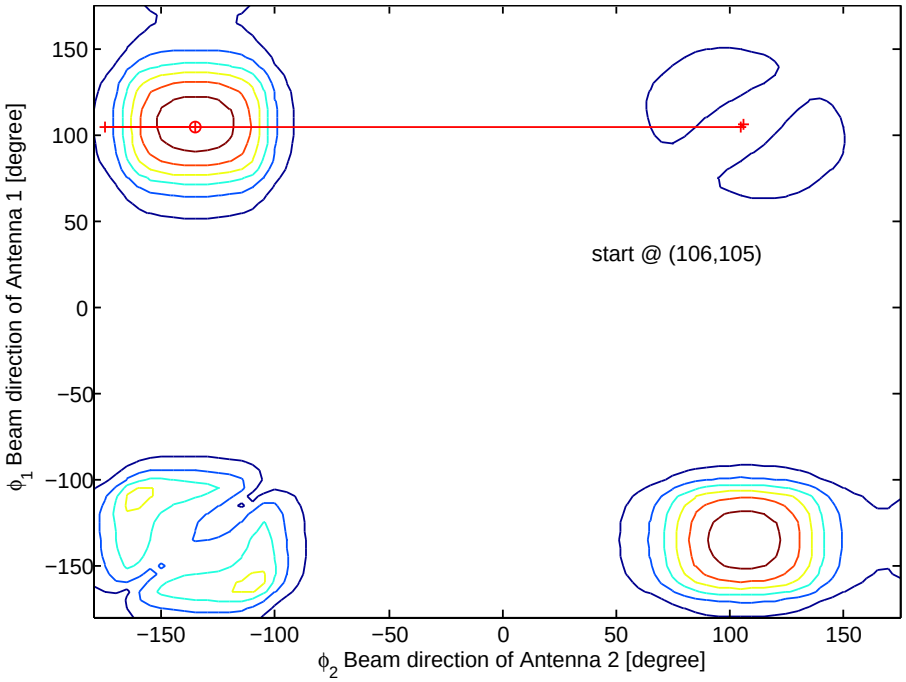

Figure 5.4 Search the radiation pattern state maximizing the capacity merit function with grid search.

where $\mathbf{r}$ is the n-th column vector of $\mathbf{R}$, $\mathbf{r}_{n^-}$ is the sub-vector of $\mathbf{r}$ with the n-th element removed and $\mathbf{R}_{n^-}$ is the sub-matrix of $\mathbf{R}$ with the n-th row and column removed. Eq. (5.18) can be used to find the maximum ascending direction. The simulation results of radiation pattern selection with Newton's method is illustrated in Fig. 5.3. The figure illustrates the quick convergence of the method to a quasi-optimal solution. Newton's method can converge to the global maximum if the initial value is carefully selected.

Newton's method requires to update the searching direction at each iteration step according to Eq. (5.18). In order to remove the computational burden of the matrix inverse in Eq. (5.18), we propose a grid search method to solve the optimization problem. For each reconfigurable antenna at the receiver, we discretized the beam direction so that we only need to search the maximum in a N_r-dimensional grid. The proposed grid search method starts from a selected initial value, and at each step it searches for the maximum within the range of the beam direction of a single antenna. Fig. 5.4 illustrates the path of the grid search method.

5.4 Numerical Results

This section describes a set of simulations for evaluating the ergodic capacity of SPS-MIMO systems using the Monte-Carlo method. In all the simulations, unless mentioned otherwise, we assume a $(2, 2)$ MIMO system with antennas with dynamic radiation patterns at the transmitter side and omni-directional antennas at the receiver side, both separated by half wavelength. We also assume the MIMO channel is uncorrelated at the receiver side. At the transmitter side, unless mentioned otherwise, a single-clustered MIMO channel with a mean arriving angle of the cluster at $\phi_c = 0^\circ$ and an arriving angular spread $\sigma_c = 15^\circ$.

The first simulation results illustrate the ergodic capacity gain of the dynamic radiation pattern compared to the omni-directional radiation pattern. The theoretical SPS-MIMO system capacity gain in this case is given by

$$\Delta\bar{C} \approx \log_2 G_p + \log_2 G_d \tag{5.19}$$

According to Eq. (5.17) and Eq. (5.19), for $\sigma_c = 15^\circ$, the maximum theoretical capacity gain is 8.2 bits/Hz/s. Such remarkable capacity improvement is validated by the results presented in Fig. 5.5, in which at SNR=15 dB the narrow beam case (beamwidth is 20°) provides a 7.6 bits/Hz/s capacity gain. For the wide beam case (beamwidth is 90°), the capacity gain is 3.9 bits/Hz/s, which also fits our estimation of 4 bits/Hz/s gain given by Eq. (5.16) and Eq. (5.19). Fig. 5.6 shows the ergodic capacity of the MIMO system with the

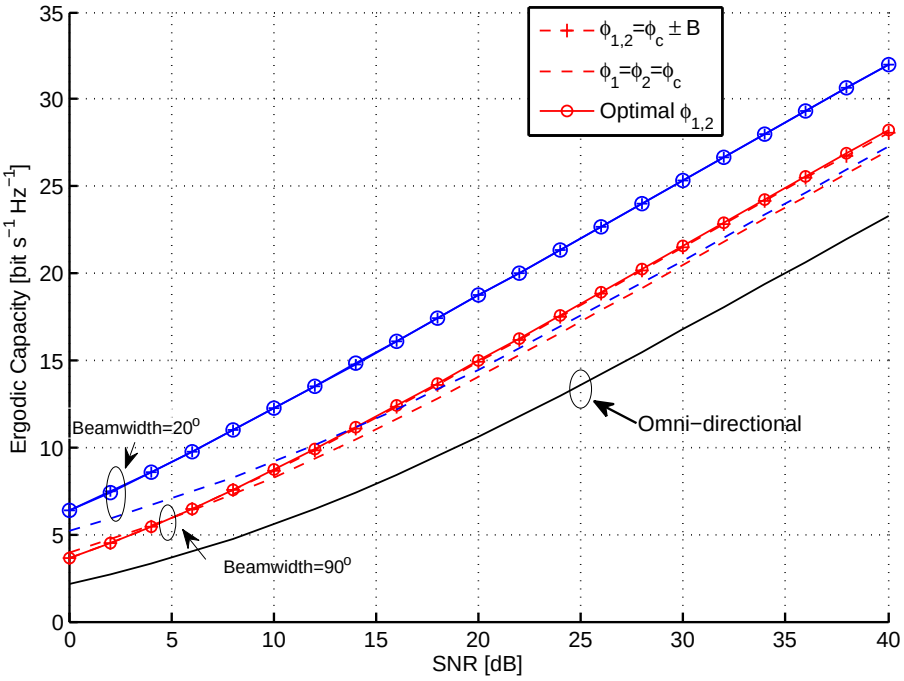

Figure 5.5 Ergodic channel capacity of a $(2, 2)$ MIMO system using abstract dynamic radiation patterns. The circled lines give the maximum ergodic capacity with optimal radiation patterns. The lines with '+' markers give the ergodic capacity with radiation patterns which fully decorrelate the channel. The dotted lines give the ergodic capacity with radiation patterns aiming to the cluster mean angle to maximize the power gain.

actual CRLH-LWA radiation pattern from Eq. (5.1) deployed. At SNR=15 dB, the capacity gain is about 7.2 and 3.6 bits/Hz/s, for $N_c = 20$ (narrow beam) and $N_c = 10$ (wide beam), respectively. That is to say, the capacity can be at least doubled at low SNR by steering the patterns to proper directions. It is also interesting to observe that, as predicted by Eq. (5.7), a multiplexing gain of 2 can be obtained in the correlated channel at high SNR. However, adjustable radiation patterns at both transmitting antennas decreases the SNR value at which the maximum multiplexing gain can be reached (i.e., the linear section of the capacity).

The second set of simulation results depicts the search of the optimal directions of the MIMO system with CRLH-LWA. Fig. 5.7 shows that the optimal directions are just the mean angle of the cluster if the beamwidth of the radiation patterns are wide enough. However, Fig. 5.8 shows that if we use radiation patterns with narrow beam, the mean angle of the cluster is no longer the optimal choice, because radiation pattern with high directivity will cause high correlation and thus reduce channel capacity. The optimal solution is now to slightly offset the two radiation patterns on each side of the mean cluster arrival angle (note

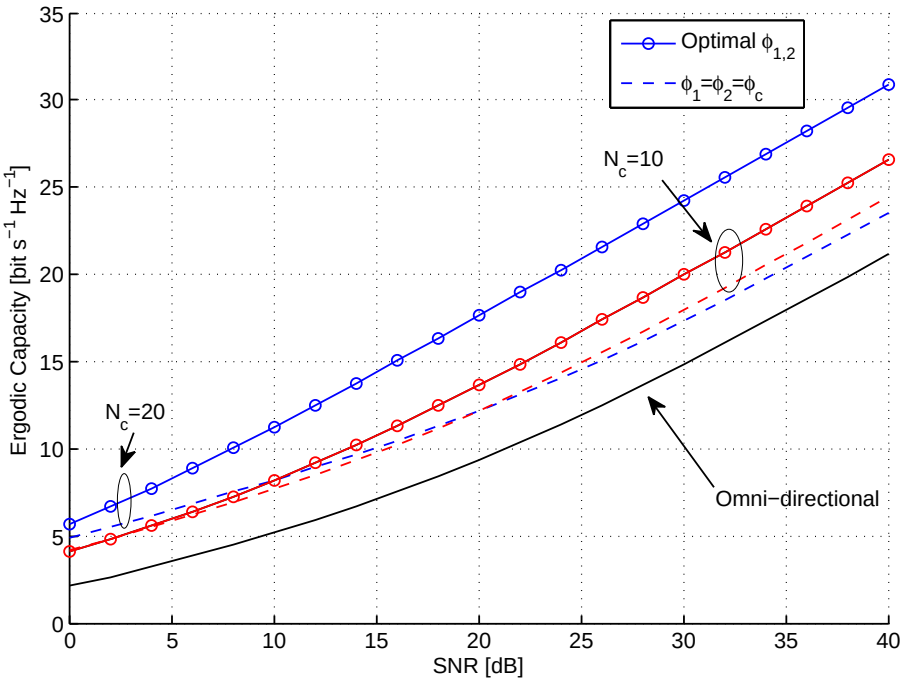

Figure 5.6 Ergodic channel capacity of a $(2, 2)$ MIMO system deploying dynamic radiation patterns using CRLH-LWA. The circled line gives the maximum ergodic capacity with optimal radiation pattern directions. The dotted line gives the ergodic capacity with radiation pattern directions aiming to the cluster mean angle to maximize the power gain.

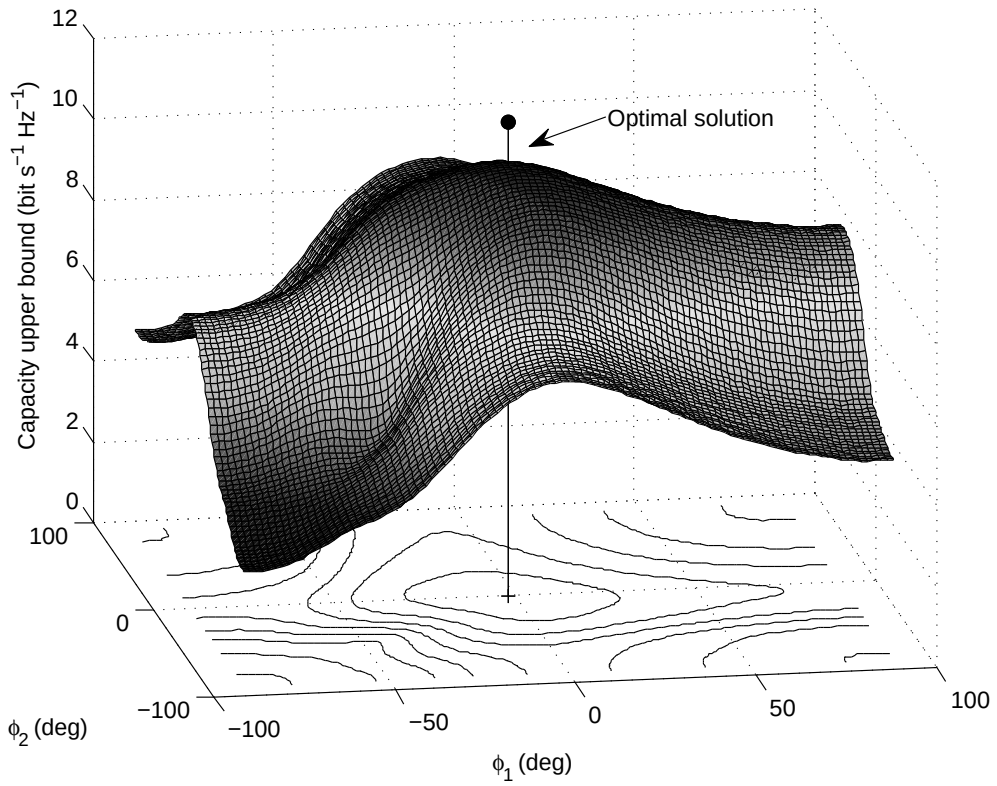

Figure 5.7 Searching radiation pattern directions that maximize the ergodic channel capacity of a $(2, 2)$ SPS-MIMO using two 8-cell CRLH-LWA's. SNR=10 dB.

that there exists two optimal solutions due to the symmetry of the problem). This motivates the utilization of $\phi_{1,2} = \phi_c \pm B$ as an heuristic solution.

The third simulation set shows how the CRLH-LWA antennas are used to maximize channel capacity in channels with more clusters and more antennas. In Fig. 5.9, we assume a 2-cluster MIMO channel, with mean angles $\phi_{c,1} = 0°$, $\phi_{c,2} = 60°$ and equal angle spread $\sigma_c = 15°$ for both clusters. For the $(2, 2)$ MIMO system, we steer the direction of each CRLH-LWA to a cluster mean angle to maximize the power gain. However, since the two clusters are separated far enough, the decorrelation gain is not significant. For the $(4, 4)$ MIMO system, the four directional antennas are partitioned into two groups to deal with the two clusters using the algorithm proposed in the previous section. The simulated ergodic capacity shows that about 9 bits/Hz/s capacity gain can be achieved at SNR=15 dB using 20-cell CRLH-LWA's for the $(4, 4)$ case.

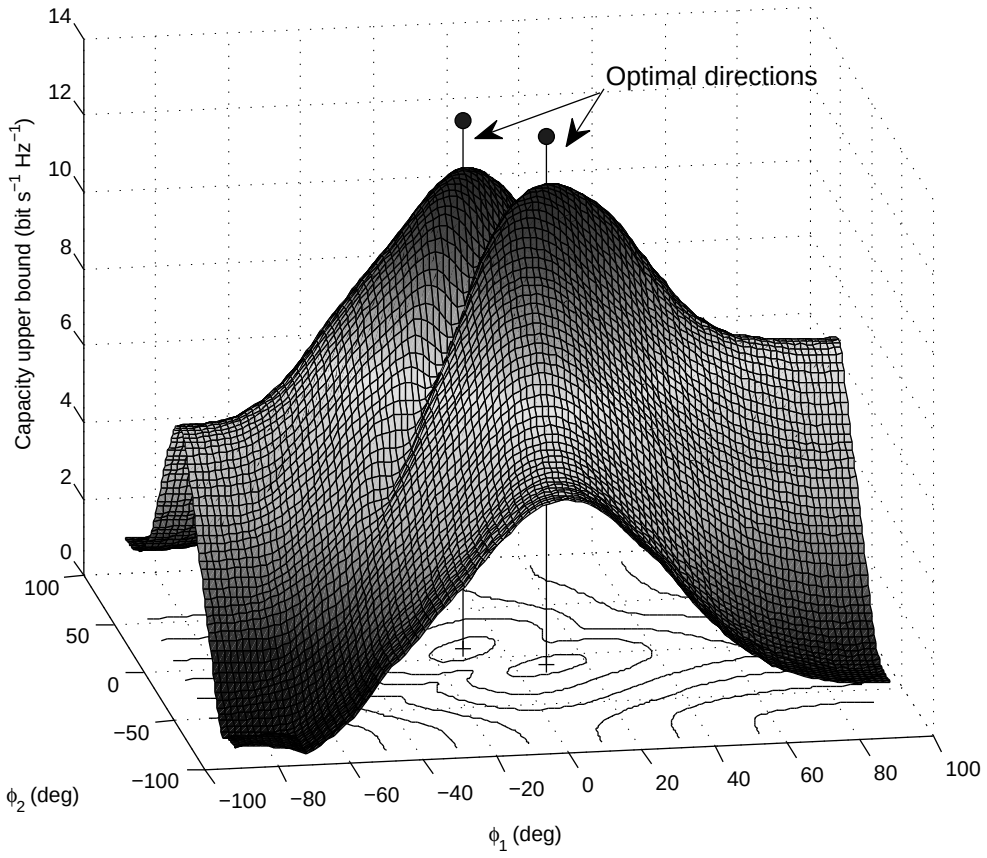

Figure 5.8 Searching radiation pattern directions that maximize the ergodic channel capacity of a $(2, 2)$ SPS-MIMO using two 20-cell CRLH-LWA's. SNR=10 dB.

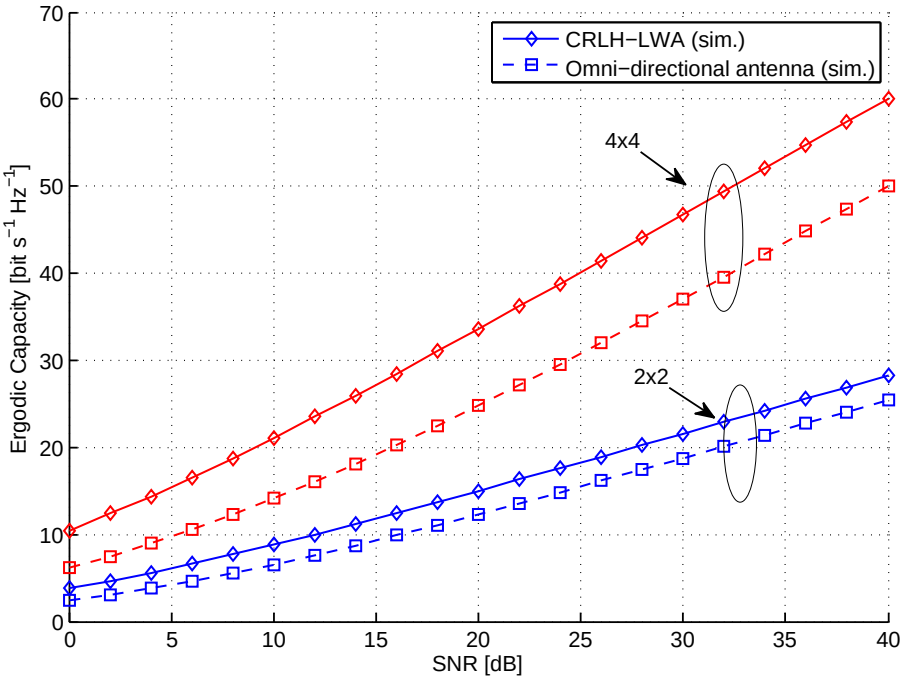

Figure 5.9 Ergodic channel capacity of a two-cluster MIMO channel using 20-cell CRLH-LWA's at the receiver and omni-directional antennas at the transmitter. The mean angles are $\phi_c = [0°, 60°]$ and the angle spreads are $\sigma_c = [15°, 15°]$.

5.5 Chapter Summary

In this chapter, we have studied the ergodic capacity performance of MIMO systems with dynamic radiation patterns in a clustered channel. Both analytical and simulation results show that the MIMO channel capacity benefits from high directivity of the radiation pattern and obtains a power gain. Furthermore, the channel capacity also takes advantage from the direction-steerable feature that matches the distribution of the propagation power to help decorrelating the clustered channel. Simulation indicates that, by using CRLH-LWA's, the ergodic channel capacity of a $(2, 2)$ MIMO system can be at least doubled at low SNR by steering the radiation patterns to proper directions. Searching methods for the statistical optimal directions are also proposed in this chapter. We also showed by theoretical analysis and simulations that aiming all the radiation patterns to the cluster mean angle can be a near optimal solution if the radiation pattern has a wide beam.

CHAPTER 6

PS-MIMO SYSTEMS WITH INSTANTANEOUS SELECTION

MIMO systems are capable of increasing data transmission rates and/or improve the transmission reliability over fading channels by exploiting the created spatial subchannels. These spatial resources can be utilized under different circumstances. When the propagation channels are in deep fades, spatial subchannels can be used as diversity branches to transmit data replicas. Through combining the diversity branches, the probability for the system to suffer deep fades is significantly decreased. The spatial subchannels can be used to transmit multiple symbol streams in parallel, which is known as spatial multiplexing. Under this scenarios, the data rate is multiplied by the minimum of the number of transmitting and receiving antennas, over spatially uncorrelated channels.

Although theoretically promising, the above benefits are not guaranteed in real applications due to a few deficiencies of the MIMO systems. First, real propagation channels are usually correlated, which reduces the effective degree of freedom and the number of effective diversity branches. Second, the number of antennas is often limited by device dimensions. To overcome these limitations, researchers have recently proposed to deploy reconfigurable antennas at the transmit or/and receive side(s) of MIMO systems. Reconfigurable antennas are capable to be switched or tuned to produce a number of radiation patterns. This produces additional diversity branches in the angular domain and is able to increase the diversity order while full spatial multiplexing gain is maintained without adding more antennas.

In this chapter, the ergodic capacity of instantaneous PS-MIMO systems over spatially correlated Rayleigh fading channels is investigated. For every channel realization, the radiation patterns of the receiving antennas are selected to maximize the instantaneous channel capacity. We assume the spatial correlation can be separated between the transmitter and the receiver side. Perfect channel state information is assumed available at the receiver only. Our research methodology and contributions in this chapter are as follows. First, we analyze the diversity order of correlated IPS-MIMO. Next, an approximation to the ergodic channel capacity of IPS-MIMO with OSTBC coding is derived. Based on the approximated channel capacity, we present two selection algorithms and illustrate the possibility to achieve performance-cost trade-off. Then we evaluate the system performance of the proposed algorithms by numerical simulations.[1]

[1]Part of the work presented in this chapter was published in: X. Li and J.-F. Frigon, "Algorithms for

6.1 Diversity Order

6.1.1 Diversity Order of Conventional MIMO

We assume that the CSI is perfectly known at the receiver but unavailable at the transmitter. For MIMO systems with CSI at the receiver side only, it is reasonable to assume that the transmitting power is equally allocated among transmit antennas [2]. In this case, the instantaneous capacity of a MIMO channel is given by

$$C(\mathbf{H}) = \log_2 \det\left(\mathbf{I}_{N_r} + \frac{\gamma}{N_t}\mathbf{H}\mathbf{H}^H\right), \tag{6.1}$$

where $\mathbf{H}$ is the channel matrix, γ is the SNR per receive antenna [2]. The channel outage probability, the probability that the instantaneous channel capacity of a fading channel cannot support the target transmission rate r, is defined by

$$P_{out} = \Pr\left\{C(\mathbf{H}) < r\right\}. \tag{6.2}$$

Though the diversity order of a fading channel is usually defined by the average error rate, it has been proved that the outage probability is the best achievable average error rate. Therefore we adopt the definition of the diversity order by the asymptotic magnitude slope of the outage probability versus SNR in the log-log scale, i.e.

$$d = -\lim_{\gamma\to\infty} \frac{\log P_{out}}{\log \gamma}. \tag{6.3}$$

In order to evaluate the diversity order of instantaneous PS-MIMO systems, we start from the diversity order of the conventional (N_t, N_r) MIMO as the following.

Proposition 6.1. *Over a Rayleigh fading MIMO channel with arbitrary correlation, the cumulative distribution function (CDF) of the Frobenius norm square of the channel matrix* $\mathbf{H}$ *can be approximated by*

$$F_{\|\mathbf{H}\|_F^2}(x) \triangleq \Pr\{\|\mathbf{H}\|_F^2 \le x\} \approx \frac{x^{\mathrm{rank}(\mathbf{R})}}{(\mathrm{rank}(\mathbf{R}))!\prod_{n=1}^{\mathrm{rank}(\mathbf{R})}\lambda_n} \tag{6.4}$$

as $x \to 0^+$, *where* $\mathbf{R} = \mathbb{E}\left[\mathrm{vec}\,(\mathbf{H})\,\mathrm{vec}\,(\mathbf{H})^H\right]$ *is the channel correlation matrix, and* $\lambda_1, \ldots, \lambda_{\mathrm{rank}(\mathbf{R})}$ *are the non-zero eigenvalues of* $\mathbf{R}$.

pattern selection mimo systems over spatially correlated channels," in *Proc. IEEE International Conference on Communications (ICC'12).* 2012, pp. 3969–3973.

Proof. See Appendix A in which the asymptotic approximation of $F_{\|\mathbf{H}\|_F^2}(x)$ as $x \to 0^+$ over Nakagami-m fading channels is given in Eq. (A.10), which proves Proposition 6.1 as a special case when the Nakagami-m fading figure $m = 1$. □

Corollary 6.1. *Denote the channel matrix of the (N_t, N_r) MIMO system (without selection) by $\mathbf{H}$, the diversity order of the MIMO system over Rayleigh fading channels is equal to the rank of the channel correlation matrix*

$$d^{\text{MIMO}} = \text{rank}(\mathbf{R}), \tag{6.5}$$

where $\mathbf{R} = \mathbb{E}\Big[\text{vec}\,(\mathbf{H})\,\text{vec}\,(\mathbf{H})^H\Big]$. If $\mathbf{R}$ has full rank, the diversity order equals to

$$d^{\text{MIMO}} = N_t N_r. \tag{6.6}$$

Proof. Let $\lambda_1, \ldots, \lambda_M$ be non-zero eigenvalues of $\mathbf{H}\mathbf{H}^H$. Eq. (6.1) can then be expressed by

$$C(\mathbf{H}) = \log_2 \prod_{m=1}^{M} (1 + \frac{\gamma}{N_t}\lambda_m). \tag{6.7}$$

In order to evaluate the diversity order, we will bound the capacity outage probability using upperbounds and lowerbounds on the mutual information. First, applying the inequality between the geometric and arithmetic means to Eq. (6.7), we have the following mutual information upperbound

$$C(\mathbf{H}) \leq M \log_2 \left(1 + \frac{\gamma}{MN_t} \|\mathbf{H}\|_F^2\right). \tag{6.8}$$

Therefore, the first lowerbound of the channel outage probability for rate r is given by

$$\begin{aligned} P_{out}^{\text{MIMO}} &\geq \Pr\left(M \log_2(1 + \frac{\gamma}{MN_t} \|\mathbf{H}\|_F^2) < r\right) \\ &= F_{\|\mathbf{H}\|_F^2}\left(\frac{N_t M(2^{r/M} - 1)}{\gamma}\right) \end{aligned} \tag{6.9}$$

because $2^{r/M} - 1 > \frac{r}{M} \ln 2$, we have the second lowerbound of the channel outage probability

$$P_{out}^{\text{MIMO}} > F_{\|\mathbf{H}\|_F^2}\left(\frac{rN_t}{\gamma} \ln 2\right). \tag{6.10}$$

Second, using Taylor's expansion of the logarithm function, we obtain a lowerbound of the

mutual information, i.e.

$$\begin{aligned} C(\mathbf{H}) &= \sum_{m=1}^{M} \log_2(1 + \frac{\gamma}{N_t}\lambda_m) \\ &> \frac{\gamma}{N_t} \sum_{m=1}^{M} \lambda_m \\ &= \frac{\gamma}{N_t} \|\mathbf{H}\|_F^2 . \end{aligned} \tag{6.11}$$

Thus the outage probability for rate r is upper-bounded by

$$P_{out}^{\text{MIMO}} \leq F_{\|\mathbf{H}\|_F^2}\left(\frac{rN_t}{\gamma}\right). \tag{6.12}$$

Applying Eq. (6.9) and Eq. (6.12) to Eq. (6.3), the diversity order of (N_t, N_r) MIMO is bounded by

$$\lim_{\gamma\to\infty} \frac{\ln F_{\|\mathbf{H}\|_F^2}(\ln 2 \cdot rN_t/\gamma)}{\ln(1/\gamma)} \leq d^{\text{MIMO}} \leq \lim_{\gamma\to\infty} \frac{\ln F_{\|\mathbf{H}\|_F^2}(rN_t/\gamma)}{\ln(1/\gamma)}. \tag{6.13}$$

Eq. (6.5) is proved by applying Proposition 6.1 to the exponential approximation of $F_{\|\mathbf{H}\|_F^2}(x)$. □

In the following, we illustrate the diversity order of conventional MIMO systems in Rayleigh fading channels given in Corollary 6.1 and upper and lower bounds of the outage probability presented in Eq. (6.20), Eq. (6.10) and Eq. (6.12) by numerical simulations. We generate MIMO channel matrices by Weichselberger's unitary-independent-unitary model proposed in [51], i.e.,

$$\mathbf{H} = \mathbf{U}_r(\sqrt{\mathbf{\Omega}} \odot \mathbf{G})\mathbf{U}_r^T, \tag{6.14}$$

where $\mathbf{U}_t$ is the spatial eigenbasis at the transmitter side, $\mathbf{U}_r$ is the spatial eigenbasis at the receiver side, $\sqrt{\mathbf{\Omega}}$ is the element-wise square root of Weichselberger's coupling matrix $\mathbf{\Omega}$, and $\mathbf{G}$ is an independent and identically distributed (i.i.d.) random matrix with zero mean and unit variance elements. The elements of the coupling matrix, which are called the coupling coefficients, are the eigenvalues of the channel correlation matrix $\mathbf{R}$. The (m, n)-th coupling coefficient $[\mathbf{\Omega}]_{m,n}$ specifies the mean amount of energy that is coupled from the m-th eigenmode of the transmit side to the n-th eigenmode of the receive side, and the sum of all coupling coefficients is identical to the total channel power tr$\mathbf{R}$. In our simulations, we assume a MIMO system with 2 transmit antennas and 2 receive antennas. The Weichselberger's

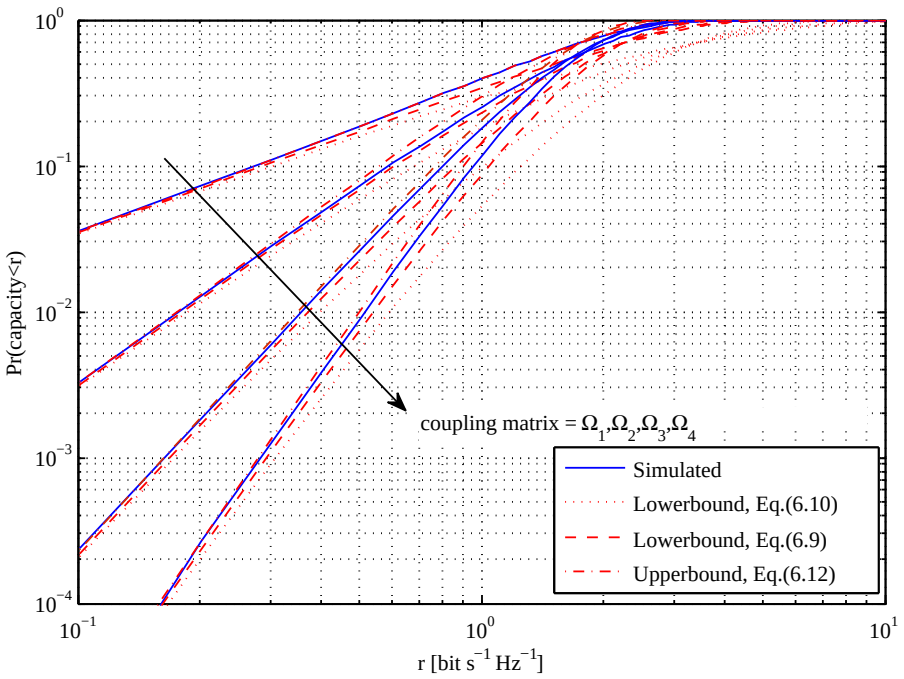

Figure 6.1 Simulated and bounds of the outage probability of $(2, 2)$ conventional MIMO systems over Rayleigh fading channels versus rate. $\gamma = 0$ dB.

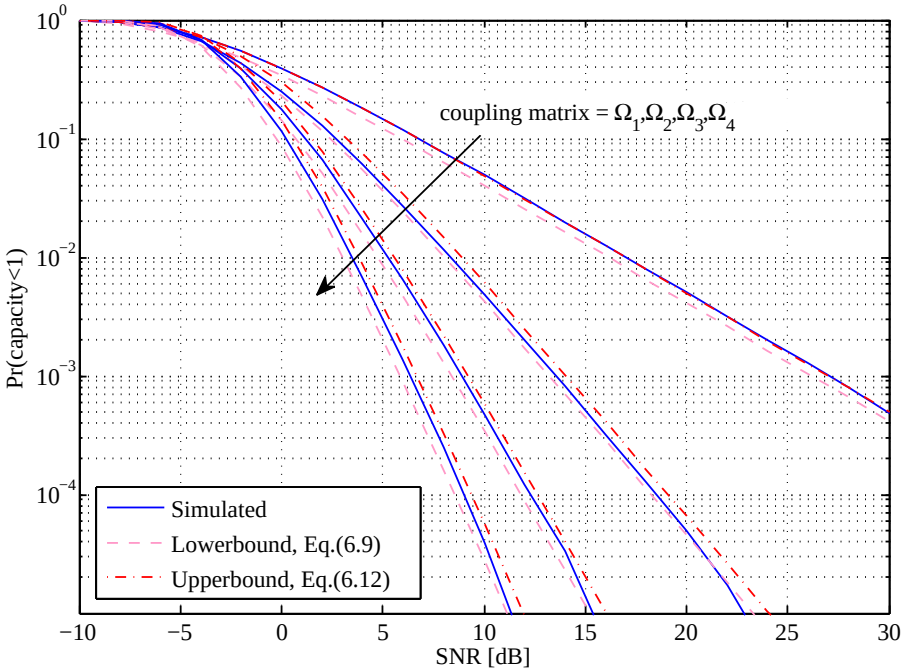

Figure 6.2 Simulated and bounds of the outage probability of $(2, 2)$ conventional MIMO systems over Rayleigh fading channels versus SNR. $r = 1$ bit/s/Hz.

coupling matrices selected for simulations are as follows,

$$\mathbf{\Omega}_1 = \begin{bmatrix} 4 & 0 \\ 0 & 0 \end{bmatrix}, \mathbf{\Omega}_2 = \begin{bmatrix} 3 & 0 \\ 0 & 1 \end{bmatrix}, \mathbf{\Omega}_3 = \begin{bmatrix} 2 & 1 \\ 0 & 1 \end{bmatrix}, \mathbf{\Omega}_4 = \begin{bmatrix} 1 & 1 \\ 1 & 1 \end{bmatrix}.$$

Since the entries of the Weichselberger's coupling matrix are the eigenvalues of the channel correlation matrix $\mathbf{R}$ [51], the rank of the correlation generating matrix is equal to the number of non-zero entries in the coupling matrix, i.e., the rank of the selected channel correlation matrix varies from 1 to 4.

In Fig. 6.1 and Fig. 6.2, we show the simulated and the derived bounds of the capacity outage probability versus rate and SNR, respectively. The simulations show that for both cases the outage probability is tightly bounded by the lowerbound Eq. (6.10) and the upperbound Eq. (6.12) in the small rate region and in the high SNR regime, respectively. The slope of each capacity CDF curve for small outage probability is, as indicated in Corollary 6.1, the rank of the channel correlation matrix. The lowerbound Eq. (6.9) is not as tight at high rate or low SNR but still provides the correct asymptotic slope for diversity order.

6.1.2 Diversity Order of IPS-MIMO

With the approach similar to the proof of Corollary 6.1, we derive the diversity order of the IPS-MIMO system as follows.

Corollary 6.2. *For the $(N_t|P_t, N_r|P_r)$ IPS-MIMO system over Rayleigh fading channels, the diversity order defined by Eq.* (6.3) *is equal to the rank of the correlation generating matrix* $\mathbf{R}_G = \mathbb{E}\Big[\mathrm{vec}\,(\mathbf{H}_G)\,\mathrm{vec}\,(\mathbf{H}_G)^H\Big]$, i.e.

$$d^{\mathrm{PS-MIMO}} = \mathrm{rank}(\mathbf{R}_G), \tag{6.15}$$

If $\mathbf{R}_G$ has full rank, the diversity order of the IPS-MIMO system is equal to the product of the numbers of antennas and the numbers of radiation patterns at the transmitter and the receiver:

$$d^{\mathrm{PS-MIMO}} = N_t N_r P_t P_r. \tag{6.16}$$

Proof. Assume a given generating channel $\mathbf{H}_G$. We select the channel state ψ_a which maximizes the instantaneous channel capacity of the IPS-MIMO system and select the channel

state ψ_b which maximizes the channel power of the IPS-MIMO system. Thus we have

$$C(\mathbf{H}_{\psi_b}) \leq C(\mathbf{H}_{\psi_a}) < C(\mathbf{H}_G) \tag{6.17}$$

and

$$\|\mathbf{H}_{\psi_a}\|_F^2 \leq \|\mathbf{H}_{\psi_b}\|_F^2 < \|\mathbf{H}_G\|_F^2. \tag{6.18}$$

We first start from Eq. (6.17) to find an upperbound of $C(\mathbf{H}_{\psi_a})$ and the lowerbound of $P_{out}^{\text{PS-MIMO}}$. Based on Eq. (6.8) and Eq. (6.17), we have

$$C(\mathbf{H}_{\psi_a}) < C(\mathbf{H}_G) < \tilde{M} \log_2 \left(1 + \frac{\gamma}{\tilde{M} N_t P_t} \|\mathbf{H}_G\|_F^2\right), \tag{6.19}$$

where $\tilde{M} = \text{rank}(\mathbf{R}_G)$. Similar to Eq. (6.9) and Eq. (6.10), the outage probability of the IPS-MIMO system for the rate r is lowerbounded by

$$P_{out}^{\text{PS}-\text{MIMO}} > F_{\|\mathbf{H}_G\|_F^2} \left(\frac{N_t P_t \tilde{M}(2^{r/\tilde{M}} - 1)}{\gamma}\right) \tag{6.20}$$

$$> F_{\|\mathbf{H}_G\|_F^2} \left(\frac{r N_t P_t}{\gamma} \ln 2\right) \tag{6.21}$$

In the following we find a lowerbound for the channel capacity of IPS-MIMO and the corresponding upperbound of the outage probability. Based on Eq. (6.8) and Eq. (6.18), we have

$$C(\mathbf{H}_{\psi_a}) > C(\mathbf{H}_{\psi_b}) > \frac{\gamma}{N_t} \|\mathbf{H}_{\psi_b}\|_F^2 \geq \frac{\gamma}{N_t P_t P_r} \|\mathbf{H}_G\|_F^2. \tag{6.22}$$

The upperbound of the outage probability is straightforward as follows

$$P_{out}^{\text{PS}-\text{MIMO}} < F_{\|\mathbf{H}_G\|_F^2} \left(\frac{r N_t P_t}{\gamma}\right). \tag{6.23}$$

The outage probability of the IPS-MIMO system of the target rate r is upperbounded and lowerbounded by

$$F_{\|\mathbf{H}_G\|_F^2} \left(\frac{r N_t P_t \ln 2}{\gamma}\right) < P_{out}^{\text{PS}-\text{MIMO}} < F_{\|\mathbf{H}_G\|_F^2} \left(\frac{r N_t P_t}{\gamma}\right). \tag{6.24}$$

The upperbound and lowerbound of $P_{out}^{\text{PS}-\text{MIMO}}$ have the identical exponential order $\text{rank}(\mathbf{R}_G)$,

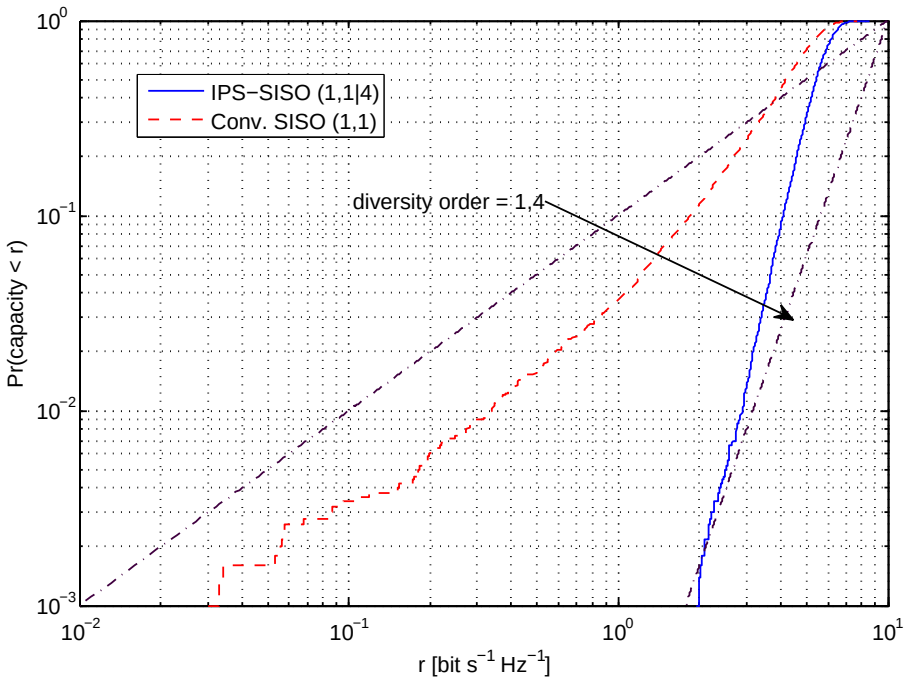

Figure 6.3 Simulated outage probability of a $(1, 1|4)$ IPS-SISO system with orthogonal radiation patterns versus rate. Ideal scattering at the transmitter and receiver. $\gamma = 0$ dB.

which proves Eq. (6.15). □

Corollary 6.2 suggests that IPS-MIMO systems are able to achieve higher diversity order by pattern selection comparing to conventional MIMO systems of the same antenna dimension. Specifically, the full rank IPS-MIMO increases its diversity order by P-fold comparing to the conventional MIMO system.

We use Monte-Carlo simulations to provide illustrations for Corollary 6.2. In Fig. 6.1 and Fig. 6.2, we show the simulated and the derived bounds of the capacity outage probability versus rate and SNR, respectively. The simulation shows that for both cases the capacity outage probability is tightly bounded by the lowerbound Eq. (6.10) and the upperbound Eq. (6.12) in the small rate region and in the high SNR regime, respectively. The slope of each capacity CDF curve for small outage probability is, as indicated by Corollary 6.1, the rank of the total arbitrary covariance matrix. The lowerbound Eq. (6.9) is not as tight at high rate or low SNR but still provides the correct asymptotic slope for diversity order.

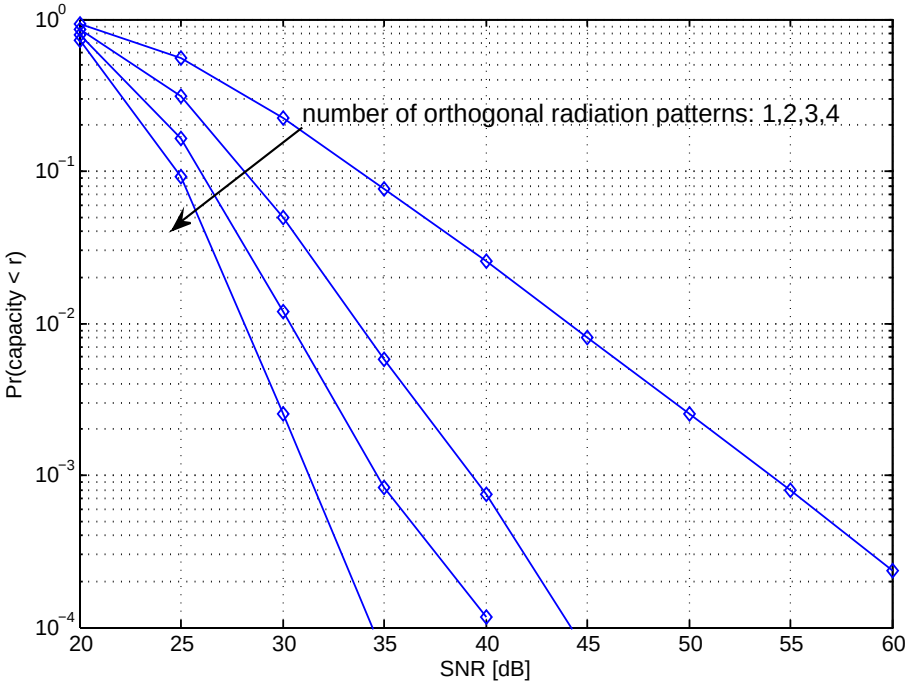

Figure 6.4 Impact of the number of orthogonal radiation states, P, per receive antenna, on the outage probability of $(1, 1|P)$ IPS-SISO versus SNR curves. Ideal scattering at the transmitter and receiver. $r = 8$ bit/s/Hz.

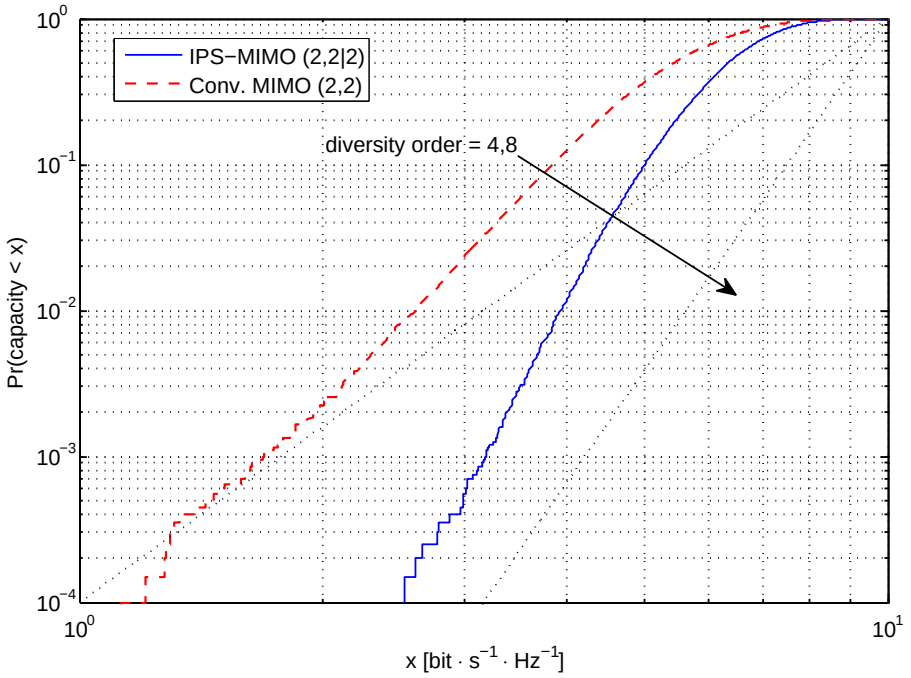

Figure 6.5 Simulated outage probability of a $(2, 2|2)$ IPS-MIMO versus SNR. ULA with half-wavelength spacing at the transmitter and receiver. Ideal scattering. $\gamma = 10$dB.

6.2 Capacity of IPS-MIMO with OSTBC

The instantaneous channel capacity of a MIMO system using OSTBC when the channel configuration is ψ is

$$C_{\psi}^{\text{OSTBC}} = \log_2\left(1 + \gamma\|\mathbf{H}_{\psi}\|_{\text{F}}^2\right) \tag{6.25}$$

where γ is the equivalent signal-to-noise ratio (SNR). The instantaneous channel capacity of IPS-MIMO with OSTBC (IPS-OSTBC) is the maximum of OSTBC channel capacities among all possible channel states

$$C^{\text{PS-OSTBC}} = \max_{\psi\in\Psi} C_{\psi}^{\text{OSTBC}}, \tag{6.26}$$

where Ψ is the complete set of all available pattern states.

In this section, we first introduce the exact ergodic channel capacity of OSTBC derived by Hamdi [52]. Then we extend Hamdi's method to the high oder and joint MGF cases to obtain the (co)variances of C_{ψ}^{OSTBC} ($\psi \in \Psi$). Since the distribution of channel capacity can be approximated by the Gaussian distribution, the channel capacity covariances are used in the rest of this section for approximating the mean channel capacity of the IPS-OSTBC with Clark's algorithm which is a good approximation to calculate the mean value of the maximum of correlated Gaussian variables.

6.2.1 Ergodic Capacity of Conventional OSTBC Systems

In this subsection, the exact ergodic capacity of conventional OSTBC systems are discussed and presented. This exact result will be used in future sections of this chapter as a basis for deriving the ergodic capacity of PS-OSTBC systems.

In [52], Hamdi notices that the ergodic capacity of a scalar channel is a conditional integral of $\log_2(1 + x)$. By representing the logarithm in an equivalent form in which x appears only as an exponent

$$\ln(1 + x) = \int_0^{\infty} \frac{1}{z}(1 - e^{-xz})e^{-z}dz \qquad (\text{for } x > 0), \tag{6.27}$$

Hamdi converts the ergodic capacity of an OSTBC system to a scalar integral of a function

related to the MGF of the squared Frobenius norm of the channel [52]

$$\begin{aligned}\mathbb{E}[C^{\text{OSTBC}}] &= \int_{\mathbb{C}^N}\int_0^\infty \frac{\log_2 e}{z}\left(1-e^{-\bar{\gamma}z\mathbf{h}^H\mathbf{h}}\right)e^{-z}f_{\mathbf{h}}(\mathbf{h})dzd\mathbf{h}\\ &= \log_2 e\int_0^\infty \frac{e^{-z}}{z}\left[\int_{\mathbb{C}^N}\left(1-e^{-\bar{\gamma}z\mathbf{h}^H\mathbf{h}}\right)f_{\mathbf{h}}(\mathbf{h})d\mathbf{h}\right]dz\\ &= \log_2 e\int_0^\infty \frac{e^{-z}}{z}\left[1-\mathcal{M}_{\|\mathbf{H}\|_{\text{F}}^2}(-\bar{\gamma}z)\right]dz, \end{aligned} \tag{6.28}$$

where $\mathbf{h}=\text{vec}\,(\mathbf{H})$ and $\bar{\gamma}$ is the SNR at the receiver side. Eq. (6.28) is a general result for any fading channel. In this chapter, only PS-OSTBC systems over Rayleigh fading channels are considered. Since the closed-form MGF of the squared Frobenius norm of Rayleigh fading channels is readily known, for a certain channel configuration ψ_n and the corresponding channel matrix $\mathbf{H}_{\psi_n}$, the MGF of $\|\mathbf{H}_\psi\|_{\text{F}}^2=\mathbf{h}_\psi^H\mathbf{h}_\psi$ is

$$\mathcal{M}_{\|\mathbf{H}_\psi\|_{\text{F}}^2}(s)=\mathbb{E}\left[e^{s\|\mathbf{H}_\psi\|_{\text{F}}^2}\right]=\frac{1}{\det(\mathbf{I}_N-s\mathbf{R}_{\psi_n})}. \tag{6.29}$$

From Eq. (6.28) and Eq. (6.29), the ergodic capacity of a PS-OSTBC system, with channel configuration ψ, over Rayleigh fading channels can be evaluated by numerically computing the scalar integral as the following

$$\mathbb{E}\left[C_\psi^{\text{OSTBC}}\right]=\log_2 e\int_0^\infty\frac{e^{-z}}{z}\left[1-\frac{1}{\det(\mathbf{I}_N+\bar{\gamma}z\mathbf{R}_\psi)}\right]dz. \tag{6.30}$$

In the following, we present two approaches for evaluating the improper integral in Eq. (6.30) to obtain the exact ergodic capacity of OSTBC systems. For the first approach, the improper integral in Eq. (6.30) is converted to a definite integral over $[0,1]$ by the change of variables. For the second approach, the improper integral in Eq. (6.30) is converted in terms of special functions.

Let $\zeta\triangleq\bar{\gamma}z$ and let

$$J(\zeta)\triangleq\frac{1}{\zeta}\left[1-\frac{1}{\det(\mathbf{I}_N+\zeta\mathbf{R}_\psi)}\right].$$

Eq. (6.30) is rewritten as

$$\mathbb{E}\left[C_\psi^{\text{OSTBC}}\right]=\log_2 e\int_0^\infty e^{-\zeta/\bar{\gamma}}J(\zeta)d\zeta. \tag{6.31}$$

Expand the rational fraction $J(\zeta)$ into partial fractions as

$$\begin{aligned} J(\zeta) &= \frac{1}{\zeta}\left[1 - \frac{1}{\prod_{k=1}^{K}(1+\tilde{\lambda}_k\zeta)^{M_k}}\right] \\ &= \sum_{k=1}^{K}\sum_{m_k=1}^{M_k}\frac{A_{k,m_k}}{(1+\tilde{\lambda}_k\zeta)^{m_k}} \end{aligned} \tag{6.32}$$

where $\tilde{\lambda}_1, \ldots, \tilde{\lambda}_K$ are the K distinct non-zero eigenvalues of $\mathbf{R}_\psi$, M_k is the order of the k-th non-zero eigenvalue $\tilde{\lambda}_k$ and A_{k,m_k} ($k = 1, \ldots, K$ and $m_k = 1, \ldots, M_k$) are the coefficients of the partial fractions. A_{k,m_k} is derived by

$$A_{k,m_k} = \frac{1}{\tilde{\lambda}_k^{M_k-m_k}(M_k-m_k)!}\frac{\partial^{M_k-m_k}}{\partial\zeta^{M_k-m_k}}\Big[(1+\tilde{\lambda}_k\zeta)^{M_k}J(\zeta)\Big]\Big|_{\zeta=-\tilde{\lambda}_k^{-1}}. \tag{6.33}$$

Substituting Eq. (6.32) to Eq. (6.31) and applying [53, Eq (34)], the ergodic channel capacity of the reconfigurable OSTBC system with the channel configuration ψ over Rayleigh fading environments is expressed by

$$\mathbb{E}\Big[C_\psi^{\mathrm{OSTBC}}\Big] = \bar{\gamma}\log_2 e\sum_{k=1}^{K}\sum_{m_k=1}^{M_k} A_{k,m_k}\,{}_2F_0(1, m_k; -\bar{\gamma}\tilde{\lambda}_k^{(\psi)}) \tag{6.34}$$

where ${}_2F_0(a, b; z)$ is a generalized hypergeometric function.[2]

As a special case, when the covariance matrix $\mathbf{R}_\psi$ has no multi-fold non-negative eigenvalues, $J(\zeta)$ can be rewritten as

$$\begin{aligned} J(\zeta) &= \frac{1}{\zeta}\left[1 - \frac{1}{\prod_{k=1}^{K}(1+\tilde{\lambda}_k\zeta)}\right] \\ &= \sum_{k=1}^{K}\frac{\bar{A}_k}{\zeta+\tilde{\lambda}_k^{-1}}, \end{aligned} \tag{6.35}$$

[2]The generalized hypergeometric function ${}_2F_0(a, b; z)$ is defined by

$${}_2F_0(a, b; z) \triangleq \sum_{k=0}^{\infty}\frac{(a)_k(b)_k z^k}{k!},$$

where $(x)_k \triangleq \prod_{n=1}^{k}(x+n-1)$. See [54].

where $\bar{A}_k$ can be obtained by the Matlab function RESIDUE. Thus, Eq. (6.31) becomes

$$\begin{aligned}\mathbb{E}\left[C_{\psi}^{\text{OSTBC}}\right] &= \log_2 e \int_0^{\infty} e^{-\zeta/\bar{\gamma}} \sum_{k=1}^{K} \frac{\bar{A}_k}{\zeta + \tilde{\lambda}_k^{-1}} d\zeta \\ &= \log_2 e \sum_{k=1}^{K} -\bar{A}_k e^{1/\bar{\gamma}\tilde{\lambda}_k} \text{Ei}\left(-\frac{1}{\tilde{\lambda}_k \bar{\gamma}}\right), \end{aligned} \tag{6.36}$$

where $\text{Ei}(x) \triangleq -\int_{-x}^{\infty} e^{-t}/t\, dt$ is the exponential integral [54], which is closely related to generalized hypergeometric functions. In this way, the integral in Eq. (6.31) is converted to a weighted sum of exponential integrals.

6.2.2 Gaussian Approximation to the Channel Capacity

The exact distribution of the MIMO channel capacity have been found for spatial multiplexing and diversity systems over Rayleigh fading channels. But for practical uses, these exact results involve complicated computations and are too complex. For our needs, approximating the capacity distribution by a real Gaussian distribution (*Gaussian approximation*) is more favorable. Gaussian approximation is a moment matching technique which only requires that the mean and variance be matched by the first two central moments of the channel capacity distribution. Its accuracy has been numerically and theoretically verified for both spatial multiplexing and diversity systems.

The *Gaussian approximation* of the MIMO channel capacity was first observed in [55] for spatial multiplexing systems over i.i.d. channels, and it is later extended to correlated cases for either spatial multiplexing or diversity MIMO systems. Later, Kamath *et al.* proved that the capacity distribution of spatial multiplexing MIMO over i.i.d. Rayleigh fading channels converges to a Gaussian distribution when the transmitting and receiving antenna numbers increase to infinity at a constant rate [56]. Hachem *et al.* proved that for fully correlated channels the capacity distribution is also asymptotically Gaussian for large dimensional MIMO systems [57]. This asymptotic convergence motivates the Gaussian approximation approach. For MIMO systems with limited number of antennas, Shin *et al.* have derived exact expressions of the first four orders of central moments of channel capacity, which are namely the mean, variance, skewness and kurtosis [53]. The skewness and excess kurtosis can measure the difference between the probability distribution function of the channel capacity and the approximated Gaussian distribution in terms of symmetry and flatness, respectively, and enable theoretical justification of Gaussian approximation. Calculated skewness and excess kurtosis show that Gaussian approximation is very accurate for most cases, and is still acceptable for highly correlated channels with as few as two antennas at both ends, operating at a

SNR regime lower than 30 dB, which is the region of interest for most wireless communication scenarios.

Gaussian approximation is also applicable to the capacity distribution of diversity MIMO systems such as OSTBC or MRC. Qian *et al.* has proved that the capacity distribution of OSTBC or MRC over i.i.d. Rayleigh fading channels is asymptotically Gaussian [58]. Perez *et al.* have proposed a framework to use Gaussian distribution to approximate the STBC capacity CDF of STBC systems with arbitrary correlation, as long as the mean and variance of the effective SNR is known [59]. The accuracy of Gaussian approximation of OSTBC capacity has been verified in aforementioned literatures either by numerical experiments or theoretical analysis.

Apparently, though, Gaussian approximation results in errors, especially in the tails of the capacity distribution. Therefore, in our analysis we only utilize the Gaussian approximation method to approximate the ergodic capacity in the cases in which the tail distribution of the capacity is not a major concern.

6.2.3 Expected Value of the Maximum of Correlated Gaussians

In 1961, Clark derived the exact joint distribution and the first four moments of two arbitrarily correlated real Gaussian randoms [60]. Assuming three correlated Gaussians, namely c_1, c_2 and c_3, with their mean values, variances and correlation coefficients known, Clark gave the mean and variance of the maximum of the first two Gaussians [60]:

$$\begin{aligned}\mathbb{E}[\max\{c_1,c_2\}] =& \mathbb{E}[c_1]\,\Phi(\alpha)+\mathbb{E}[c_2]\,\Phi(-\alpha)+a\varphi(\alpha),\\ \mathrm{Var}[\max\{c_1,c_2\}] =& \mathbb{E}\left[c_1^2\right]\Phi(\alpha)+\mathbb{E}\left[c_2^2\right]\Phi(-\alpha)\\ &+a\varphi(\alpha)\left(\mathbb{E}[c_1]+\mathbb{E}[c_2]\right)-\left(\mathbb{E}[\max\{c_1,c_2\}]\right)^2,\end{aligned} \tag{6.37}$$

where $\varphi(x)=\frac{1}{\sqrt{2\pi}}\exp(-\frac{x^2}{2})$ and $\Phi(x)=\int_{-\infty}^{x}\varphi(t)dt$ are the standard Gaussian density function and distribution function, respectively, and parameters a and α are given by

$$a=\sqrt{\mathrm{Var}[c_1]+\mathrm{Var}[c_2]-\rho_{12}\mathrm{Var}[c_1]\,\mathrm{Var}[c_2]}, \tag{6.38}$$

$$\alpha=\frac{\mathbb{E}[c_1]-\mathbb{E}[c_2]}{a}, \tag{6.39}$$

$$\rho_{12}=\frac{\mathrm{Cov}[c_1,c_2]}{\sqrt{\mathrm{Var}[c_1]\,\mathrm{Var}[c_2]}}. \tag{6.40}$$

By assuming the maximum of any pair of Gaussians is still Gaussian, Clark then proposed

an iterative process to evaluate the mean of the maximum of a finite set of Gaussian randoms by making use of the recursion

$$\max\{c_1, c_2, , c_3\} = \max\{\max\{c_1, c_2\}, c_3\}. \tag{6.41}$$

For each iteration, the covariance of the newly generated $\max\{c_1, c_2\}$ and other Gaussian randoms is updated by [60]

$$\mathrm{Cov}[\max\{c_1, c_2\}, c_3] \approx \mathrm{Cov}[c_1, c_3]\, \Phi(\alpha) + \mathrm{Cov}[c_2, c_3]\, \Phi(-\alpha). \tag{6.42}$$

6.2.4 Capacity Covariance of Two Correlated OSTBC

In Section 6.2.1, the exact expression of ergodic OSTBC capacity was discussed. To find the ergodic capacity of PS-OSTBC with Clark's algorithm, the variance and covariance of $C_{\psi}^{\mathrm{OSTBC}}$ ($\psi \in \Psi$) are required. However, the direct MGF method requires a double matrix integral, which is tedious to handle.

In Hamdi's method, Eq. (6.27) transforms the first moment of OSTBC capacity to a single integral of a function related to the MGF. By extending this idea to the multivariate case, the multivariate joint moments can be written as multidimensional scalar integrals with the integrands being functions related to the (joint) MGF's. Specifically for the bivariate case, the joint non-central moment $\mathbb{E}\left[C_{\psi_1}^{\mathrm{OSTBC}} C_{\psi_2}^{\mathrm{OSTBC}}\right]$ ($\psi_1, \psi_2 \in \Psi$) is a double scalar integral which is given by

$$\begin{aligned}
&\mathbb{E}\left[C_{\psi_1}^{\mathrm{OSTBC}} C_{\psi_2}^{\mathrm{OSTBC}}\right] \\
=&(\log_2 e)^2 \int_0^{\infty}\int_0^{\infty} \frac{e^{-(\zeta_1+\zeta_2)/\bar{\gamma}}}{\zeta_1\zeta_2} \\
&\times \left[1 - \mathcal{M}_{\|\mathbf{H}_{\psi_1}\|_{\mathrm{F}}^2}(-\zeta_1) - \mathcal{M}_{\|\mathbf{H}_{\psi_2}\|_{\mathrm{F}}^2}(-\zeta_2) + \mathcal{M}_{\|\mathbf{H}_{\psi_1}\|_{\mathrm{F}}^2, \|\mathbf{H}_{\psi_2}\|_{\mathrm{F}}^2}(-\zeta_1, -\zeta_2)\right] d\zeta_1 d\zeta_2
\end{aligned} \tag{6.43}$$

The covariance of $C_{\psi_1}^{\mathrm{OSTBC}}$ and $C_{\psi_2}^{\mathrm{OSTBC}}$ is defined by

$$\mathrm{Cov}\left[C_{\psi_1}^{\mathrm{OSTBC}}, C_{\psi_2}^{\mathrm{OSTBC}}\right] = \mathbb{E}\left[C_{\psi_1}^{\mathrm{OSTBC}} C_{\psi_2}^{\mathrm{OSTBC}}\right] - \mathbb{E}\left[C_{\psi_1}^{\mathrm{OSTBC}}\right] \mathbb{E}\left[C_{\psi_2}^{\mathrm{OSTBC}}\right]. \tag{6.44}$$

We substitute Eq. (6.43) and Eq. (6.30) into the definition of the OSTBC capacity covariance

Eq. (6.44), and obtain

$$\begin{aligned}
&\mathrm{Cov}\left[C_{\psi_1}^{\mathrm{OSTBC}}, C_{\psi_2}^{\mathrm{OSTBC}}\right] \\
=&(\log_2 e)^2 \int_0^\infty \int_0^\infty \frac{e^{-(\zeta_1+\zeta_2)/\bar{\gamma}}}{\zeta_1\zeta_2} \\
&\times \left[\mathcal{M}_{\|\mathbf{H}_{\psi_1}\|_{\mathrm{F}}^2,\|\mathbf{H}_{\psi_2}\|_{\mathrm{F}}^2}(-\zeta_1,-\zeta_2) - \mathcal{M}_{\|\mathbf{H}_{\psi_1}\|_{\mathrm{F}}^2}(-\zeta_1)\mathcal{M}_{\|\mathbf{H}_{\psi_2}\|_{\mathrm{F}}^2}(-\zeta_2)\right] d\zeta_1 d\zeta_2. \qquad (6.45)
\end{aligned}$$

To calculate Eq. (6.45), we need the expressions of the MGF's $\mathcal{M}_{\|\mathbf{H}_{\psi_1}\|_{\mathrm{F}}^2}$, $\mathcal{M}_{\|\mathbf{H}_{\psi_2}\|_{\mathrm{F}}^2}$ and $\mathcal{M}_{\|\mathbf{H}_{\psi_1}\|_{\mathrm{F}}^2,\|\mathbf{H}_{\psi_2}\|_{\mathrm{F}}^2}$ for Rayleigh fading channels. $\mathcal{M}_{\|\mathbf{H}_{\psi_1}\|_{\mathrm{F}}^2}$ and $\mathcal{M}_{\|\mathbf{H}_{\psi_2}\|_{\mathrm{F}}^2}$ have already been given in Eq. (6.29). In the following, we will derive $\mathcal{M}_{\|\mathbf{H}_{\psi_1}\|_{\mathrm{F}}^2,\|\mathbf{H}_{\psi_2}\|_{\mathrm{F}}^2}$.

First, without loss of generality, we assume two channel configuration states $\psi_1, \psi_2 \in \psi$. The corresponding channel vectors of these two channel configuration states are selected from the channel generating matrix by

$$\begin{aligned}
\mathbf{h}_1 &= \mathrm{vec}\left(\mathbf{S}(\psi_1)\mathbf{H}_G\right), \\
\mathbf{h}_2 &= \mathrm{vec}\left(\mathbf{S}(\psi_2)\mathbf{H}_G\right). \qquad (6.46)
\end{aligned}$$

The probability distribution of $\mathbf{h}_2$ conditioned to $\mathbf{h}_1$ is still multivariate complex Gaussian of the same dimension as that of $\mathbf{h}_1$ and $\mathbf{h}_2$, which yields [61, Theorem 2.2.5]

$$\mathbf{h}_2|\mathbf{h}_1 \sim \mathcal{CN}_{N_t N_r}\left(\mathbf{A}\mathbf{h}_1, \tilde{\mathbf{R}}_{2\cdot 1}\right), \qquad (6.47)$$

where the conditional mean is $\mathbf{h}_1$ left-multiplied by

$$\mathbf{A} = \mathbf{I}_{N_t} \otimes \left(\mathbf{R}_{21}\mathbf{R}_{11}^{-}\right), \qquad (6.48)$$

and the conditional variance matrix is

$$\begin{aligned}
\tilde{\mathbf{R}}_{2\cdot 1} &= \mathbf{R}_t \otimes \mathbf{R}_{r,2\cdot 1} \\
&= \mathbf{R}_t \otimes [\mathbf{R}_r(\psi_2,\psi_2) - \mathbf{R}_r(\psi_2,\psi_1)\mathbf{R}_r(\psi_1,\psi_1)^{-}\mathbf{R}_r(\psi_1,\psi_2)]. \qquad (6.49)
\end{aligned}$$

The superscript $(\cdot)^{-}$ in Eq. (6.48) and Eq. (6.49) is the generalized matrix inverse operator of the matrix. [3]

Next, by performing repeated integrals conditioned to $\mathbf{h}_2|\mathbf{h_1}$ and $\mathbf{h}_1$, successively, we

[3] A generalized inverse matrix of the matrix $\mathbf{A}$ is any matrix $\mathbf{A}^{-}$ such that $\mathbf{A}\mathbf{A}^{-}\mathbf{A} = \mathbf{A}$. See [62].

obtain

$$
\begin{aligned}
&\mathcal{M}_{\|\mathbf{H}_{\psi_1}\|_{\mathrm{F}}^2,\|\mathbf{H}_{\psi_2}\|_{\mathrm{F}}^2}(-s_1,-s_2) \\
&= \int_{\mathbb{C}^{N_t N_r}} e^{-s_1 \mathbf{h}_1^H \mathbf{h}_1} \left[\int e^{-s_2 \mathbf{h}_2^H \mathbf{h}_2} f_{\mathbf{h}_2|\mathbf{h}_1}(\mathbf{h}_2) d\mathbf{h}_2 \right] f_{\mathbf{h}_1}(\mathbf{h}_1) d\mathbf{h}_1 \\
&= \frac{1}{\pi^N \det(\mathbf{I}_N + s_2 \tilde{\mathbf{R}}_{2\cdot 1}) \det \tilde{\mathbf{R}}_{11}} \\
&\qquad \times \int_{\mathbb{C}^N} \exp\left(-s_1 \mathbf{h}_1^H \mathbf{h}_1 - s_2 \mathbf{h}_1^H \mathbf{A}^H (\mathbf{I}_N + s_2 \tilde{\mathbf{R}}_{2\cdot 1})^{-1} \mathbf{A} \mathbf{h}_1 - \mathbf{h}_1^H \tilde{\mathbf{R}}_{11}^{-1} \mathbf{h}_1 \right) d\mathbf{h}_1 \\
&= \frac{1}{\det\left[(\mathbf{I}_N + s_2 \tilde{\mathbf{R}}_{2\cdot 1})(\mathbf{I}_N + s_1 \tilde{\mathbf{R}}_{11} + s_2 \mathbf{A}^H (\mathbf{I}_N + s_2 \tilde{\mathbf{R}}_{2\cdot 1})^{-1} \mathbf{A} \tilde{\mathbf{R}}_{11}) \right]} \\
&= \frac{1}{\det\left(\mathbf{I}_N + s_1 \tilde{\mathbf{R}}_{\psi_1} + s_2 \tilde{\mathbf{R}}_{\psi_2} + s_1 s_2 [\tilde{\mathbf{R}}_{\psi_1} \tilde{\mathbf{R}}_{\psi_2} - (\mathbf{I}_N + s_1 \tilde{\mathbf{R}}_{\psi_1}) \tilde{\mathbf{R}}_{\psi_2 \psi_1} (\mathbf{I}_N + s_1 \tilde{\mathbf{R}}_{\psi_1})^{-1} \tilde{\mathbf{R}}_{\psi_1 \psi_2}] \right)}.
\end{aligned}
\tag{6.50}
$$

The third equation of Eq. (6.50) is derived directly from Eq. (6.47) and Eq. (6.30). See Appendix B for detailed derivation.

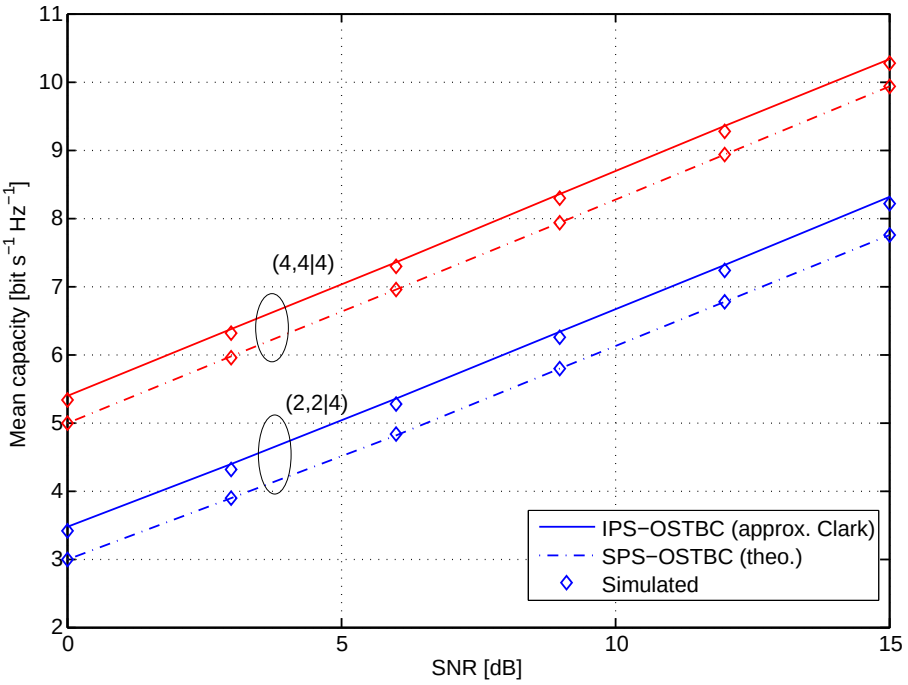

Figure 6.6 Approximated ergodic capacity of correlated IPS-OSTBC. The cluster configuration is TGn Model A. Each receive antenna can provide 4 radiation patterns with beamwidth=120°, equally spaced from 0° to 180°.

Finally, by substituting Eq. (6.50) and Eq. (6.29) into Eq. (6.43), we obtain the capacity

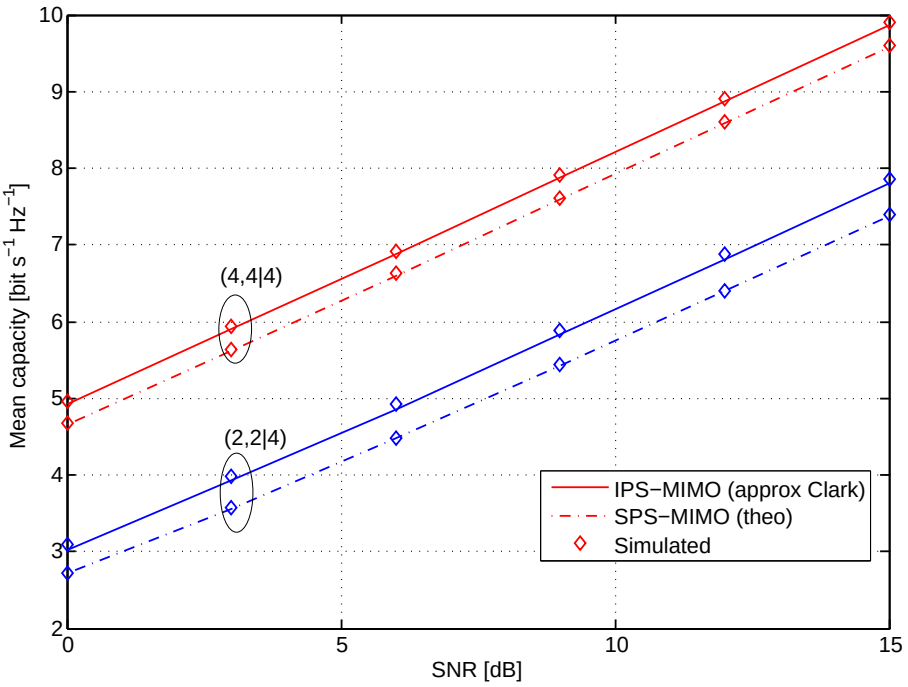

Figure 6.7 Approximated ergodic capacity of correlated IPS-OSTBC. The cluster configuration is TGn Model B. The deployed reconfigurable antennas are the same as Fig. 6.6.

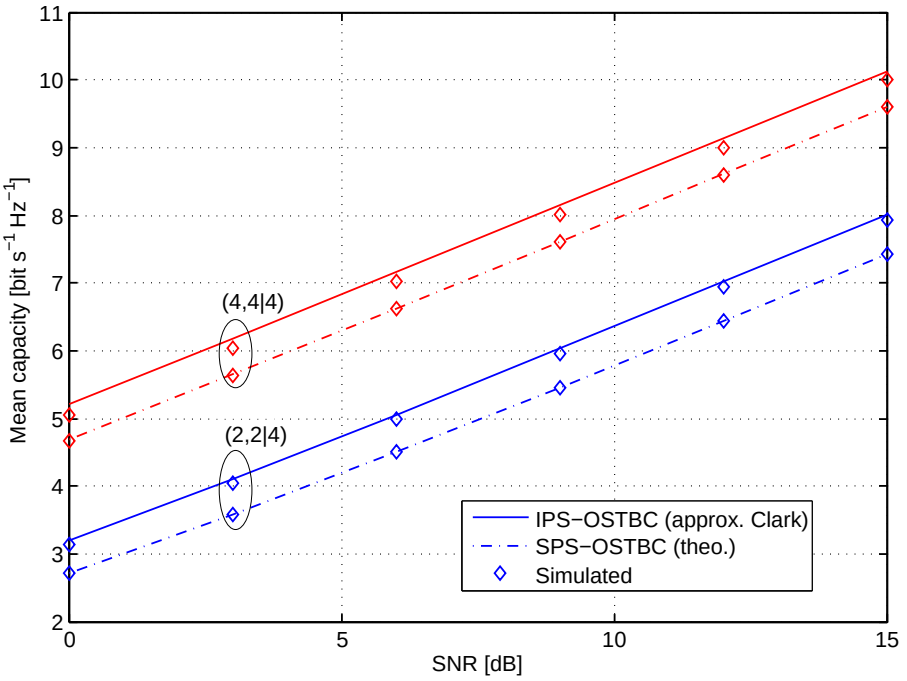

Figure 6.8 Approximated ergodic capacity of correlated IPS-OSTBC. The cluster configuration is TGn Model C. The deployed reconfigurable antennas are the same as Fig. 6.6.

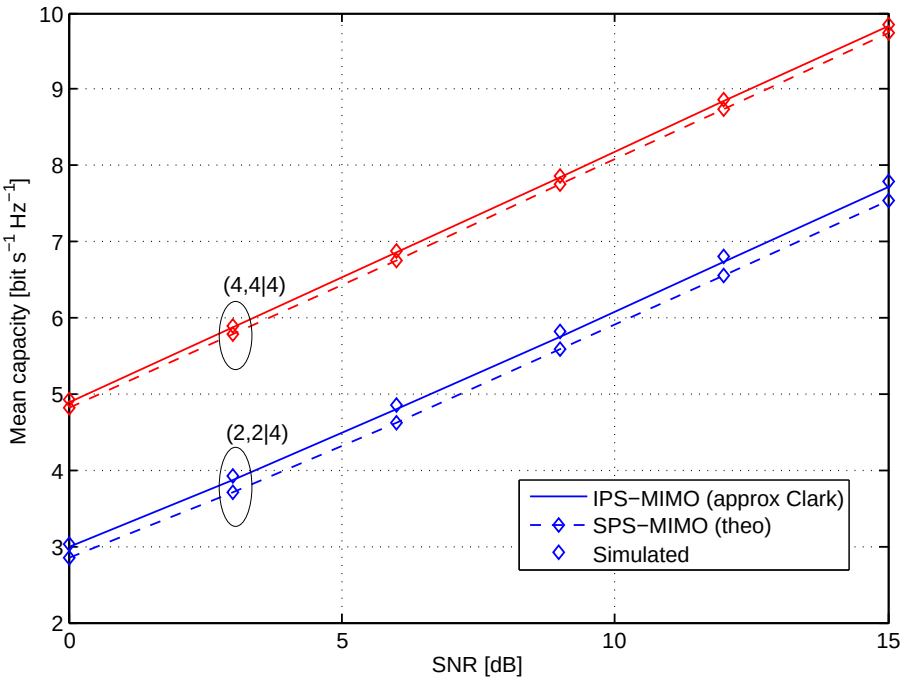

Figure 6.9 Approximated ergodic capacity of correlated IPS-OSTBC. The cluster configuration is TGn Model D. The deployed reconfigurable antennas are the same as Fig. 6.6.

correlation as the following

$$\begin{aligned}
&\mathbb{E}\left[C_{\psi_1}^{\text{OSTBC}} C_{\psi_2}^{\text{OSTBC}}\right] \\
&= (\log_2 e)^2 \int_0^\infty \int_0^\infty \frac{e^{-(\zeta_1+\zeta_2)/\bar{\gamma}}}{\zeta_1 \zeta_2} \\
&\times \left[\frac{1}{\det\left(\mathbf{I}_N + s_1\tilde{\mathbf{R}}_{\psi_1} + s_2\tilde{\mathbf{R}}_{\psi_2} + s_1 s_2[\tilde{\mathbf{R}}_{\psi_1}\tilde{\mathbf{R}}_{\psi_2} - (\mathbf{I}_N + s_1\tilde{\mathbf{R}}_{\psi_1})\tilde{\mathbf{R}}_{\psi_2\psi_1}(\mathbf{I}_N + s_1\tilde{\mathbf{R}}_{\psi_1})^{-1}\tilde{\mathbf{R}}_{\psi_1\psi_2}]\right)} \right. \\
&\left. +1 - \frac{1}{\det(\mathbf{I}_N + \zeta_1\tilde{\mathbf{R}}_{\psi_1})} - \frac{1}{\det(\mathbf{I}_N + \zeta_2\tilde{\mathbf{R}}_{\psi_2})} \right] d\zeta_1 d\zeta_2. \qquad (6.51)
\end{aligned}$$

And, by substituting Eq. (6.50) and Eq. (6.29) into Eq. (6.45), we obtain the OSTBC capacity

covariance as the following

$$\begin{aligned}
&\mathrm{Cov}\Big[C_{\psi_1}^{\mathrm{OSTBC}}, C_{\psi_2}^{\mathrm{OSTBC}}\Big] \\
&= (\log_2 e)^2 \int_0^\infty \int_0^\infty \frac{e^{-(\zeta_1+\zeta_2)/\bar{\gamma}}}{\zeta_1\zeta_2} \\
&\quad \times \Bigg[\frac{1}{\det\Big\{\mathbf{I}_N + s_1\tilde{\mathbf{R}}_{\psi_1} + s_2\tilde{\mathbf{R}}_{\psi_2} + s_1 s_2[\tilde{\mathbf{R}}_{\psi_1}\tilde{\mathbf{R}}_{\psi_2} - (\mathbf{I}_N + s_1\tilde{\mathbf{R}}_{\psi_1})\tilde{\mathbf{R}}_{\psi_2\psi_1}(\mathbf{I}_N + s_1\tilde{\mathbf{R}}_{\psi_1})^{-1}\tilde{\mathbf{R}}_{\psi_1\psi_2}]\Big\}} \\
&\qquad - \frac{1}{\det(\mathbf{I}_N + \zeta_1\tilde{\mathbf{R}}_{\psi_1})\det(\mathbf{I}_N + \zeta_2\tilde{\mathbf{R}}_{\psi_2})} \Bigg] d\zeta_1 d\zeta_2. \qquad (6.52)
\end{aligned}$$

By letting $\mathbf{R}_{\psi_1} = \mathbf{R}_{\psi_2} = \mathbf{R}_{\psi_1\psi_2} = \mathbf{R}_{\psi_2\psi_1}$ and substituting these equations into Eq. (6.52), the OSTBC capacity variance for the IPS-OSTBC system configured at ψ is directly obtained by

$$\begin{aligned}
\mathrm{Var}\Big[C_{\psi}^{\mathrm{OSTBC}}\Big] =& (\log_2 e)^2 \int_0^\infty \int_0^\infty \frac{e^{-(\zeta_1+\zeta_2)/\bar{\gamma}}}{\zeta_1\zeta_2} \\
&\times \left[\frac{1}{\det[\mathbf{I}_N + (\zeta_1+\zeta_2)\tilde{\mathbf{R}}_{\psi}]} - \frac{1}{\det(\mathbf{I}_N + \zeta_1\tilde{\mathbf{R}}_{\psi})\det(\mathbf{I}_N + \zeta_2\tilde{\mathbf{R}}_{\psi})} \right] d\zeta_1 d\zeta_2. \qquad (6.53)
\end{aligned}$$

Simulation

In the following, we present by numerical simulations the approximated mean capacity of a $(2, 2|4)$ IPS-MIMO system and a $(4, 4|4)$ IPS-MIMO system using OSTBC in 4 different spatial channel settings, namely, TGn A, TGn B, TGn C and TGn D [36]. The approximated mean capacity of IPS-MIMO with OSTBC is derived by Clark's algorithm. The mean, variance and correlation values of the capacity of all possible selections are calculated based on Eq. (6.30), Eq. (6.52) and Eq. (6.53). Each simulation is run with 1000 channel realizations. The simulated results in Fig. 6.6, Fig. 6.7, Fig. 6.8 and Fig. 6.9 indicate that the Clark's approximation is surprisingly accurate for various spatial channel configurations.

6.2.5 Approximating the Capacity Correlation Coefficients

For computing the mean capacity of a $(N_t, N_r|P)$ IPS-MIMO system, Clark's algorithm requires $P^{N_r} - 1$ capacity correlation coefficients, which would be computationally burdensome for systems with large P and N_r. In order to reduce the computational cost, we propose to use a simple approximation of the correlation coefficients in Clark's algorithm. The exact capacity covariance or correlation coefficient of MIMO systems is difficult to compute. For

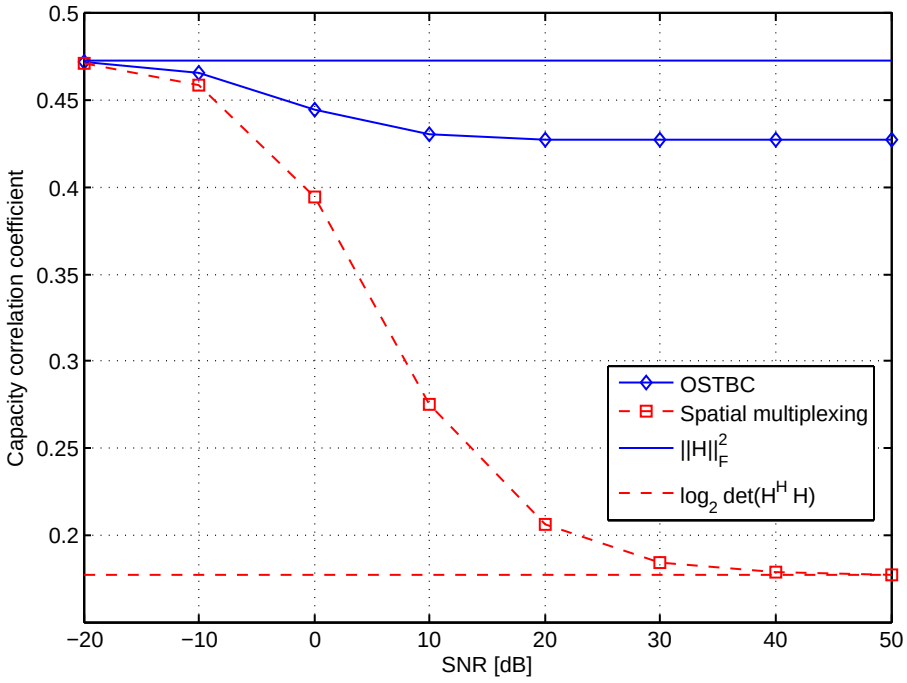

Figure 6.10 Impact of various approximations to the capacity correlation coefficient curves versus SNR.

MIMO systems using OSTBC, we can calculate the exact capacity covariance by Eq. (6.52). But when the size of Ψ, the set of channel configuration states, is too large, computing all the correlation pairs with numerical integrals is very time-consuming. Therefore, we propose to approximate the capacity correlation coefficient by an expression with lower computational costs.

Here, we examine three possible approximation methods to the channel capacity of MIMO systems using spatial multiplexing, and obtain the corresponding approximated capacity correlation coefficients. The channel capacity of spatial-multiplexing MIMO is given by

$$C^{\text{MIMO}}(\psi) = \log_2 \det(\mathbf{I} + \frac{\gamma}{N_r}\mathbf{H}_\psi^H \mathbf{H}_\psi).$$

And, the capacity correlation of spatial-multiplexing MIMO is

$$\rho(\psi_1, \psi_2) \triangleq \frac{\text{Cov}[C^{\text{MIMO}}(\psi_1), C^{\text{MIMO}}(\psi_2)]}{\sqrt{\text{Var}[C^{\text{MIMO}}(\psi_1)]\,\text{Var}[C^{\text{MIMO}}(\psi_1)]}}. \tag{6.54}$$

The first approximation to C^{MIMO} is a low SNR approximation

$$C^{\text{MIMO}} \approx \log_2(1 + \frac{\gamma}{N_r}\|\mathbf{H}\|_{\text{F}}^2).$$

The second approximation to C^{MIMO} is the approximation for the extreme low SNR

$$C^{\text{MIMO}} \approx (\log_2 e)\frac{\gamma}{N_r}\|\mathbf{H}\|_{\text{F}}^2.$$

Noticing that a linear transform does not change the correlation coefficient, the capacity correlation coefficient of MIMO channels configured to ψ_1 and ψ_2 can be approximated by

$$\rho(\psi_1, \psi_2) \approx \frac{\text{Cov}[\|\mathbf{H}_{\psi_1}\|_{\text{F}}^2, \|\mathbf{H}_{\psi_2}\|_{\text{F}}^2]}{\sqrt{\text{Var}[\|\mathbf{H}_{\psi_1}\|_{\text{F}}^2]\,\text{Var}[\|\mathbf{H}_{\psi_2}\|_{\text{F}}^2]}}. \tag{6.55}$$

The third approximation to C^{MIMO} is the high SNR approximation

$$C^{\text{MIMO}} \approx \log_2 \det(\frac{\gamma}{N_r}\mathbf{H}^H\mathbf{H}).$$

Fig. 6.10 shows how the correlation coefficient verses SNR for instantaneous capacity of a MIMO system system using spatial multiplexing with the low-SNR approximation and the high-SNR approximation of MIMO capacity, respectively. Numerical evaluations in Fig. 6.10 show that the exact and the three approximated capacity correlation coefficients do not vary significantly, which suggests that the approximated correlation coefficients may be used to replace the exact one in Clark's approximation method.

Furthermore, we notice that for highly correlated selections, the capacity correlation coefficients do not vary significantly either. Therefore, we place highly correlated selections in adjacent positions when ordering the selections in Clark's algorithm also helps to reduce the approximation error.

Next, we investigate IPS-MIMO systems using OSTBC. Similarly, in the low SNR regime, the instantaneous capacity using OSTBC of MIMO configured to ψ can be approximated by

$$C_{\psi}^{\text{OSTBC}} \approx (\bar{\gamma}\log_2 e)\|\mathbf{H}_{\psi}\|_{\text{F}}^2 \triangleq \hat{C}_{\psi}^{\text{OSTBC}}. \tag{6.56}$$

Therefore, we approximate $\rho_{\psi_1\psi_2}$, the correlation coefficient of $C_{\psi_1}^{\text{OSTBC}}$ and $C_{\psi_2}^{\text{OSTBC}}$, by $\hat{\rho}_{\psi_1\psi_2}$, the correlation coefficient of $\|\mathbf{H}_{\psi_1}\|_{\text{F}}^2$ and $\|\mathbf{H}_{\psi_2}\|_{\text{F}}^2$. We use the following lemma to find the moments generated by the joint MGF Eq. (6.50).

Lemma 6.1. *For any normal matrix $\mathbf{X} \in \mathbb{C}^N$, if its spectral radius $|\rho(\mathbf{X})| < 1$, the inverse*

of $\det(\mathbf{I}_N + \mathbf{X})$ *can be expanded as*

$$\det(\mathbf{I}_N + \mathbf{X})^{-1} = \sum_{m=0}^{\infty} \frac{1}{m!} \left[\sum_{k=1}^{\infty} \frac{(-1)^k}{k} \mathrm{tr}\mathbf{X}^k \right]^m . \tag{6.57}$$

Proof. Eq. (6.57) can be directly proved by applying the unitary diagonalization of $\mathbf{X}$ and making use of Taylor series expansions of the logarithm function and of the exponential function. Let $\lambda_1, \ldots, \lambda_N$ be the eigenvalues of $\mathbf{X}$.

$$\begin{aligned}
\det(\mathbf{I}_N + \mathbf{X})^{-1} &= \prod_{n=1}^{N} (1 + \lambda_n)^{-1} \\
&= \exp\left[- \sum_{n=1}^{N} \ln(1 + \lambda_n) \right] \\
&= \exp\left[\sum_{n=1}^{N} \sum_{k=1}^{\infty} \frac{(-1)^k}{k} \lambda_n^k \right] \\
&= \exp\left[\sum_{k=1}^{\infty} \frac{(-1)^k}{k} \mathrm{tr}\mathbf{X}^k \right] \\
&= \sum_{m=0}^{\infty} \frac{1}{m!} \left[\sum_{k=1}^{\infty} \frac{(-1)^k}{k} \mathrm{tr}\mathbf{X}^k \right]^m
\end{aligned}$$

Lemma 6.1 is proved. □

Truncating Eq. (6.57) to second order terms, we have

$$\det(\mathbf{I}_N + \mathbf{X})^{-1} = 1 - \mathrm{tr}\mathbf{X} + \frac{(\mathrm{tr}\mathbf{X})^2 + \mathrm{tr}\mathbf{X}^2}{2} + \text{high order terms.} \tag{6.58}$$

Substituting Eq. (6.58) to Eq. (6.50), we expand the joint MGF in the neighboring region around $(s_1, s_2) = (0, 0)$ into a polynomial of s_1 and s_2 as

$$\begin{aligned}
\mathcal{M}_{\|\mathbf{H}_{\psi_1}\|_{\mathrm{F}}^2, \|\mathbf{H}_{\psi_2}\|_{\mathrm{F}}^2}(-s_1, -s_2) = 1 &- s_1(\mathrm{tr}\tilde{\mathbf{R}}_{11}) - s_2(\mathrm{tr}\tilde{\mathbf{R}}_{11}) \\
&+ s_1^2 \frac{(\mathrm{tr}\tilde{\mathbf{R}}_{11})^2 + \mathrm{tr}\tilde{\mathbf{R}}_{11}^2}{2} + s_2^2 \frac{(\mathrm{tr}\tilde{\mathbf{R}}_{22})^2 + \mathrm{tr}\tilde{\mathbf{R}}_{22}^2}{2} \\
&+ s_1 s_2 (\mathrm{tr}\tilde{\mathbf{R}}_{11} \mathrm{tr}\tilde{\mathbf{R}}_{22} + \mathrm{tr}\tilde{\mathbf{R}}_{21}\tilde{\mathbf{R}}_{12}) \\
&+ \text{high order terms.}
\end{aligned}$$

We derive the first order and the second order moments about zero of $\|\mathbf{H}_{\psi_1}\|_{\mathrm{F}}^2$ and $\|\mathbf{H}_{\psi_2}\|_{\mathrm{F}}^2$ as

follows:

$$\begin{aligned}
&\mathcal{M}_1(0,0) = \mathrm{tr}\tilde{\mathbf{R}}_{11},\\
&\mathcal{M}_2(0,0) = \mathrm{tr}\tilde{\mathbf{R}}_{22},\\
&\mathcal{M}_{11}(0,0) = \mathrm{tr}\tilde{\mathbf{R}}_{11}^2 + (\mathrm{tr}\tilde{\mathbf{R}}_{11})^2,\\
&\mathcal{M}_{22}(0,0) = \mathrm{tr}\tilde{\mathbf{R}}_{22}^2 + (\mathrm{tr}\tilde{\mathbf{R}}_{22})^2,\\
&\mathcal{M}_{12}(0,0) = \mathrm{tr}\tilde{\mathbf{R}}_{11}\mathrm{tr}\tilde{\mathbf{R}}_{22} + \mathrm{tr}\tilde{\mathbf{R}}_{21}\tilde{\mathbf{R}}_{12}
\end{aligned}$$

Therefore, the mean and variance values, i.e., the first order and second order central moments, of $\|\mathbf{H}_{\psi_1}\|_{\mathrm{F}}^2$ and $\|\mathbf{H}_{\psi_2}\|_{\mathrm{F}}^2$ are

$$\begin{aligned}
&\mathbb{E}\Big[\|\mathbf{H}_{\psi_1}\|_{\mathrm{F}}^2\Big] = \mathcal{M}_1(0,0) = \mathrm{tr}\tilde{\mathbf{R}}_{11} = \mathrm{tr}\mathbf{R}_t\mathrm{tr}\mathbf{R}_{r,11},\\
&\mathbb{E}\Big[\|\mathbf{H}_{\psi_2}\|_{\mathrm{F}}^2\Big] = \mathcal{M}_2(0,0) = \mathrm{tr}\tilde{\mathbf{R}}_{22} = \mathrm{tr}\mathbf{R}_t\mathrm{tr}\mathbf{R}_{r,22},\\
&\mathrm{Var}\Big[\|\mathbf{H}_{\psi_1}\|_{\mathrm{F}}^2\Big] = \mathcal{M}_{11}(0,0) - \mathcal{M}_1^2(0,0) = \mathrm{tr}\tilde{\mathbf{R}}_{11}^2 = \mathrm{tr}\mathbf{R}_t^2\mathrm{tr}\mathbf{R}_{r,11}^2,\\
&\mathrm{Var}\Big[\|\mathbf{H}_{\psi_2}\|_{\mathrm{F}}^2\Big] = \mathcal{M}_{22}(0,0) - \mathcal{M}_2^2(0,0) = \mathrm{tr}\tilde{\mathbf{R}}_{22}^2 = \mathrm{tr}\mathbf{R}_t^2\mathrm{tr}\mathbf{R}_{r,22}^2,
\end{aligned} \tag{6.59}$$

respectively. And, the covariance of $\|\mathbf{H}_{\psi_1}\|_{\mathrm{F}}^2$ and $\|\mathbf{H}_{\psi_2}\|_{\mathrm{F}}^2$ is

$$\begin{aligned}
\mathrm{Cov}\Big[\|\mathbf{H}_{\psi_1}\|_{\mathrm{F}}^2, \|\mathbf{H}_{\psi_2}\|_{\mathrm{F}}^2\Big] &= \mathcal{M}_{12}(0,0) - \mathcal{M}_1(0,0)\mathcal{M}_2(0,0)\\
&= \mathrm{tr}\tilde{\mathbf{R}}_{12}\tilde{\mathbf{R}}_{21}\\
&= \mathrm{tr}\mathbf{R}_t^2\mathrm{tr}\mathbf{R}_{12}\mathbf{R}_{21}
\end{aligned} \tag{6.60}$$

Therefore in the low SNR regime, the mean and (co)variance of the capacity of the OSTBC system are approximated by

$$\begin{aligned}
&\mathbb{E}\Big[C_{\psi_1}^{\mathrm{OSTBC}}\Big] \approx \mathbb{E}\Big[\hat{C}_{\psi_1}^{\mathrm{OSTBC}}\Big] = (\bar{\gamma}\log_2 e)\mathrm{tr}\tilde{\mathbf{R}}_{11},\\
&\mathbb{E}\Big[C_{\psi_2}^{\mathrm{OSTBC}}\Big] \approx \mathbb{E}\Big[\hat{C}_{\psi_2}^{\mathrm{OSTBC}}\Big] = (\bar{\gamma}\log_2 e)\mathrm{tr}\tilde{\mathbf{R}}_{22},\\
&\mathrm{Var}\Big[C_{\psi_1}^{\mathrm{OSTBC}}\Big] \approx \mathrm{Var}\Big[\hat{C}_{\psi_1}^{\mathrm{OSTBC}}\Big] = (\bar{\gamma}\log_2 e)^2\mathrm{tr}\tilde{\mathbf{R}}_{11}^2,\\
&\mathrm{Var}\Big[C_{\psi_2}^{\mathrm{OSTBC}}\Big] \approx \mathrm{Var}\Big[\hat{C}_{\psi_2}^{\mathrm{OSTBC}}\Big] = (\bar{\gamma}\log_2 e)^2\mathrm{tr}\tilde{\mathbf{R}}_{22}^2,\\
&\mathrm{Cov}\Big[C_{\psi_1}^{\mathrm{OSTBC}}, C_{\psi_2}^{\mathrm{OSTBC}}\Big] \approx \mathrm{Cov}\Big[\hat{C}_{\psi_1}^{\mathrm{OSTBC}}, \hat{C}_{\psi_2}^{\mathrm{OSTBC}}\Big] = (\bar{\gamma}\log_2 e)^2\mathrm{tr}\tilde{\mathbf{R}}_{12}\tilde{\mathbf{R}}_{21}.
\end{aligned}$$

In the next step, we approximate the capacity correlation coefficient $\rho(\psi_1, \psi_2)$ by

$$\begin{aligned}\rho(\psi_1,\psi_2) &\triangleq \frac{\mathrm{Cov}\left[C_{\psi_1}^{\mathrm{MIMO}}, C_{\psi_2}^{\mathrm{MIMO}}\right]}{\sqrt{\mathrm{Var}\left[C_{\psi_1}^{\mathrm{MIMO}}\right]\mathrm{Var}\left[C_{\psi_2}^{\mathrm{MIMO}}\right]}} \\ &\approx \frac{\mathrm{Cov}\left[\hat{C}_{\psi_1}^{\mathrm{OSTBC}}, \hat{C}_{\psi_2}^{\mathrm{OSTBC}}\right]}{\sqrt{\mathrm{Var}\left[\hat{C}_{\psi_1}^{\mathrm{OSTBC}}\right]\mathrm{Var}\left[\hat{C}_{\psi_2}^{\mathrm{OSTBC}}\right]}} \\ &= \frac{\mathrm{tr}\tilde{\mathbf{R}}_{21}\tilde{\mathbf{R}}_{12}}{\sqrt{\mathrm{tr}\tilde{\mathbf{R}}_{11}^2\mathrm{tr}\tilde{\mathbf{R}}_{22}^2}} \\ &\triangleq \hat{\rho}(\psi_1,\psi_2), \end{aligned} \tag{6.61}$$

which significantly reduces the computational cost comparing to calculating the double integral for $\rho(\psi_1, \psi_2)$.

6.3 Capacity of IPS-MIMO with Spatial Multiplexing

In the previous section we proved that the maximum achievable diversity order of a pattern selection MIMO system is the rank of the total correlation matrix of the full system. In this section we propose two algorithms to select radiation patterns for the IPS-MIMO based on the instantaneous channel realization to provide capacity and diversity gains.

6.3.1 Incremental Radiation Pattern Selection

$\mathbf{Q} := \gamma\mathbf{I}_{N_t}$;
$\mathcal{N} := \{1, 2, \cdots, N_r P\}$;
$p_1^* := \arg\max_{l\in\mathcal{N}} \|\mathbf{e}_l^T\mathbf{H}\|_F^2$;
for $n = 1$ *TO* $N_r - 1$ **do**
  $\mathcal{N} := \mathcal{N} - \{P\lceil p_n/P\rceil - P + 1, \cdots, P\lceil p_n/P\rceil\}$;
  $\mathbf{h} := \mathbf{H}^H\mathbf{e}_{p_n}$;
  $\mathbf{Q} := \mathbf{Q} - \mathbf{Q}\mathbf{h}(1 + \mathbf{h}^H\mathbf{Q}\mathbf{h})^{-1}\mathbf{h}^H\mathbf{Q}$;
  $p_{n+1}^* := \arg\max_{l\in\mathcal{N}} \mathbf{e}_l^T\mathbf{H}\mathbf{Q}\mathbf{H}^H\mathbf{e}_l$;
end

Algorithm 6.1 Incremental radiation pattern selection

It is straightforward to perform an exhaustive search to find the radiation patterns ψ^*

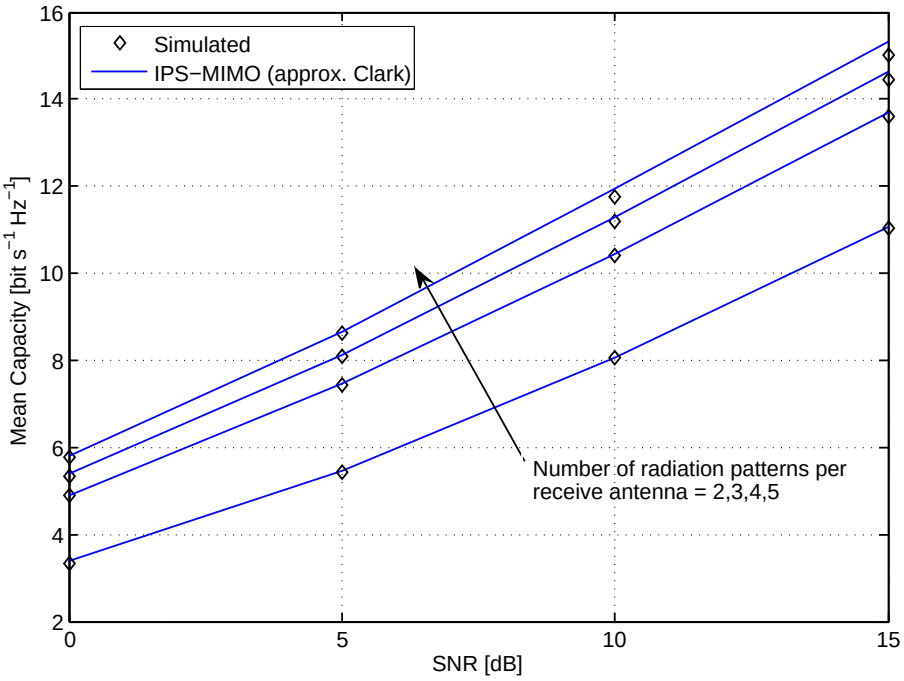

Figure 6.11 Approximated ergodic capacity of correlated IPS-MIMO

to maximize instantaneous channel capacity,

$$\psi^* = \arg\max_{\psi \in \mathbf{\Pi}} C(\mathbf{H}_\psi). \tag{6.62}$$

But this requires channel estimation for $N_r P$ receive branches and $\binom{N_r P}{N_r}$ determinant calculations. In Fig. 6.11, we present a numerical simulation of IPS-MIMO channel capacity and the theoretical approximation by Clark's method. The spatial channel for the simulation is a TGn A model with a single cluster and the radiation patterns are uniformly separated from 0° to 180° with a varying pattern number fro 2 to 5. The simulation indicates that the channel capacity of the IPS-MIMO tends to saturate when the number of radiation patterns increases, which suggests that some radiation pattern branches may not contribute much to the channel capacity.

Inspired by the incremental selection algorithm for antenna selection MIMO systems in [63], we propose the incremental radiation pattern selection algorithm for IPS-MIMO to reduce determinant calculations. We select the radiation pattern for N_r receive antennas in N_r steps. At the n-th step, we select the radiation pattern p_n^* that maximizes the instantaneous

channel capacity for the selected (N_t, n) MIMO system,

$$p_n^* = \arg \max_{p_n \in \{\text{remaining patterns}\}} C(\mathbf{H}_{(p_1^*,\ldots,p_{n-1}^*,p_n)}) \tag{6.63}$$

and remove $P-1$ rows corresponding to other patterns of this antenna from the full channel matrix $\mathbf{H}$. Notice that n is not the index of receive antenna but the order for this antenna to perform pattern selection. Applying the matrix inversion lemma, the incremental selection algorithm is further simplified in Alg. 6.1.

6.3.2 Subset Radiation Pattern Selection

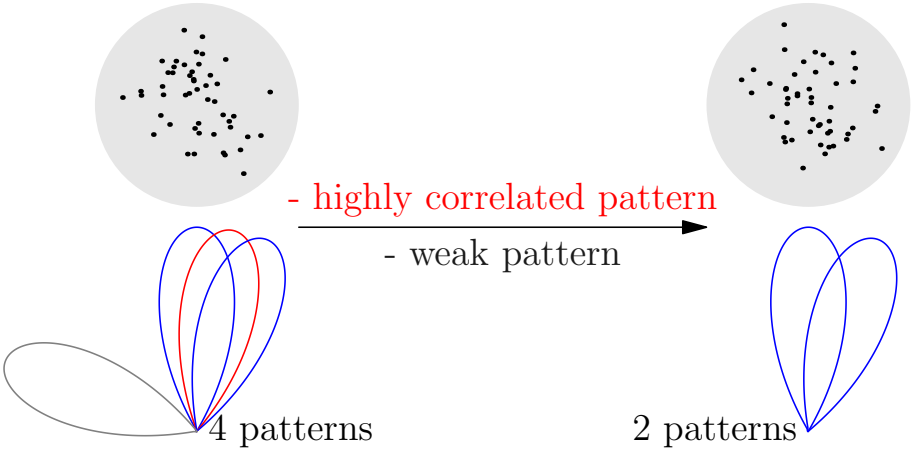

Figure 6.12 Example of the subset selection of radiation patterns. Radiation patterns corresponding to weak or highly-correlated branches are removed.

In a poor scattering propagation environment, the signal power is transmitted within limited directions and some of the radiation pattern branches are too weak to support a diversity branch. Furthermore, strong radiation pattern branches may be highly dependent and the differences between the branches are not significant enough to provide distinct diversity. Also, the incremental selection algorithm proposed in the previous section cannot reduce the channel estimation costs. For instance, the number of radiation pattern branches of a $(N_t, N_r|P)$ IPS-MIMO system is N_r^P, which may require a very long training sequence for large P to estimate the channel response and is prohibitive to implement. Noticing that for spatially correlated channels the diversity order of IPS-MIMO asserted by Corollary 6.2 cannot be achieved in the moderate SNR range, we propose to reduce the number of radiation pattern branches by temporarily inactivating branches which are too weak or highly correlated based on the channel correlation matrix, as illustrated in Fig. 6.12.

In this proposed *subset radiation pattern selection algorithm*, the activated radiation pattern branches are selected based on the long-term statistics of the propagation environment. We assume the PAS at the receive side is known to the receiver by covariance estimation techniques and the receive correlation matrix of all diversity branches can be calculated. We use the capacity correlation coefficient defined in quantify the cross-correlation between different selections by the *cross-correlation measure*.

Definition For the receive correlation matrix of the full system $\mathbf{R}_r$, the cross-correlation measure between two given pattern index vectors ψ_1 and ψ_2 is defined by

$$\varrho(\psi_1, \psi_2) = \frac{\mathrm{tr}\tilde{\mathbf{R}}_{21}\tilde{\mathbf{R}}_{12}}{\sqrt{\mathrm{tr}\tilde{\mathbf{R}}_{11}^2 \mathrm{tr}\tilde{\mathbf{R}}_{22}^2}}. \tag{6.64}$$

Note that $\varrho(\psi_1, \psi_2) = 0$ if and only if $\mathbf{R}_r(\psi_1, \psi_2)$ is a zero matrix which means no cross-correlation exists. $\varrho(\psi_1, \psi_2) = 1$ if $\psi_1 = \psi_2$ and $\mathbf{R}_r(\psi_1, \psi_1)$ has only one non-zero entry on its diagonal, which exhibits the strongest correlation.

$\Pi' := \emptyset$
for $l = 1$ *TO* L **do**
  $\psi^* := \arg\max_{\psi \in \mathbf{\Pi}} \det(\mathbf{R}_r(\psi, \psi))$;
  $\Pi' := \Pi' + \{\psi^*\}$;
  $\mathbf{\Pi} := \mathbf{\Pi} - \{\psi \in \mathbf{\Pi} | \hat{\rho}(\psi^*, \psi) > \alpha\}$;
  if $\mathbf{\Pi} = \emptyset$ **then**
    break;
  end
end
$\psi := \arg\max_{\psi \in \Pi'} C(\mathbf{H}_\psi)$;

Algorithm 6.2 Subset radiation pattern selection

We propose a subset radiation pattern selection algorithm for IPS-MIMO systems based on cross-correlation measure in Alg. 6.2. L is the maximal number of active radiation patterns for selection at each antenna and α a threshold for eliminating highly correlated branches. The last step in Alg. 6.2 can be replaced by Alg. 6.1 in favor of fast selection.

6.3.3 Numerical Results

We investigate the capacity performances of the IPS-MIMO system in the rich scattering environment and the poor scattering environment by numerical simulations.

In Fig. 6.13, the capacity CDF is plotted for a $(2, 2|4)$ IPS-MIMO system with capacity maximizing selection and the incremental selection algorithm in a rich scattering environ-

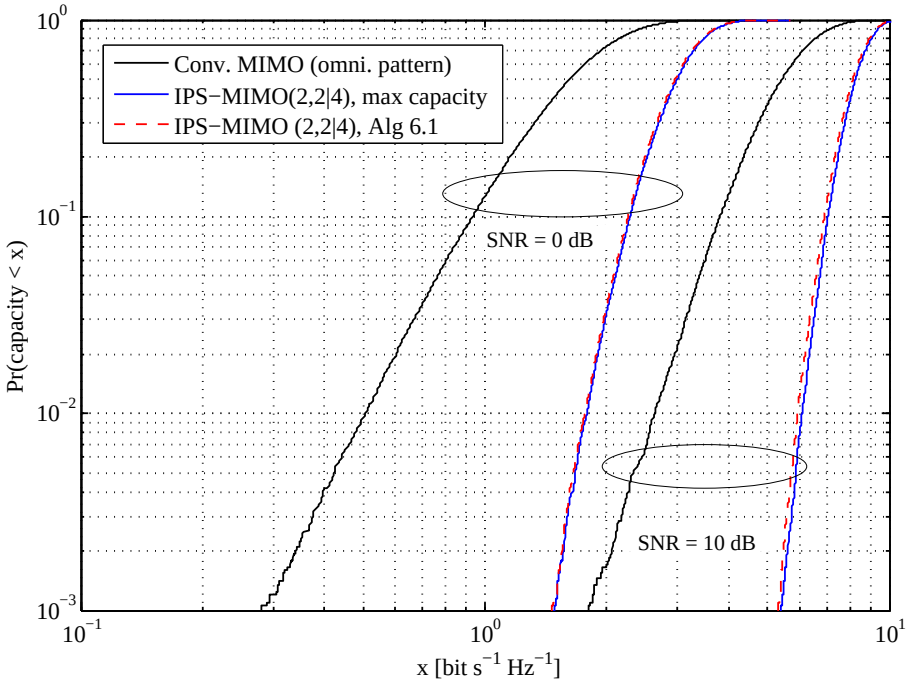

Figure 6.13 Channel capacity CDF of a $(2, 2|4)$ IPS-MIMO system. The antennas are surrounded by ideal scattering environments and separated by half wavelength.

ment. The radiation patterns at each receive antenna can be steered to 0°, 60°, 120° or 180° with pattern beamwidth 90°. The capacity CDF shows that IPS-MIMO is able to provide additional diversity gain and improve channel capacity. The results of the incremental selection algorithm almost approach the maximal capacity. Though the propagation environment is rich scattering, the overlapping radiation patterns still cause correlation. This correlated IPS-MIMO system cannot achieve the diversity order of $N_t N_r P = 16$ in the low SNR range.

In Fig. 6.14 and Fig. 6.15 we simulate the mean capacity and outage probability of the $(2, 2|4)$ IPS-MIMO system in a poor scattering single cluster environment. The cluster PAS is assume to be Laplacian distributed with the mean angle at 90° and angular spread 25°. The same radiation patterns as for the previous case are used. We show that in highly correlated spatial channels we can inactivate some radiation patterns while similar capacity performances can still be achieved. Fig. 6.15 shows that Alg. 6.2 with $L = 1$ provides no diversity gain because no pattern selection is performed. By increasing the number of activated radiation patterns, Alg. 6.2 with $L = 2$ provides similar performances as Alg. 6.1 in both mean capacity and diversity order, but the required estimation length is only a half of that of Alg. 6.1. This simulation shows that Alg. 6.2 is flexible in achieving the trade-off between system performance and complexity.

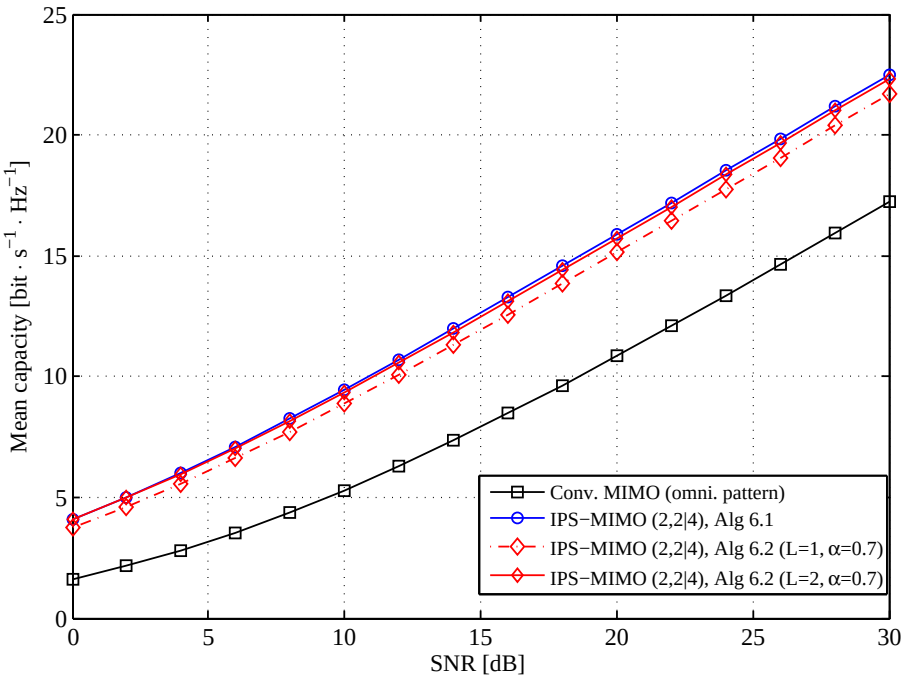

Figure 6.14 Mean capacity of a $(2, 2|4)$ IPS-MIMO system in a one-cluster spatial channel. The antennas are separated by half wavelength.

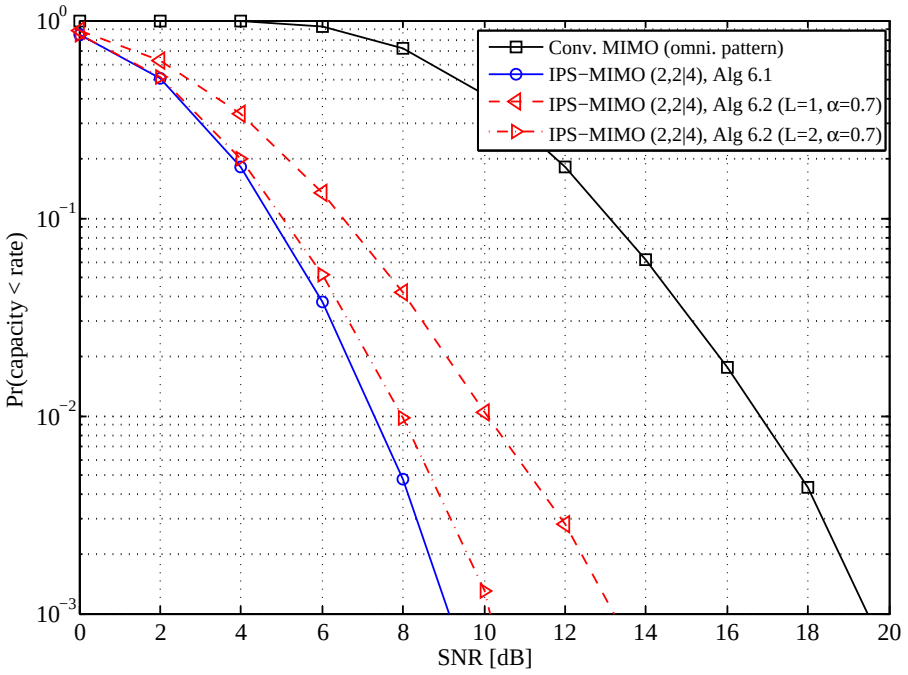

Figure 6.15 Channel outage probability of a $(2, 2|4)$ IPS-MIMO system ina one-cluster spatial channel. The antennas are separated by half wavelength.

6.4 Chapter Summary

In this chapter, we propose a framework to approximate the ergodic capacity of MIMO systems with selection diversity over arbitrarily correlated fading channels. By deriving the exact variance and covariance of the instantaneous channel capacity of the correlated OSTBC systems, we model the joint distribution of OSTBC capacity for selection as joint multivariate Gaussians. We use Clark's algorithm to find the ergodic capacity of IPS-MIMO. We also propose to use approximated covariance to reduce the computational costs. Numerical results show that the proposed framework is accurate with errors no more than 2%.

We validate by simulation that the channel capacity distribution of an IPS-OSTBC system over Rayleigh fading channels can be approximated by the skew-Normal distribution with negative skewness. The auto/cross-correlation coefficients of the mean channel capacities of each channel state are derived. By applying Clark's algorithm, we are able to approximate the mean capacity of the IPS-OSTBC. Therefore future works may extend this framework with skew-normal distribution to give more accurate results.

CHAPTER 7

SUMMARY AND CONCLUSIONS

7.1 Summary

- System Model of PS-MIMO

  The performance of a new technology referred to as PS-MIMO, which involves a state-of-the-art combination of pattern selection and spatial multiplexing, has been introduced to improve system performances in wireless communication. The potential benefits of using the PS-MIMO technology lies in the increase of directional antenna gain and additional diversity gain. The performance of the PS-MIMO technology is directly dependent on the MIMO propagation environment and PS-MIMO technology performs better than conventional MIMO in correlated channel scenarios. The reconfigurable directional antennas are steered to major propagation directions and instantaneous selection of the radiation patterns are used to provide selection diversity. Further, propagation parameters can be extracted from the measurement data and an empirical validation of a stochastic MIMO radio channel is possible. The target application of the correlation based MIMO model is link level simulation. This model originally assumes identical radiation pattern for each element of the reconfigurable antenna array. In addition, recommendations on how to use the MIMO technology are presented so that the MIMO technology achieves optimal performance.

- Estimating Channel Parameters with Reconfigurable Array

  Two joint DoA and angular spread estimation algorithm for a multiple element array with reconfigurable antennas is proposed. The generalized Capon estimation performance of the proposed method is evaluated by numerical simulations. The second proposed estimator takes advantage of the covariance matching estimation technique. Numerical simulations have shown that the mean angle and angular spread of the clustered channel can be accurately estimated compared to conventional estimation techniques.

- SPS-MIMO Systems

  The ergodic capacity of MIMO systems with dynamic radiation patterns in a clustered channel is studied. Theoretical analysis and simulation results show that the ergodic

capacity of SPS-MIMO benefits from high directivity of the radiation pattern and obtains a power gain. Furthermore, the channel capacity also takes advantage from the direction-steerable feature that matches the distribution of the propagation power to help decorrelating the clustered channel. Simulation indicates that, by using CRLH-LWA's, the ergodic channel capacity of a 2×2 MIMO system can be at least doubled at low SNR by steering the radiation patterns to proper directions. A searching method for the optimal directions is also proposed in this paper. We also showed by theoretical analysis and simulations that aiming all the radiation patterns to the cluster mean angle can be a near optimal solution if the radiation pattern has a wide beam.

- IPS-MIMO Systems

  From a reliability viewpoint, instantaneous selection provides an additional diversity dimension, which is used by IPS-MIMO systems to compensate the loss of space diversity due to spatial correlation between highly directional radiation patterns. The maximum achievable *diversity order* of the IPS-MIMO system measures the system's ability of combating fading. In this thesis, it is proved that the diversity order of the IPS-MIMO system is multiplied by the number of available radiation patterns at each antenna. More generally, the diversity order equals to the rank of the total correlation matrix which describes correlation between any pair of space diversity branches. From a rate viewpoint, IPS-MIMO increases the ergodic channel capacity due to the improved SNR by selection combining. A framework is proposed to approximate the channel capacity distribution of IPS-MIMO systems over arbitrarily correlated fading channels by a known distribution which matches low order moments of the instantaneous IPS-MIMO capacity. As a result, the approximated ergodic capacity of IPS-MIMO is found by assuming Gaussian approximation to the capacity distribution. In this thesis, by deriving the exact variance and covariance of the instantaneous channel capacity of the correlated OSTBC systems, the joint distribution of OSTBC capacity for selection is modeled by joint multivariate Gaussians. The ergodic capacity of IPS-MIMO is found by applying Clark's iterative algorithm. Simulations show that that the proposed framework is relatively accurate, with errors smaller than 2%. The PS-MIMO channel capacity distribution is negatively skewed, therefore future works may extend this framework with skew-normal distribution to give more accurate results.

- Capacity and Selection Algorithms for IPS-MIMO with Spatial Multiplexing: A capacity maximizing selection algorithm is proposed. Comparing to the exhaustive seach, the proposed selection algorithm reduces searching complexity by eliminating highly correlated or weak branches. Numerical results show that the proposed algorithm has

no distinct difference in ergodic channel capacity than the exhaustive search.

7.2 Future Works

In this thesis, we propose an iterative scheme to approximately evaluate the ergodic capacity of IPS-MIMO systems with arbitrary correlated radiation patterns. In this thesis, we have derived exact channel capacity covariance of correlated OSTBC systems for evaluating the mean capacity of IPS-OSTBC, and we have used simulated capacity covariance of correlated SM systems to verify the iterative scheme for IPS-SM. The future research may derive the exact or asymptotic channel capacity covariance of correlated SM systems so that the proposed iterative scheme can be directly extended to evaluate the mean capacity of SM systems with arbitrary radiation patterns. Another future research direction is to replace Gaussian approximation by other probability distribution such as the skew-Normal distribution which utilizes the first three moments to improve approximation accuracy. The new approximated distribution will require a novel recursion to update the statistics at each iteration step.

REFERENCES

[1] J. Winters, "On the capacity of radio communication systems with diversity in a Rayleigh fading environment," *IEEE Journal on Selected Areas in Communications*, vol. 5, no. 5, pp. 871–878, June 1987.

[2] E. Telatar, "Capacity of multi-antenna Gaussian channels," *European Transactions on Telecommunications*, vol. 10, no. 6, pp. 585–595, 1999.

[3] V. Tarokh, N. Seshadri, and A. R. Calderbank, "Space-time codes for high data rate wireless communication: Performance criterion and code construction," *IEEE Transactions on Information Theory*, vol. 44, no. 2, pp. 744–765, 1998.

[4] S. Alamouti, "A simple transmit diversity technique for wireless communications," *IEEE Journal on Selected Areas in Communications*, vol. 16, no. 8, pp. 1451–1458, 1998.

[5] D. Tse and P. Viswanath, *Fundamentals of Wireless Communications*. Cambridge University Press, 2005.

[6] G. Foschini, "Layered space-time architecture for wireless communication in a fading environment when using multi-element antennas," *Bell Labs Technical Journal*, vol. 1, no. 2, pp. 41–59, 1996.

[7] L. Zheng and D. Tse, "Diversity and multiplexing: A fundamental tradeoff in multiple-antenna channels," *IEEE Transactions on Information Theory*, vol. 49, no. 5, pp. 1073–1096, May 2003.

[8] S. Sanayei, A. Hedayat, and A. Nosratinia, "Space time codes in keyhole channels: Analysis and design," *IEEE Transactions on Wireless Communications*, vol. 6, no. 6, pp. 2006–2011, June 2007.

[9] H. Shin and J. Lee, "Capacity of multiple-antenna fading channels: Spatial fading correlation, double scattering, and keyhole," *IEEE Transactions on Information Theory*, vol. 49, no. 10, pp. 2636–2647, 2003.

[10] T. Svantesson, "Correlation and channel capacity of MIMO systems employing multi-mode antennas," *IEEE Transactions on Vehicular Technology*, vol. 51, no. 6, pp. 1304–1312, 2002.

[11] J. T. Bernhard, "Reconfigurable antennas and apertures: State of the art and future outlook," in *Proc. SPIE*, vol. 5055, 2003, pp. 1–9.

[12] D. Piazza, N. Kirsch, A. Forenza, R. Heath, and K. Dandekar, "Design and evaluation of a reconfigurable antenna array for MIMO systems," *IEEE Transactions on Antennas and Propagation*, vol. 56, no. 3, pp. 869 –881, Mar. 2008.

[13] L. Petit, L. Dussopt, and J. Laheurte, "MEMS-switched parasitic-antenna array for radiation pattern diversity," *IEEE Transactions on Antennas and Propagation*, vol. 54, pp. 2624–2631, 2006.

[14] A. Grau, M.-J. Lee, J. Romeu, H. Jafarkhani, L. Jofre, and F. De Flaviis, "A multifunctional MEMS-reconfigurable pixel antenna for narrowband MIMO communications," in *Antennas and Propagation Society International Symposium, 2007 IEEE*, June 2007, pp. 489–492.

[15] R. Harrington, "Reactively controlled directive arrays," *IEEE Transactions on Antennas and Propagation*, vol. 26, no. 3, pp. 390–395, May 1978.

[16] S. Chandran, *Adaptive Antenna Arrays: Trends and Applications*. Springer, 2004.

[17] C. Caloz and T. Itoh, "Array factor approach of leaky-wave antennas and application to 1-D/2-D composite right/left-handed (CRLH) structures," *IEEE Microwave and Wireless Components Letters*, vol. 14, no. 6, pp. 274–276, Jun. 2004.

[18] D. Piazza, D. Michele, and K. Dandekar, "Two port reconfigurable crlh leaky wave antenna with improved impedance matching and beam tuning," in *Antennas and Propagation, 2009. EuCAP 2009. 3rd European Conference on*, Mar. 2009, pp. 2046 –2049.

[19] J.-F. Frigon, C. Caloz, and Y. Zhao, "Dynamic radiation pattern diversity (DRPD) MIMO using CRLH leaky-wave antennas," in *Proc. IEEE Radio and Wireless Symposium (RWS'08)*, Jan. 2008, pp. 635–638.

[20] A. Forenza and J. Heath, R.W., "Benefit of pattern diversity via two-element array of circular patch antennas in indoor clustered MIMO channels," *IEEE Transactions on Communications*, vol. 54, no. 5, pp. 943–954, 2006.

[21] X. Li and J.-F. Frigon, "Capacity analysis of MIMO systems with dynamic radiation pattern diversity." in *Proc. IEEE VTS Vehicular Technology Conference (VTC'09 Spring)*, Barcelona, Spain, Apr. 2009, pp. 1–5.

[22] F. Fazel, A. Grau, H. Jafarkhani, and F. Flaviis, "Space-time-state block coded MIMO communication systems using reconfigurable antennas," *IEEE Transactions on Wireless Communications*, vol. 8, no. 12, pp. 6019–6029, 2009.

[23] J. D. Boerman and J. T. Bernhard, "Performance study of pattern reconfigurable antennas in MIMO communication systems," *IEEE Transactions on Antennas and Propagation*, vol. 56, no. 1, pp. 231–236, Jan. 2008.

[24] L. Dong, H. Ling, and R. W. Heath, "Multiple-input multiple-output wireless communication systems using antenna pattern diversity," in *Proc. IEEE Global Telecommunications Conference (GLOBECOM'02)*, vol. 1. IEEE, 2002, pp. 997–1001.

[25] A. Grau, H. Jafarkhani, and F. De Flaviis, "A reconfigurable multiple-input multiple-output communication system," *IEEE Transactions on Wireless Communications*, vol. 7, no. 5, pp. 1719–1733, 2008.

[26] Z. Xu, S. Sfar, and R. S. Blum, "Analysis of MIMO systems with receive antenna selection in spatially correlated Rayleigh fading channels," *IEEE Transactions on Vehicular Technology*, vol. 58, no. 1, pp. 251–262, 2009.

[27] A. Gorokhov, D. Gore, and A. Paulraj, "Performance bounds for antenna selection in MIMO systems," in *Proc. IEEE International Conference on Communications (ICC'03)*, vol. 5. IEEE, 2003, pp. 3021–3025.

[28] A. F. Molisch, M. Z. Win, Y.-S. Choi, and J. H. Winters, "Capacity of MIMO systems with antenna selection," *IEEE Transactions on Wireless Communications*, vol. 4, no. 4, pp. 1759–1772, 2005.

[29] L. Dai, S. Sfar, and K. Letaief, "Optimal antenna selection based on capacity maximization for MIMO systems in correlated channels," *IEEE Transactions on Communications*, vol. 54, no. 3, pp. 563–573, 2006.

[30] A. Dua, K. Medepalli, and A. Paulraj, "Receive antenna selection in MIMO systems using convex optimization," *IEEE Transactions on Wireless Communications*, vol. 5, no. 9, p. 2353, 2006.

[31] H. Zhang, H. Dai, Q. Zhou, and B. Hughes, "On the diversity order of spatial multiplexing systems with transmit antenna selection: A geometrical approach," *IEEE Transactions on Information Theory*, vol. 52, no. 12, pp. 5297–5311, 2006.

[32] D. Love, "On the probability of error of antenna-subset selection with space-time block codes," *IEEE Transactions on Communications*, vol. 53, no. 11, pp. 1799–1803, 2005.

[33] R. Narasimhan, "Spatial multiplexing with transmit antenna and constellation selection for correlated MIMO fading channels," *IEEE Transactions on Signal Processing*, vol. 51, no. 11, pp. 2829–2838, 2003.

[34] ——, "Transmit antenna selection based on outage probability for correlated MIMO multiple access channels," *IEEE Transactions on Wireless Communications*, vol. 5, no. 10, p. 2945, 2006.

[35] M. Steinbauer, A. F. Molisch, and E. Bonek, "The double-directional radio channel," *IEEE Antennas and Propagation Magazine*, vol. 43, no. 4, pp. 51–63, 2001.

[36] V. Erceg, L. Schumacher, P. Kyritsi, A. Molisch, D. Baum, A. Gorokhov, C. Oestges, Q. Li, K. Yu, N. Tal *et al.*, "TGn channel models," *IEEE 802.11-03/940r4*, 2004.

[37] C. Oestges and B. Clerckx, *MIMO Wireless Communications: From Real-World Propagation to Space-Time Code Design*. Academic Press, 2010.

[38] Q. Spencer, B. Jeffs, M. Jensen, and A. Swindlehurst, "Modeling the statistical time and angle of arrival characteristicsof an indoor multipath channel," *IEEE Journal on Selected Areas in Communications*, vol. 18, no. 3, pp. 347–360, 2000.

[39] N. Czink, E. Bonek, L. Hentila, J. Nuutinen, and J. Ylitalo, "Cluster-based MIMO channel model parameters extracted from indoor time-variant measurements," in *Proc. IEEE Global Telecommunications Conference (GLOBECOM'06)*, San Francisco, CA, USA, 2006.

[40] R. R. Müller, "A random matrix model of communication via antenna arrays," *IEEE Transactions on Information Theory*, vol. 48, no. 9, pp. 2495–2506, 2002.

[41] A. Saleh and R. Valenzuela, "A statistical model for indoor multipath propagation," *IEEE Journal on Selected Areas in Communications*, vol. 5, no. 2, pp. 128–137, 1987.

[42] J. Wallace and M. Jensen, "Statistical characteristics of measured MIMO wireless channel data and comparison to conventional models," in *Proc. IEEE VTS 54th Vehicular Technology Conference (VTC'01 Fall)*, vol. 2, 2001, pp. 1078–1082.

[43] H. Ozcelik, M. Herdin, W. Weichselberger, J. Wallace, and E. Bonek, "Deficiencies of 'Kronecker' MIMO radio channel model," *Electronics Letters*, vol. 39, no. 16, pp. 1209–1210, Aug. 2003.

[44] W. Weichselberger, "Spatial structure of multiple antenna radio channels," Ph.D. dissertation, Institut für Nachrichtentechnik und Hochfrequenztechnik, 2003.

[45] S. Valaee, B. Champagne, and P. Kabal, "Parametric localization of distributed sources," *IEEE Transactions on Signal Processing*, vol. 43, no. 9, pp. 2144–2153, Sept. 1995.

[46] F. G. Bass and I. M. Fuks, *Wave Scattering from Statistically Rough Surfaces*. Pergamon Press ltd., 1979.

[47] J. Capon, "High-resolution frequency-wavenumber spectrum analysis," *Proc. IEEE*, vol. 57, no. 8, pp. 1408–1418, Aug. 1969.

[48] A. Hassanien, S. Shahbazpanahi, and A. Gershman, "A generalized Capon estimator for localization of multiple spread sources," *IEEE Transactions on Signal Processing*, vol. 52, no. 1, pp. 280–283, 2004.

[49] G. Foschini and M. Gans, "On limits of wireless communications in a fading environment when using multiple antennas," *Wireless Personal Communications*, vol. 6, no. 3, pp. 311–335, 1998.

[50] M. Chiani, M. Win, and A. Zanella, "On the capkacity of spatially correlated MIMO Rayleigh-fading channels," *IEEE Transactions on Information Theory*, vol. 49, no. 10, pp. 2363–2371, 2003.

[51] W. Weichselberger, M. Herdin, H. Ozcelik, and E. Bonek, "A stochastic MIMO channel model with joint correlation of both link ends," *IEEE Transactions on Wireless Communications*, vol. 5, no. 1, pp. 90–100, 2006.

[52] K. Hamdi, "Capacity of MRC on correlated Rician fading channels," *IEEE Transactions on Communications*, vol. 56, no. 5, pp. 708–711, May 2008.

[53] H. Shin, M. Win, J. H. Lee, and M. Chiani, "On the capacity of doubly correlated MIMO channels," *IEEE Transactions on Wireless Communications*, vol. 5, no. 8, pp. 2253–2265, Aug. 2006.

[54] A. Jeffrey and D. Zwillinger, *Table of Integrals, Series, and Products*, 7th ed. Elsevier, 2007.

[55] P. Smith and M. Shafi, "On a Gaussian approximation to the capacity of wireless MIMO systems," in *Proc. IEEE International Conference on Communications (ICC'02)*, vol. 1, 2002, pp. 406–410.

[56] M. Kamath and B. Hughes, "The asymptotic capacity of multiple-antenna Rayleigh-fading channels," *IEEE Transactions on Information Theory*, vol. 51, no. 12, pp. 4325–4333, Dec. 2005.

[57] W. Hachem, O. Khorunzhiy, P. Loubaton, J. Najim, and L. Pastur, "A new approach for mutual information analysis of large dimensional multi-antenna channels," *IEEE Transactions on Information Theory*, vol. 54, no. 9, pp. 3987–4004, Sept. 2008.

[58] R. Qian, Y. Qi, P. Tao, W. Wang, and J. Yang, "A simple approach of Gaussian approximation for channel capacity in multiple-antenna systems," in *Proc. IEEE VTS Vehicular Technology Conference (VTC'11 Fall)*, Sept. 2011, pp. 1–5.

[59] J. Perez, J. Ibanez, L. Vielva, and I. Santamaria, "Closed-form approximation for the outage capacity of orthogonal STBC," *IEEE Communications Letters*, vol. 9, no. 11, pp. 961–963, Nov. 2005.

[60] C. Clark, "The greatest of a finite set of random variables," *Operations Research*, pp. 145–162, 1961.

[61] T. Kollo and D. von Rosen, *Advanced Multivariate Statistics with Matrices*. Springer, 2005, vol. 579.

[62] G. Seber and A. Lee, *Linear Regression Analysis*. John Wiley and Sons, 2002.

[63] A. Gorokhov, D. Gore, and A. Paulraj, "Receive antenna selection for MIMO spatial multiplexing: Theory and algorithms," *IEEE Transactions on Signal Processing*, vol. 51, no. 11, pp. 2796–2807, 2003.

[64] M. Nakagami, "The m-distribution: A general formula of intensity distribution of rapid fading," *Statistical Method of Radio Propagation*, 1960.

[65] J. Luo, J. Zeidler, and S. McLaughlin, "Performance analysis of compact antenna arrays with MRC in correlated Nakagami fading channels," *IEEE Transactions on Vehicular Technology*, vol. 50, no. 1, pp. 267–277, 2001.

[66] R. Muirhead, *Aspects of Multivariate Statistical Theory*. John Wiley and Sons, Inc., 1982.

[67] M. Kiessling and J. Speidel, "Asymptotically tight bound on SER of MIMO zero-forcing receivers with correlated fading," in *Proc. IEEE International Symposium on Information Theory (ISIT'04)*, June 2004, p. 504.

APPENDIX A

DISTRIBUTION OF $\|\mathbf{H}\|_F^2$ OVER NAKAGAMI FADING CHANNELS

In this appendix, we will provide the exact distribution of $\|\mathbf{H}\|_F^2$ (the Frobenius norm square of the channel matrix $\mathbf{H}$) over arbitrarily correlated Nakagami-m fading channels. This result will be used to prove Proposition 6.1 and calculate Eq. (6.20), Eq. (6.21) and Eq. (6.23).

For a MIMO system equipped with N_t transmit and N_r receive antennas, the channel matrix $\mathbf{H} = \left[h_{n_r,n_t} \triangleq A_{n_r,n_t} e^{j\phi_{n_r,n_t}}\right]_{n_r,n_t=1}^{N_r,N_t}$ contains $N_t N_r$ subchannel coefficients. We assume that the phase ϕ_{n_r,n_t} is independent and uniformly distributed within $[-\pi, \pi]$ and the amplitude A_{n_r,n_t}, which may exhibit arbitrary correlation, follows the Nakagami-m distribution with the fading figure m (assuming all subchannels have an identical fading figure). The probability density function (PDF) of A_{n_r,n_t} is [64]

$$f_{A_{n_r,n_t}}(x) = \frac{2}{\Gamma(m)} \left(\frac{m}{\Omega_{n_r,n_t}}\right)^m x^{2m-1} e^{-mx^2/\Omega_{n_r,n_t}},\ x \geq 0, \quad (n_{t/r} = 1, \ldots, N_{t/r}) \tag{A.1}$$

where $\Omega_{n_r,n_t} = \mathbb{E}[|A_{n_r,n_t}|^2]$ is the average power of the subchannel coefficient between the transmit antenna n_t and the receive antenna n_r, m is the fading figure of the subchannel and $\Gamma(\cdot)$ is the Gamma function. Note that the Nakagami-m fading channel includes the Rayleigh fading channel as a special case when $m = 1$.

The MGF of $\|\mathbf{H}\|_F^2$ over Nakagami-m fading channels is given according to [65, Eq. (15)]

$$\begin{aligned} \mathcal{M}_{\|\mathbf{H}\|_F^2}(s) &= \mathbb{E}\left[e^{s\|\mathbf{H}\|_F^2}\right] \\ &= \det(\mathbf{I}_{N_t N_r} - s\mathbf{R})^{-m} \\ &= \det(\mathbf{I}_N - s\mathbf{\Lambda})^{-m}, \end{aligned} \tag{A.2}$$

where $\mathbf{R} = \mathbb{E}\left[\mathrm{vec}\,(\mathbf{H})\,\mathrm{vec}\,(\mathbf{H})^H\right]$ is the channel correlation matrix, $N = \mathrm{rank}(\mathbf{R})$ is the rank of the channel correlation matrix, and $\mathbf{\Lambda}$ is a diagonal matrix with all N positive eigenvalues of $\mathbf{R}$ on the main diagonal of $\mathbf{\Lambda}$. Using an approach developed in [66, Theorem 8.3.4], we expand Eq. (A.2) in the form of the weighted sum of MGF's of the Gamma distribution as

follows

$$\begin{aligned}\mathcal{M}_{\|\mathbf{H}\|_F^2}(s) &= \det(\mathbf{I}_N - s\mathbf{\Lambda})^{-m} \\ &= \det(t^{-1}\mathbf{\Lambda})^{-m} \sum_{k=0}^{\infty} \frac{1}{k!(1-ts)^{mN+k}} \sum_{\kappa} (m)_\kappa C_\kappa(\mathbf{I}_N - t\mathbf{\Lambda}^{-1}),\end{aligned} \tag{A.3}$$

where $0 < t < \infty$ is an auxiliary which determines the convergence speed of the series. The inner summation is over all partitions κ of k into no more than m parts[1], $(m)_\kappa$ is the generalized hypergeometric coefficient[2] of m corresponding to κ, and $C_\kappa(\cdot)$ is the zonal polynomial[3] corresponding to κ.

Since $(1-ts)^{-(mN+k)}$ is the MGF of the Gamma distribution with the parameters $mN+k$ and t, we rewrite the MGF Eq. (A.3) in the form of the weighted sum of the MGF's of the Gamma distribution by

$$\mathcal{M}_{\|\mathbf{H}\|_F^2}(s) = \sum_{k=0}^{\infty} c_k (1-ts)^{-(mN+k)}, \tag{A.4}$$

where the weight c_k is

$$c_k = \frac{1}{k! \det(t^{-1}\mathbf{\Lambda})^m} \sum_{\kappa} (m)_\kappa C_\kappa(\mathbf{I}_N - t\mathbf{\Lambda}^{-1}). \tag{A.5}$$

Therefore, the cumulative distribution function (CDF) of $\|\mathbf{H}\|_F^2$ over Nakagami-m fading channels is the weighted sum of the Gamma distribution CDF's:

$$F_{\|\mathbf{H}\|_F^2}(x) = \sum_{k=0}^{\infty} c_k F_\Gamma(x; mN+k, t), \tag{A.6}$$

where $F_\Gamma(x; mN+k, t)$ is the CDF of the Gamma distribution with the parameters $mN+k$

[1]Let k be a positive integer. The partition κ of k into no more than m parts is written as $\kappa = (k_1, k_2, \ldots, k_m)$ where $k_1 \geq \cdots \geq k_m \geq 0$ are non-negative integers satisfying $\sum_{i=1}^m k_i = k$. See [66, Section 7.2.1].

[2]Let $\kappa = (k_1, k_2, \ldots, k_m)$ and let α be a complex number. The generalized hypergeometric coefficient, denoted by $(\alpha)_\kappa$, is defined by

$$(\alpha)_\kappa = \prod_{i=1}^{m} \left(\alpha - \frac{i-1}{2}\right)_{k_i},$$

where $(x)_k = \prod_{i=1}^{k}(x+i-1)$ is the Pochhammer symbol and $(x)_0 = 1$. See [66, Section 7.2.3, (41) and Theorem 7.2.7]. Note that $(\alpha)_{(0)} \equiv 1$.

[3]Let $\mathbf{A}$ be a $m \times m$ Hermitian matrix with eigenvalues $\lambda_1, \ldots, \lambda_m$ and let $\kappa = (k_1, k_2, \ldots, k_m)$. The zonal polynomial of $\mathbf{A}$ corresponding to κ, denoted by $C_\kappa(\mathbf{A})$, is a symmetric, homogeneous polynomial of degree k in the eigenvalues. See [66, Section 7.2.1] for the definition and calculation of $C_\kappa(\mathbf{A})$.

As κ varies over all partitions of k into no more than m parts, the sum of the corresponding zonal polynomials is $\sum_\kappa C_\kappa(\mathbf{A}) = (\lambda_1 + \ldots + \lambda_m)^k = (\mathrm{tr}\mathbf{A})^k$. If $k = 0$, $C_{(0)}(\mathbf{A}) \equiv 1$.

and t, which is known as

$$F_{\Gamma}(x; mN+k, t) = \int_0^x \frac{\tau^{mN+k-1} e^{-\tau/t}}{t^{mN+k}(mN+k-1)!} d\tau. \tag{A.7}$$

Substituting the Gamma CDF Eq. (A.7) into Eq. (A.6), we present the exact CDF of $\|\mathbf{H}\|_{\mathrm{F}}^2$ over Nakagami-m fading channels by

$$F_{\|\mathbf{H}\|_F^2}(x) = \sum_{k=0}^{\infty} c_k \int_0^x \frac{\tau^{mN+k-1} e^{-\tau/t}}{t^{mN+k}(mN+k-1)!} d\tau. \tag{A.8}$$

After having obtained the exact distribution of $\|\mathbf{H}\|_{\mathrm{F}}^2$ in Eq. (A.8), we study the limiting behavior of $F_{\|\mathbf{H}\|_{\mathrm{F}}^2}(x)$ as $x \to 0^+$. First, we use the first order approximation to Eq. (A.8) near $x = 0$ and get

$$F_{\|\mathbf{H}\|_F^2}(x) \approx \sum_{k=0}^{\infty} c_k \cdot \frac{x^{mN+k}}{t^{mN+k}(mN+k)!}, \quad (\text{when } x \to 0^+). \tag{A.9}$$

Then, we neglect the summands indexed by $k > 0$ in Eq. (A.9), for they are infinitesimals of orders higher than mN, and we get

$$\begin{aligned} F_{\|\mathbf{H}\|_F^2}(x) &\approx c_0 \cdot \frac{x^{mN}}{t^{mN}(mN)!} \\ &\approx \frac{x^{mN}}{(mN)! \det \mathbf{\Lambda}^m}, \quad (\text{when } x \to 0^+) \end{aligned} \tag{A.10}$$

where $c_0 = \det(t^{-1}\mathbf{\Lambda})^{-m}$ for $(m)_\kappa \equiv 1$ and $C_\kappa(\mathbf{I}_N - t\mathbf{\Lambda}^{-1}) \equiv 1$ when $k = 0$. Note that the auxiliary t disappears in Eq. (A.10) and Eq. (A.10) is only related to the channel correlation matrix and the fading figure. We can conclude from Eq. (A.10) that the exponential order of $F_{\|\mathbf{H}\|_F^2}(x)$ over Nakagami-m fading channels as $x \to 0^+$ is the product of the Nakagami fading figure and the rank of the channel correlation matrix, i.e.,

$$\lim_{x \to 0^+} \frac{\ln F_{\|\mathbf{H}\|_{\mathrm{F}}^2}(x)}{\ln x} = m \ \mathrm{rank}(\mathbf{R}). \tag{A.11}$$

For Proposition 6.1, since the Rayleigh fading is a special case of the Nakagami-m fading when $m = 1$, Proposition 6.1 is proven according to Eq. (A.10). And, the exponential order of $F_{\|\mathbf{H}\|_F^2}(x)$ as $x \to 0^+$ over Rayleigh fading channels is the rank of the channel correlation matrix according to Eq. (A.11).

APPENDIX B

COVARIANCE OF THE CAPACITY OF TWO CORRELATED MIMO OSTBC SYSTEMS OVER RAYLEIGH FADING CHANNELS

In this appendix, we will give the detailed derivation of Eq. (6.50), the MGF and the (co)variance second order statistics of in details the exact covariance of the instantaneous capacity of two correlated MIMO OSTBC systems over Rayleigh fading channels. We give the detailed derivation of $c_1 \triangleq C_{\psi_1}^{\text{OSTBC}}$ and $c_2 \triangleq C_{\psi_2}^{\text{OSTBC}}$. We will make use of Eq. (6.47) and the following equality derived from the PDF of the multi-variate Gaussian distribution:

$$\int_{\mathbb{C}^N} e^{-\mathbf{x}^H \mathbf{K} \mathbf{x}} d\mathbf{x} = \frac{\pi^N}{\det \mathbf{K}}, \tag{B.1}$$

where $\mathbf{K}$ is a positive definite square matrix.

The cross-correlation of the capacity can be evaluated as

$$\begin{aligned}
&\mathbb{E}[c_1 c_2] \\
=&\int_{\mathbb{C}^N} \log_2(1+\gamma \mathbf{h}_1^H \mathbf{h}_1) f_{\mathbf{h}_1}(\mathbf{h}_1) \int_{\mathbb{C}^N} \log_2(1+\gamma \mathbf{h}_2^H \mathbf{h}_2) f_{\mathbf{h}_2|\mathbf{h}_1}(\mathbf{h}_2|\mathbf{h}_1) d\mathbf{h}_2 d\mathbf{h}_1 \\
=&(\log_2 e)^2 \int_{\mathbb{C}^N} \ln(1+\gamma \mathbf{h}_1^H \mathbf{h}_1) f_{\mathbf{h}_1}(\mathbf{h}_1) \left[\int_0^\infty \frac{e^{-z_2}}{z_2} \left(1 - \mathcal{M}(-\gamma z_2; \mathbf{A}\mathbf{h}_1, \tilde{\mathbf{R}}_{2\cdot 1})\right) dz_2 \right] d\mathbf{h}_1 \\
=&(\log_2 e)^2 \int_0^\infty \int_0^\infty \int_{\mathbb{C}^N} \frac{e^{-(z_1+z_2)}}{z_1 z_2} \left(1 - e^{-\gamma z_1 \mathbf{h}_1^H \mathbf{h}_1}\right) \cdot \left(1 - \frac{e^{-\mathbf{h}_1^H \mathbf{A}^H (\gamma z_2^{-1} \mathbf{I}_N + \tilde{\mathbf{R}}_{2\cdot 1})^{-1} \mathbf{A}\mathbf{h}_1}}{\det(\mathbf{I}_N + \gamma z_2 \tilde{\mathbf{R}}_{2\cdot 1})}\right) \\
&\qquad \times f_{\mathbf{h}_1}(\mathbf{h}_1) d\mathbf{h}_1 d\zeta_1 d\zeta_2 \\
=&(\log_2 e)^2 \int_0^\infty \int_0^\infty \frac{e^{-(z_1+z_2)}}{z_1 z_2} \left[1 - \frac{1}{\det(\mathbf{I}_N + \gamma z_1 \tilde{\mathbf{R}}_1)} - \frac{1}{\det(\mathbf{I}_N + \gamma z_2 \tilde{\mathbf{R}}_{2\cdot 1})} \right. \\
&\qquad \left. \times \int_{\mathbb{C}^N} (1 - e^{-\gamma z_1 \mathbf{h}_1^H \mathbf{h}_1}) \cdot e^{-\gamma z_2 \mathbf{h}_1^H \mathbf{A}^H (\mathbf{I}_N + \gamma z_2 \tilde{\mathbf{R}}_{2\cdot 1})^{-1} \mathbf{A}\mathbf{h}_1} f_{\mathbf{h}_1}(\mathbf{h}_1) d\mathbf{h}_1 \right] dz_1 dz_2 \\
=&(\log_2 e)^2 \int_0^\infty \int_0^\infty d\zeta_1 d\zeta_2 \frac{e^{-(\zeta_1+\zeta_2)/\gamma}}{\zeta_1 \zeta_2} \left[1 - \frac{1}{\det(\mathbf{I}_N + \zeta_1 \tilde{\mathbf{R}}_1)} - \frac{1}{\det(\mathbf{I}_N + \zeta_2 \tilde{\mathbf{R}}_{2\cdot 1})} \right. \\
&\qquad \left. \times \int_{\mathbb{C}^N} \left(e^{-\mathbf{h}_1^H \mathbf{A}^H (\zeta_2^{-1} \mathbf{I}_N + \tilde{\mathbf{R}}_{2\cdot 1})^{-1} \mathbf{A}\mathbf{h}_1} - e^{-\mathbf{h}_1^H [\mathbf{A}^H (\zeta_2^{-1} \mathbf{I}_N + \tilde{\mathbf{R}}_{2\cdot 1})^{-1} \mathbf{A} + \zeta_1 \mathbf{I}_N] \mathbf{h}_1}\right) f_{\mathbf{h}_1}(\mathbf{h}_1) d\mathbf{h}_1 \right] \\
=&(\log_2 e)^2 \int_0^\infty \int_0^\infty d\zeta_1 d\zeta_2 \frac{e^{-(\zeta_1+\zeta_2)/\gamma}}{\zeta_1 \zeta_2} \left[1 - \frac{1}{\det(\mathbf{I}_N + \zeta_1 \tilde{\mathbf{R}}_1)} - \frac{1}{\det(\mathbf{I}_N + \zeta_2 \tilde{\mathbf{R}}_{2\cdot 1})} \right.
\end{aligned}$$

$$\times\left(\frac{1}{\det(\mathbf{I}_N+\tilde{\mathbf{R}}_1\mathbf{A}^H(\zeta_2^{-1}\mathbf{I}_N+\tilde{\mathbf{R}}_{2\cdot1})^{-1}\mathbf{A})}-\frac{1}{\det(\mathbf{I}_N+\tilde{\mathbf{R}}_1[\mathbf{A}^H(\zeta_2^{-1}\mathbf{I}_N+\tilde{\mathbf{R}}_{2\cdot1})^{-1}\mathbf{A}+\zeta_1\mathbf{I}_N])}\right)\Bigg]$$

$$=(\log_2 e)^2\int_0^\infty\int_0^\infty d\zeta_1 d\zeta_2\frac{e^{-(\zeta_1+\zeta_2)/\gamma}}{\zeta_1\zeta_2}\left[1-\frac{1}{\det(\mathbf{I}_N+\zeta_1\tilde{\mathbf{R}}_1)}-\frac{1}{\det(\mathbf{I}_N+\zeta_2\tilde{\mathbf{R}}_{2\cdot1})}\right.$$

$$\left.\times\left(\frac{1}{\det(\mathbf{I}_N+\mathbf{A}\tilde{\mathbf{R}}_1\mathbf{A}^H(\zeta_2^{-1}\mathbf{I}_N+\tilde{\mathbf{R}}_{2\cdot1})^{-1})}-\frac{1}{\det(\mathbf{I}_N+\zeta_1\tilde{\mathbf{R}}_1+\zeta_2\tilde{\mathbf{R}}_1\mathbf{A}^H(\mathbf{I}_N+\zeta_2\tilde{\mathbf{R}}_{2\cdot1})^{-1}\mathbf{A})}\right)\right]$$

$$=(\log_2 e)^2\int_0^\infty\int_0^\infty\frac{e^{-(\zeta_1+\zeta_2)/\gamma}}{\zeta_1\zeta_2}\left[1-\frac{1}{\det(\mathbf{I}_N+\zeta_1\tilde{\mathbf{R}}_1)}-\frac{1}{\det(\mathbf{I}_N+\zeta_2\tilde{\mathbf{R}}_2)}\right.$$

$$\left.+\frac{1}{\det(\mathbf{I}_N+\zeta_1\tilde{\mathbf{R}}_1)\det(\mathbf{I}_N+\zeta_2\tilde{\mathbf{R}}_{2\cdot1}+\zeta_2\mathbf{A}(\mathbf{I}_N+\zeta_1\tilde{\mathbf{R}}_1)^{-1}\tilde{\mathbf{R}}_1\mathbf{A}^H)}\right]d\zeta_1 d\zeta_2 \tag{B.2}$$

where

$$\begin{aligned}
&\det(\mathbf{I}_N+\zeta_2\tilde{\mathbf{R}}_{2\cdot1}+\zeta_2\mathbf{A}(\mathbf{I}_N+\zeta_1\tilde{\mathbf{R}}_1)^{-1}\tilde{\mathbf{R}}_1\mathbf{A}^H)\\
=&\det(\mathbf{I}_N+\zeta_2\tilde{\mathbf{R}}_2-\zeta_2\mathbf{A}\left(\frac{\tilde{\mathbf{R}}_1}{\mathbf{I}_N+\zeta_1\tilde{\mathbf{R}}_1}-\tilde{\mathbf{R}}_1\right)\mathbf{A}^H)\\
=&\det(\mathbf{I}_N+\zeta_2\tilde{\mathbf{R}}_2-\zeta_1\zeta_2\mathbf{A}\left(\frac{\tilde{\mathbf{R}}_1^2}{\mathbf{I}_N+\zeta_1\tilde{\mathbf{R}}_1}\right)\mathbf{A}^H)\\
=&\det(\mathbf{I}_N+\zeta_2\tilde{\mathbf{R}}_2-\zeta_1\zeta_2\tilde{\mathbf{R}}_{21}(\mathbf{I}_N+\zeta_1\tilde{\mathbf{R}}_1)^{-1}\tilde{\mathbf{R}}_{12})\\
=&\det(\mathbf{I}_N+\zeta_2\tilde{\mathbf{R}}_2)\det\left(\mathbf{I}_N-\zeta_1\zeta_2\tilde{\mathbf{R}}_{21}(\mathbf{I}_N+\zeta_1\tilde{\mathbf{R}}_1)^{-1}\tilde{\mathbf{R}}_{12}(\mathbf{I}_N+\zeta_2\tilde{\mathbf{R}}_2)^{-1}\right).
\end{aligned}$$

Therefore,

$$\begin{aligned}
&\mathbb{E}[c_1c_2]\\
&=(\log_2 e)^2\int_0^\infty\int_0^\infty\frac{e^{-(\zeta_1+\zeta_2)/\gamma}}{\zeta_1\zeta_2}\left[1-\frac{1}{\det(\mathbf{I}_N+\zeta_1\tilde{\mathbf{R}}_1)}-\frac{1}{\det(\mathbf{I}_N+\zeta_2\tilde{\mathbf{R}}_2)}\right.\\
&\left.+\frac{1}{\det(\mathbf{I}_N+\zeta_1\tilde{\mathbf{R}}_1)\det(\mathbf{I}_N+\zeta_2\tilde{\mathbf{R}}_2)\det[\mathbf{I}_N-\zeta_1\zeta_2\tilde{\mathbf{R}}_{21}(\mathbf{I}_N+\zeta_1\tilde{\mathbf{R}}_1)^{-1}\tilde{\mathbf{R}}_{12}(\mathbf{I}_N+\zeta_2\tilde{\mathbf{R}}_2)^{-1}]}\right]d\zeta_1 d\zeta_2.
\end{aligned} \tag{B.3}$$

Using the similar method, $\mathbb{E}[c_n^2]$ $(n = 1, 2)$ is derived by

$$\mathbb{E}\Big[c_n^2\Big] = (\log_2 e)^2 \int_0^\infty \int_0^\infty \frac{e^{-(\zeta_1+\zeta_2)/\gamma}}{\zeta_1\zeta_2} \times \left[1 - \frac{1}{\det(\mathbf{I}_N + \zeta_1\tilde{\mathbf{R}}_n)} - \frac{1}{\det(\mathbf{I}_N + \zeta_2\tilde{\mathbf{R}}_n)} + \frac{1}{\det(\mathbf{I}_N + (\zeta_1+\zeta_2)\tilde{\mathbf{R}}_n)}\right] d\zeta_1\zeta_2. \tag{B.4}$$

Therefore, the variance of the capacity c_n $(n = 1, 2)$ is

$$\begin{aligned}\mathrm{Var}[c_n] &= \mathbb{E}\Big[c_n^2\Big] - \mathbb{E}[c_n]^2 \\ &= (\log_2 e)^2 \int_0^\infty \int_0^\infty \frac{e^{-(\zeta_1+\zeta_2)/\gamma}}{\zeta_1\zeta_2} \\ &\quad \times \left\{\frac{1}{\det[\mathbf{I}_N + (\zeta_1+\zeta_2)\tilde{\mathbf{R}}_n]} - \frac{1}{\det[\mathbf{I}_N + (\zeta_1+\zeta_2)\tilde{\mathbf{R}}_n + \zeta_1\zeta_2\tilde{\mathbf{R}}_n^2]}\right\} d\zeta_1\zeta_2. \end{aligned} \tag{B.5}$$

The covariance of the capacity of two correlated channels is

$$\begin{aligned}&\mathrm{Cov}[c_1, c_2] \\ &= \mathbb{E}[c_1 c_2] - \mathbb{E}[c_1]\,\mathbb{E}[c_2] \\ &= (\log_2 e)^2 \int_0^\infty \int_0^\infty \frac{e^{-(\zeta_1+\zeta_2)/\gamma}}{\zeta_1\zeta_2} \\ &\times \left\{\frac{1}{\det(\mathbf{I}_N + \zeta_1\tilde{\mathbf{R}}_1)\det(\mathbf{I}_N + \zeta_2\tilde{\mathbf{R}}_2)\det[\mathbf{I}_N - \zeta_1\zeta_2\tilde{\mathbf{R}}_{21}(\mathbf{I}_N + \zeta_1\tilde{\mathbf{R}}_1)^{-1}\tilde{\mathbf{R}}_{12}(\mathbf{I}_N + \zeta_2\tilde{\mathbf{R}}_2)^{-1}]}\right. \\ &\quad \left. - \frac{1}{\det(\mathbf{I}_N + \zeta_1\tilde{\mathbf{R}}_1)\det(\mathbf{I}_N + \zeta_2\tilde{\mathbf{R}}_2)}\right\} d\zeta_1\zeta_2. \end{aligned} \tag{B.6}$$

APPENDIX C

V-BLAST SYSTEMS WITH RECONFIGURABLE ANTENNAS

We consider a V-BLAST system with reconfigurable antennas deployed at the receiver side. The channel is assumed flat fading. With the complete channel state information at the transmitter. For the covariance matrices we assume without loss of generality $R_{nn} = N_0 I$ and $R_{ss} = E_s I$. The signal to noise ratio (SNR) is defined by $\gamma = E_s/N_0$. for V-BLAST IPS-MIMO systems with the zero-forcing (ZF) receiver, the SNR at the k-th substream with channel state p is

$$\gamma_k^{(p)} = 1/\left[(\mathbf{H}_{(p)}^H \mathbf{H}_{(p)})^{-1}\right]_{kk}, \tag{C.1}$$

where $[\cdot]_{kk}$ extracts the k-th element on the main diagonal of the square matrix.

Assume the MIMO channel is uncorrelated at the transmitter, i.e., $\mathbf{R}_t = \mathbf{I}_{N_t}$. This assumption is valid when antennas at the transmitter side are separated far enough. We assume that each reconfigurable antenna deployed provides P radiation patterns, and these radiation patterns are orthogonal with each other:

$$\int_{2\pi} g_{r,m}^{(p)}(\phi_r) g_{r,n}^{(q)*}(\phi_r) d\phi_r = 0, \quad \text{where } m, n = 1, \cdots, N_r . m \neq n . p, q = 1, \cdots, P. \tag{C.2}$$

In this case, channel matrices received by different radiation pattern configurations at the receiver side are uncorrelated and independent, i.e.,

$$\mathbf{R}(\psi, \psi') = \mathbf{1}_{N_t} \otimes \mathbf{0}_{N_r}, \quad (\text{where } \psi \neq \psi' \text{ and } \psi, \psi' \in \Psi.) \tag{C.3}$$

Therefore, the substream SNR of each radiation pattern configuration are independent. [67] suggests that the MGF of the substream SNR of ZF receivers can be approximated by

$$M_{\gamma,k}^{(p)}(s) \approx \frac{1}{|\mathbf{I} + s\gamma \mathbf{O}^{(p)}|} \cdot \frac{\mathrm{tr}\mathbf{O}^{(p)} N_t - 1}{\mathrm{tr}\mathbf{O}^{(p)} (\mathbf{I} + s\gamma \mathbf{O}^{(p)})^{-1} N_t - 1} \tag{C.4}$$

At high SNR reign, the MGF can be approximated as

$$\overline{M}_{\gamma,k}^{(p)}(s) = \frac{\mathrm{tr}\mathbf{O}^{(p)} N_t - 1}{|\mathbf{O}^{(p)}| \cdot \begin{pmatrix} N_R \\ N_t - 1 \end{pmatrix}} \cdot (s\gamma)^{-D} \tag{C.5}$$

where $D = N_r - N_t + 1$ is the space diversity order of the p-th branch of the conventional ZF transmission scheme.

We select the maximum substream SNR:

$$\gamma_k = \max_{p=1}^{P} \gamma_k^{(p)} \tag{C.6}$$

As $\mathbf{H}^{(p)}$ are independent, the substream SNR $\gamma_k^{(p)}$ are also independent. Therefore we derive the approximated MGF of γ_k as

$$\overline{M}_{\gamma,k}(s) = s^{-(DP-P+1)} \cdot (\beta_k \gamma)^{-DP} \cdot \frac{(DP-P)!}{\left[(D-1)! \cdot \begin{pmatrix} N_R \\ N_t - 1 \end{pmatrix}\right]^P} \prod_{p=1}^{P} \frac{\mathrm{tr}\mathbf{O}^{(p)} N_t - 1}{|\mathbf{O}^{(p)}|} \tag{C.7}$$

Thus the asymptotic symbol error rate (SER) at high SNR of substream k is

$$\overline{P}_k(\gamma) \approx b \cdot c^{-(DP-P-1)} \cdot (\beta_k \gamma)^{-DP} \cdot \frac{(2DP-2P+1)!!}{2^{DP-P+1} \cdot \left((D-1)!\binom{N_R}{N_t-1}\right)^P} \prod_{p=1}^{P} \frac{\mathrm{tr}\mathbf{O}^{(p)} N_t - 1}{|\mathbf{O}^{(p)}|} \tag{C.8}$$

Eq. (C.8) indicates that the diversity order of a ZF decoding V-BLAST system is multiplied by the number of orthogonal radiation patterns if reconfigurable antennas are deployed.